

University of Massachusetts Medical School

eScholarship@UMMS

GSBS Dissertations and Theses

Graduate School of Biomedical Sciences

2006-07-08

Development of Pharmacological Magnetic Resonance Imaging Methods and their Application to the Investigation of Antipsychotic Drugs: a Dissertation

Karl F. Schmidt

University of Massachusetts Medical School

Let us know how access to this document benefits you.

Follow this and additional works at: https://escholarship.umassmed.edu/gsbs_diss



Part of the [Animal Experimentation and Research Commons](#), [Chemical Actions and Uses Commons](#), and the [Diagnosis Commons](#)

Repository Citation

Schmidt KF. (2006). Development of Pharmacological Magnetic Resonance Imaging Methods and their Application to the Investigation of Antipsychotic Drugs: a Dissertation. GSBS Dissertations and Theses. <https://doi.org/10.13028/w7am-qc46>. Retrieved from https://escholarship.umassmed.edu/gsbs_diss/114

This material is brought to you by eScholarship@UMMS. It has been accepted for inclusion in GSBS Dissertations and Theses by an authorized administrator of eScholarship@UMMS. For more information, please contact Lisa.Palmer@umassmed.edu.

A Dissertation Presented

By

Karl F. Schmidt

Submitted to the Faculty of the
University of Massachusetts Graduate School of Biomedical Sciences, Worcester
in partial fulfillment of the requirements for the degree of

DOCTOR OF PHILOSOPHY

July 8, 2006

Program in Neuroscience

COPYRIGHT

Portions of this dissertation appear in the following publications and copyrighted manuscripts:

Schmidt KF, Febo M, Shen Q, Luo F, Sicard KM, Ferris CF, Stein EA, Duong TQ. Hemodynamic and metabolic changes induced by cocaine in anesthetized rat observed with multimodal functional MRI. *Psychopharmacology (Berl)* 185: 479-86 (2006)

Liu ZM, Schmidt KF, Sicard KM, Duong TQ. Imaging oxygen consumption in forepaw somatosensory stimulation in rats under isoflurane anesthesia. *Magn Reson Med* 52: 277-285 (2004)

Schmidt KF, Lemdiasov RA, Brevard M; Chen W, Fox GB, King JA, Ludwig R, Ferris CF. Simultaneous measurement of spin-echo BOLD and cerebral blood flow in the conscious rat using a three coil imaging and restraint system. Copyright © 2006 *Journal of Neuroscience Methods*, under review

Ferris CF, Febo M, Luo F, Schmidt K, Brevard M, Harder JA, Kulkarni P, Messenger T, King JA. Functional magnetic resonance imaging in conscious animals: a new tool in behavioural neuroscience research. *J Neuroendocrinol.* 2006 May;18(5):307-18.

**Development of Pharmacological Magnetic Resonance Imaging Methods
and Their Application to the Investigation of Antipsychotic Drugs**

A Dissertation Presented

By

Karl F. Schmidt

Approved as to style and content by:

David Weaver, Ph.D., Chair of Committee

Jean King, Ph.D., Member of Committee

Glenn Gaudette, Ph.D., Member of Committee

Daniel Kilpatrick, Ph.D., Member of Committee

Lino Becerra, Ph.D., External Member of Committee

Craig Ferris, Ph.D., Thesis Advisor

Anthony Carruthers, Ph.D., Dean of the Graduate School of Biomedical Sciences

Ph.D. Program in Neuroscience
June 16, 2006

ACKNOWLEDGMENTS

I have been unusually fortunate as a graduate student to have had the opportunity to train under the direction of two mentors with very different interests and expertise. Dr. Timothy Duong was responsible for my training in my first years at UMASS Medical School and, following his progression to Emory University, I have had the great fortune to complete my training under the direction of Dr. Craig Ferris. I owe a tremendous debt of gratitude to both mentors, for their invaluable instruction in the technical aspects of MRI and in the application of MRI to pertinent problems in neuroscience. For years now, Dr. David Weaver has provided me with tireless and unwavering support in my scholastic and research efforts, without which I am confident that my progress would have stalled or failed, long ago. Similarly, the additional members of my research committee, Drs. Jean King, Glenn Gaudette, and Josie Harder, have provided me with the critical direction and support that I have needed in my research efforts, and I am truly grateful.

I would like to thank the members of the examination committee, some of whom have already suffered through too many of my presentations, for contributing their valuable time in this final exercise, especially Drs. Lino Becerra and Daniel Kilpatrick.

My colleagues at the CCNI have provided me with a broader education than I could possibly have anticipated. To be surrounded by such diverse medical and technical expertise has been a rare opportunity, and I thank Dr. Marcelo Febo, Mat Brevard, Tara Messenger, Dr. Li Zhixin, Dr. Ken Sicard, Dr. Praveen Kulkarni, Dr. Steve Bird, Dr. Nils

Henninger, Dr. Wei Chen, and Dr. Feng Luo (now at Abbott Laboratories), as well as Govind Nair (now at Emory University) for their help and instruction over the past years.

I owe this opportunity to pursue my doctorate to my mentors at Harvard Medical School, Drs. Mitch Albert, Yanping Sun, and Mary Mazzanti, for their training in prior years. I sincerely appreciate the support and direction given by Dr. Tony Carruthers in my first months at UMASS, and on a continuing basis thereafter, as well as the loving support and encouragement of my family. Several studies were made possible with the gracious financial support of Abbott Laboratories, and the valuable direction of Drs. Gerard Fox, Yanping Luo, Pamela Skoubis, Vincent Hradil, and Chih-Liang Chin. Overall, funding for this research was provided by Abbott Laboratories, the American Heart Association (SDG-0430020N), the National Institute on Drug Abuse (R01-DA13517), the National Institutes of Health (R01-EY014211), the University of Massachusetts Medical School, and the Whitaker Foundation (RG-02-0005).

Finally, the word *support* does not begin to describe the emotional investment and daily contributions of another that have ultimately made this pursuit possible. What small portion of this effort that is mine to give, is dedicated to my loving wife, Rebecca.

ABSTRACT

Pharmacological magnetic resonance imaging (phMRI) is the use of functional MRI techniques to elucidate the effects that psychotropic drugs have on neural activity within the brain; it is an emerging field of research that holds great potential for the investigation of drugs that act on the central nervous system by revealing the changes in neural activity that mediate observable changes in behavior, cognition, and perception. However, the realization of this potential is hampered by several unanswered questions: Are the MRI measurements reliable surrogates of changing neural activity in the presence of pharmacological agents? Is it relevant to investigate psychiatric phenomena such as reward or anxiolysis in anesthetized, rather than conscious animals? What are the methods that yield reproducible and meaningful results from phMRI experiments, and are they consistent in the investigations of different drugs?

The research presented herein addresses many of these questions with the specific aims of

- 1) Developing pharmacological MRI methodologies that can be used in the conscious animal,
- 2) Validating these methodologies with the investigation of a non-stimulant, psychoactive compound, and

3) Applying these methodologies to the investigation of typical and atypical antipsychotic drugs, classes of compounds with unknown mechanisms of therapeutic action

Building on recent developments in the field of functional MRI research, we developed new techniques that enable the investigator to measure localized changes in metabolism commensurate with changing neural activity. We tested the hypothesis that metabolic changes are a more reliable surrogate of changes in neural activity in response to a cocaine challenge, than changes observed in the blood-oxygen-level-dependent (BOLD) signal alone. We developed a system capable of multi-modal imaging in the conscious rat, and we tested the hypothesis that the conscious brain exhibits a markedly different response to systemic morphine challenge than the anesthetized brain. We identified and elucidated several fundamental limitations of the imaging and analysis protocols used in phMRI investigations, and developed new tools that enable the investigator to avoid common pitfalls. Finally, we applied these phMRI techniques to the investigation of neuroleptic compounds by asking the question: does treatment with typical or atypical antipsychotic drugs modulate the systems in the brain which are direct or indirect (i.e. downstream) substrates for a dopaminergic agonist?

The execution of this research has generated several new tools for the neuroscience and drug discovery communities that can be used in neuropsychiatric investigations into the action of psychotropic drugs, while the results of this research provide evidence that supports several answers to the questions that currently limit the utility of phMRI investigations. Specifically, we observed that metabolic change can be measured to

resolve discrepancies between anomalous BOLD signal changes and underlying changes in neural activity in the case of systemically administered cocaine. We found clear differences in the response to systemically administered morphine between conscious and anesthetized rats, and observed that only conscious animals exhibit a phMRI response that can be explained by the pharmacodynamics of morphine and corroborated by behavioral observations. We identified fundamental and drug-dependent limitations in the protocols used to perform phMRI investigations, and designed tools and alternate methods to facilitate protocol development.

By applying these techniques to the investigation of neuroleptic compounds, we have gained a new perspective of the alterations in dopaminergic signaling induced by treatment with antipsychotic medications, and have found effects in many nuclei outside of the pathways that act as direct substrates for dopamine. A clearer picture of how neuroleptics alter the intercommunication of brain nuclei would be an invaluable resource for the classification of investigational antipsychotic drugs, and would provide the basis for future studies that examine the neuroplastic changes that confer therapeutic efficacy following chronic treatment with antipsychotic medications.

TABLE OF CONTENTS

COPYRIGHT	ii
SIGNATURE PAGE	iii
ACKNOWLEDGMENTS	iv
ABSTRACT	vi
LIST OF TABLES	xiii
LIST OF FIGURES	xiv
LIST OF ABBREVIATIONS.....	xvii
CHAPTER I: Introduction	1
Background and Rationale.....	1
The basics of MRI.....	5
Changing hemodynamics associated with changing neuronal metabolism.....	10
The BOLD signal and functional MRI	12
Noninvasive Measurement of Cerebral Blood Flow using MRI	14
Antipsychotic medications.....	18
The history of antipsychotic drug development.....	18
Receptor affinity and the enduring mystery of therapeutic action.....	20
Activation of neural networks and their visualization by fMRI	23
CHAPTER II: Measuring $\Delta CMRO_2$ by multi-modal imaging in the anesthetized rat.....	34
Introduction.....	35
Theory.....	35
Materials and methods	39
Animal Preparation	39

MRI experiments	40
Data analysis	41
Results.....	43
Discussion.....	45
CHAPTER III: Measurement of changes in CMRO ₂ following cocaine administration in the anesthetized rat.....	57
Introduction.....	58
Materials and methods.....	60
Animal Preparation.....	60
MRI Experiments.....	61
Data analysis.....	62
Results.....	64
Discussion.....	66
CHAPTER IV: Whole brain analysis of multiple subjects mandates spin echo MRI acquisition: development of a 3 coil system for multi-modal imaging in conscious animals	77
Introduction.....	78
Materials and Methods.....	81
Results.....	82
Discussion.....	87
CHAPTER V: Conscious animals exhibit a BOLD response to morphine that differs from anesthetized animals	100
Introduction.....	101
Materials and Methods.....	104
Animal preparation	104
MRI experiments	105

Data analysis	106
Results.....	107
Discussion.....	109
Transient BOLD changes observed in anesthetized vs. conscious rats	109
Conscious, but not anesthetized, animals exhibit BOLD signal changes consistent with the pharmacodynamics of morphine.....	111
Limitations of the technique	113
Implications for pharmacological functional MRI	114
CHAPTER VI: BOLD signal changes in response to intracerebral ventricular apomorphine challenge in the conscious rat are modulated by pretreatment with neuroleptics.....	127
Introduction.....	128
Materials and methods.....	130
Animal preparation	131
MRI methods	131
Data analysis	132
Results.....	134
Discussion.....	138
ICV administration of apomorphine in the conscious animal	138
Regional correlation among animals pretreated with vehicles alone.....	138
Effects of pretreatment with haloperidol, clozapine, olanzapine and the selective D ₃ antagonist SB277011	140
Implications for the characterization of known and novel antipsychotic drugs	141
CHAPTER VII: Comprehensive discussion.....	155
Impact of findings.....	156
Considerations for phMRI data analysis.....	159

Future directions	160
Investigation of the function of antipsychotic drugs.....	160
Further improvements in phMRI methodology are required.....	162
Final comments.....	164
BIBLIOGRAPHY.....	165
APPENDIX A: Supplemental groupwise correlation analyses	186
APPENDIX B: Considerations in Choosing an Imaging Method for phMRI experiments	194
Experiments using the conscious animal	194
Considerations for selecting the functional imaging modality, image acquisition protocol, and route of drug administration	195

LIST OF TABLES

Table 1 – 1: Profiles of receptor blockade among atypical antipsychotic medications and haloperidol	29
Table 2 – 1: Respiration rate, heart rate, and mean arterial blood pressure during baseline and electrical forepaw stimulation.....	48
Table 3 – 1: Quantitative changes in BOLD, CBF, estimated CMRO ₂ and the parameter M in various regions of interest following intravenous administration of 1.0 mg/kg cocaine.	72
Table 5 – 1: Changes in heart rate (HR) and respiration rate (RR) following saline or morphine administration in conscious and anesthetized rats.....	121

LIST OF FIGURES

Figure 1 – 1: MRI of the ^1H Nucleus.....	28
Figure 1 – 2: Hemodynamic changes following increased neural activation.	31
Figure 1 – 3: Continuous Arterial Spin Labeling (CASL).....	33
Figure 2 – 1: Anatomical images, quantitative CBF, the parameter M and changes in BOLD, CBF, and CMRO ₂ following electrical forepaw stimulation from a single animal	50
Figure 2 – 2: Group average EPI images, quantitative CBF, and changes in CBF, BOLD and CMRO ₂	52
Figure 2 – 3: Dynamic changes in BOLD, CBF, and CMRO ₂	53
Figure 2 – 4: Changes in BOLD, CBF and CMRO ₂ are correlated over the observed ranges of signal change.	54
Figure 2 – 5: Monte Carlo simulation of error propagation through the biophysical model	56
Figure 3 – 1: Group average changes in BOLD, CBF, estimated CMRO ₂	71
Figure 3 – 2: Time dependent changes in BOLD, CBF, and CMRO ₂ for a single subject	73
Figure 3 – 3: Relationship among CBF, BOLD, and CMRO ₂ changes following intravenous administration of 1.0 mg/kg cocaine obtained from different brain regions. 75	
Figure 3 – 4: Estimates of changes in CBV from this study are correlated with reported changes in CBV following a similar dose of cocaine that were measured using MION contrast agent	76
Figure 4 – 1: Three coil imaging and integrated restraint system.....	92
Figure 4 – 2: Simulated B1 field strength near the arterial labeling coil and active decoupling electronics.	93
Figure 4 – 3: Arterial spin labeling contrast in pseudo-CASL with SE BOLD weighted acquisition.....	95

Figure 4 – 4: Effect size artifacts are visible in activation maps using statistical thresholds.	97
Figure 4 – 5: BOLD and CBF changes within the hindpaw primary somatosensory cortex following electrical stimulation.	99
Figure 5 – 1: Regions of interest investigated.	117
Figure 5 – 2: Changes in BOLD signal intensity in the thalamus correlate with physiological changes observed following morphine administration in anesthetized rats.	119
Figure 5 – 3: Group average SE BOLD signal changes within S1 in conscious and anesthetized rats following morphine or vehicle injection.	123
Figure 5 – 4: Late onset changes in the BOLD signal among all regions investigated in conscious and anesthetized rats.	124
Figure 5 – 4: Late onset changes in the BOLD signal among all regions investigated in conscious and anesthetized rats.	125
Figure 5 – 5: The frequency of struggle events decreases following morphine administration in conscious rats.	126
Figure 6 – 1: Criteria for selection of functional imaging protocol, location of the intracerebral ventricular cannula, and regions of interest defined.	144
Figure 6 – 2: BOLD signal changes induced by apomorphine exhibit complex temporal dynamics and intersubject variability.	145
Figure 6 – 3: Correlation analysis of BOLD signal changes under electrical forepaw stimulation in anesthetized rats.	147
Figure 6 – 4: Correlation analysis of BOLD signal changes following apomorphine challenge in conscious rats pre-treated with saline or DMSO.	149
Figure 6 – 5: Correlation analysis of BOLD signal changes following apomorphine challenge in conscious rats pretreated with haloperidol.	150
Figure 6 – 6: Correlation analysis of BOLD signal changes following apomorphine challenge in conscious rats pretreated with clozapine.	151
Figure 6 – 7: Correlation analysis of BOLD signal changes following apomorphine challenge in conscious rats pretreated with olanzapine.	152

Figure 6 – 8: Correlation analysis of BOLD signal changes following apomorphine challenge in conscious rats pretreated with SB277011.....	153
Figure 6 – 9: Common features between different pretreatment groups.	154
Figure A – 1: Standard errors of group mean correlation matrices in saline and DMSO pretreatment groups (N = 6).....	187
Figure A – 2: Standard errors of group mean correlation matrices in haloperidol and clozapine pretreatment groups (N = 6)	188
Figure A – 3: Standard errors of group mean correlation matrices in olanzapine and SB277011 pretreatment groups (N = 6).....	189
Figure A – 4: Correlations observed among sensory and motor pathways in electrical forepaw stimulation analysis.....	190
Figure A – 5: Correlation between regions of the mesolimbic dopamine network following ICV apomorphine administration.....	191
Figure A – 6: Correlation between regions associated with nociception and sensory information processing following ICV apomorphine administration.....	192
Figure A – 7: Correlation between regions associated with motor control and sensory information processing following ICV apomorphine administration.....	193
Figure B – 1: Considerations for phMRI study design based on experiences gleaned from the present studies.....	200

LIST OF ABBREVIATIONS

5-HT	Serotonin
5-HT _{2A}	The serotonin receptor subtype 2A
AFNI	Analysis of Functional Neuro Images
ASL	Arterial spin labeling
bpm	beats per minute or breaths per minute
BOLD	Blood oxygenation level dependent
CA	Contrast agent
CASL	Continuous arterial spin labeling
CBF/rCBF	Cerebral blood flow / regional cerebral blood flow
CBV/rCBV	Cerebral blood volume / regional cerebral blood volume
CG	Cingulate cortex
CMRO ₂	Cerebral metabolic rate of oxygen
CMRGlu	Cerebral metabolic rate of glucose
CNS	Central nervous system
CPu	Caudate putamen
Ctx	Cortex
D ₁₋₅	Dopamine receptor subtypes 1 – 5
EPI	Echo planar imaging
EPS	Extrapyramidal symptoms
fMRI	Functional magnetic resonance imaging
FSE	Fast spin echo
FOV	Field of view
GE	Gradient echo
Hip	Hippocampus
HP	Hind paw
HR	Heart rate

ICV	Intracerebral ventricular
IP	Intraperitoneal
IV	Intravenous
LGP	Lateral globus pallidus
M1	Primary motor area
MION	Monocrystalline Iron Oxide Nanocolloid
MOR/KOR/DOR	μ / κ / δ opioid receptor
MRI	Magnetic resonance imaging
NAc	Nucleus accumbens
NMR	Nuclear magnetic resonance
PAG	Periaqueductal gray
PET	Positron emission tomography
phMRI	Pharmacological magnetic resonance imaging, or pharmacological fMRI
R2	Transverse relaxivity (1/T2)
R2*	Transverse relaxivity (1/T2*)
RARE	Rapid acquisition with relaxation enhancement
ROI	Region of interest
RR	Respiration rate
S1	Primary somatosensory cortex
S2	Secondary somatosensory cortex
SC	Subcutaneous
SE	Spin echo
SN	Substantia nigra
SNpc	Substantia nigra pars compacta
SPECT	Single photon emission computed tomography
T1	Longitudinal relaxation rate, or spin-lattice relaxation rate
T2	Transverse relaxation rate, or spin-spin relaxation rate

T2*	Transverse relaxation rate plus relaxation due to macroscopic field inhomogeneities
TE	Echo time
thk	Slice thickness
TR	Repetition time
VPL	Ventral posterolateral nucleus of the thalamus
VTA	Ventral tegmental area

CHAPTER I

INTRODUCTION

Background and Rationale

Many drugs that affect the central nervous system confer their effects through mechanisms that are still a mystery. This is especially true among drugs that are implicated in the treatment or in the pathology of psychiatric diseases. Drugs of abuse and antipsychotic agents are two pertinent examples; in the case of both classes of drugs, the molecular properties of the chemicals themselves are well understood. For example, it is largely known with which receptors and neurotransmitter transporters these chemicals interact, where in the brain neurons harboring these receptors and transporters exist, and generally, it is known what the acute effects on activity within these neurons are, following administration of a particular compound from either of these drug classes (Nestler et al., 2001; Squire et al., 2003; Katzung, 2004).

What is not known, in these two examples, is what connects the psychiatrically relevant changes in behavior and cognition to the acute effects of the drugs themselves. For example, cocaine, amphetamine, and methylphenidate are psychostimulants with varying liability for abuse, and each of these drugs prevents reuptake of dopamine, norepinephrine, and serotonin (Rothman and Baumann, 2003). Based on the dogma that increased synaptic dopamine in the nucleus accumbens (NAc) causes the reinforcement that leads to drug abuse (Koob and Bloom, 1988; Nestler et al., 2001; Squire et al., 2003),

it is surprising that methylphenidate, which has a higher affinity for the dopamine transporter than either cocaine or amphetamine (Han and Gu, 2006) has a lower liability for abuse (Nestler et al., 2001). Differences in the route of administration of these drugs may partially explain this difference in abuse liability; it has been shown that the rate of receptor occupancy by cocaine is correlated with its reinforcing characteristics (Woolverton and Wang, 2004; Nelson et al., 2006), a phenomenon described as the *rate hypothesis*. The evidence supporting the rate hypothesis (Gorelick, 1998) is one example of the complex neural response to psychotropic drugs that obscures any simple connections between the observed behavioral and cognitive effects, and the fundamental molecular actions of the drug. In the second example, the linkage between the molecular actions of antipsychotic drugs and their therapeutic effects is also obscure, and unanswered questions regarding the mechanisms by which these drugs confer therapeutic benefit are discussed in detail later in this, and in following chapters.

Neuroimaging can be used to investigate the complex cascade of changes in neural activity that translate the acute molecular actions of a psychotropic drug on a subset of neurons in the brain to the relevant changes in behavior and cognition observed in the animal (human and lower species) as a whole. Neuroimaging studies have been beneficial for the study of drugs' effects on nociception (Becerra et al., 2001; Malisza and Docherty, 2001), for the development of integrative theories that describe pathological states such as addiction (Volkow et al., 2004), and are recognized for their growing utility in the design of novel drugs that act on the CNS (Wise and Tracey, 2006). Functional MRI (fMRI) offers a unique capability among other neuroimaging modalities such as

positron emission tomography (PET) and single photon emission computed tomography (SPECT) by providing high temporal resolution to resolve dynamic changes in neural activity following the administration of a psychoactive drug. Additionally, the non-invasive nature of fMRI, and the widespread use of MRI in clinical settings suggest that fMRI of psychoactive drugs, termed pharmacological functional MRI or pharmacological MRI (phMRI), is well positioned to translate observations made in lower species to observations made in the clinic.

While phMRI neuroimaging studies offer a valuable view of the changes in neural activity that occur throughout the whole brain following the administration of psychoactive drugs, several unanswered questions complicate the application of phMRI techniques and limit the inferences that can be made from the results obtained from phMRI experiments. Three of these open questions are addressed in the research that follows:

- 1) Are the MRI measurements reliable surrogates of changing neural activity in the presence of pharmacological agents?

- 2) Is it relevant to investigate psychiatric phenomena such as reward or anxiolysis in anesthetized, rather than conscious animals? And

- 3) what are the methods that yield reproducible and meaningful results from phMRI experiments, and are they consistent in the investigations of different drugs?

With an improved understanding of the capabilities and limitations of phMRI techniques, we apply phMRI to the investigation of antipsychotic drugs in an effort to

resolve the effect that acute treatment with these drugs has on the brain's response to altered dopaminergic signaling, the neural pathway that is universally implicated in pharmacological treatments of psychosis.

In the research that follows, we test the hypothesis that hemodynamic and metabolic markers, such as cerebral blood flow (CBF) and cerebral metabolic rate of oxygen consumption ($CMRO_2$), can be reliably measured by phMRI to infer changes in neural activity following sensory and pharmacological stimuli. We develop new technology for performing simultaneous measurements of spin-echo blood-oxygenation-level-dependent (SE BOLD) contrast and CBF in the conscious animal. We test the hypothesis that conscious animals will exhibit a differential fMRI response to a non-stimulant psychoactive drug in comparison to anesthetized animals, and that the response observed in the conscious animal is better explained by the pharmacodynamics of the drug itself. And, in the final study, we test the hypothesis that dopaminergic signaling, observed in the conscious rat, can be modulated by pretreatment with antipsychotic drugs, observing that many regions of the brain beyond the immediate dopaminergic pathways are affected by these treatments.

The remaining sections of this chapter provide the necessary background for the studies that follow, and, hopefully, provide the context and resources to adequately understand the current state of the art. It is hoped that the results and advances described in the following chapters will provide valuable direction for future phMRI studies, and that the modulation of dopaminergic signaling by acute pretreatment with antipsychotic

medications will provide a template for the comparison of novel antipsychotic drugs under investigation.

The basics of MRI

A fascinating aspect of nuclear magnetic resonance (NMR) imaging is the beguiling simplicity of the grayscale images that are now commonplace in clinical and research settings. In fact, the acquisition of even the most basic MR image is the result of several interdependent experiments performed on the subject or sample that reproduce physical phenomena which took more than 29 years to understand (Bloch et al., 1946; Purcell et al., 1946; Damadian, 1971; Lauterbur, 1973; Kumar et al., 1975) in research that warranted the award of three Nobel Prizes (Physics in 1952, Chemistry in 1991, and Physiology or Medicine in 2003). Although the accelerating pace of research in MRI has extended the capabilities of this non-invasive imaging modality beyond the imaginations of its original discoverers, we are continually reminded of their contributions. Every MRI scan reflects the fundamental process of MR image formation through the presence of image artifacts and in the effort required to elicit and detect the inherently weak NMR signal. Consequently, a basic understanding of the process of MR image formation is essential in order to interpret the results of contemporary MRI experiments, all of which build on these fundamental techniques.

Image formation can be considered to consist of two components. The first component concerns the origin and generation of the NMR signal that is detected, while the second component concerns the manipulation of the experimental setting to localize

and spatially encode the signal, enabling two or three dimensional image reconstruction. The NMR signal can be observed in atoms whose nuclei contain a non-integer nuclear magnetic moment, called *spin* (Rohlf, 1994; Buxton, 2002; Hornak, 2002). This nuclear spin, likened to electrical charge distributed on the surface of spinning subatomic particles, exists as quanta of $\frac{1}{2}$ of the nuclear magneton in each of the protons and neutrons that comprise the nucleus of stable atoms. Subatomic particles within the same nuclear orbit pair with one another in a manner that cancels the collective magnetic moment, but, in nuclear orbits that contain an odd number of protons and neutrons, there exists a residual magnetic moment that will interact with external magnetic fields.

Most MRI is based on the interaction between the magnetic field of the MRI scanner and hydrogen atoms (spin $\frac{1}{2}$ nuclei) bound in water molecules. In addition to ^1H , some isotopes with non-zero nuclear magnetic dipole moments that are used conjointly in MRI studies include: ^{23}Na (Lee et al., 1986), ^{13}C & ^{31}P (H. Bomsdorf, 1988), ^{19}F (Nelson et al., 1985), ^{17}O (Pekar et al., 1991; Fiat and Kang, 1992; Fiat et al., 1993; Fiat and Kang, 1993), ^{129}Xe (Albert et al., 1996), and ^3He (Middleton et al., 1995). The dependence of NMR signal intensity on, among other factors, the abundance of the nucleus being investigated, and the high biological abundance (63%) of ^1H in the body (Hornak, 2002), explain the extensive use of ^1H MRI.

In the presence of an external magnetic field, the nuclear magnetic moment of a non-zero spin nucleus can assume an orientation nearly aligned with or nearly counter-aligned with the external field, the counter aligned orientation having slightly higher energy (Figure 1-1, panel a; Figures and Tables are found at the end of each chapter).

Given a population of such spins that we will call a *spin-packet*, in the presence of a strong external magnetic field a slightly larger number of nuclear spins will align themselves in the lower energy configuration. The small difference between spins in the high and low energy states (0.0005% in a 1.5T external field at room temperature) causes the spin-packet to exhibit a non-zero magnetic moment, and enables the spin-packet to absorb and emit photons with an energy that corresponds to the transition between the high and low energy states of the individual spins contained within. The frequency of this radiation is known as the Larmor frequency (Rohlf, 1994).

We can think of the net magnetic moment of the spin-packet (Figure 1-1, panel b) as being analogous to a spinning top with a bar magnet inserted through the middle along the axis of rotation. Under fully relaxed conditions, the magnetic moment is aligned with the external magnetic field. Like a spinning top in the presence of gravitational forces, if we displace the spin-packet's magnetic moment from alignment with the external magnetic field by bombardment with radiation at the Larmor frequency (Figure 1-1, panel c), intrinsic angular momentum causes the spin-packet's magnetic moment to precess (i.e. gyrate) about the axis of the external magnetic field, emitting radiation at the Larmor frequency until it reaches the fully relaxed condition or until the spins contained within dephase. When multiple spin-packets precess in synchrony, the emitted radiation can be detected as a rapidly fading signal called the *free induction decay* (FID) (Figure 1-1, panel d) (Bloch et al., 1946).

Two important factors govern the detection of the NMR signal and the characteristics of the FID, following displacement of the spin-packet's magnetic moment

by excitation with radiation at the Larmor frequency. The first factor governs the strength of the emitted NMR signal, and is important during the repeated excitations used to collect the FIDs that are necessary to reconstruct an image. This factor is the rate at which the spin-packet's magnetic moment returns to alignment with the external magnetic field, a rate that is referred to as *longitudinal*, or *spin-lattice* relaxation and that is characterized by a time constant (T1). The second factor concerns the rate at which the emitted signal is eroded by growing phase differences between the precessions of neighboring spins. Small differences in the rates of precession between neighboring spin-packets due to microscopic and macroscopic inhomogeneities in the external magnetic field are unavoidable, and the effects of cancellation rapidly erode the detected signal in a process described by *transverse*, or *spin-spin* relaxation, which is also characterized by time constants measuring the rate of signal loss due to microscopic effects (T2) or microscopic plus macroscopic effects (T2*). T1, T2, and T2* are important factors that differ between tissues or samples of interest (Fullerton and Cameron, 1988) in MRI experiments, and images are deliberately *weighted* to reflect T1 and T2 or T2* contrast within specified ranges of these parameters.

The second component of image formation addresses the spatial encoding of the FID, and describes the acquisition of many FIDs to collect the information necessary to reconstruct a 2-dimensional image. The concept originally put forth by Kumar, Ernst and others (Kumar et al., 1975; Edelstein et al., 1980) to use phase and Larmor frequency modulation by introducing spatially linear gradients in the X, Y, and Z directions within the confines of the static external magnetic field remains the basis of the MRI techniques

in use today. By introducing a spatially linear gradient in the magnetic field in one direction, and simultaneously irradiating the sample with RF energy spanning a range of frequencies, it is possible to excite only a thin slice of the sample being investigated. A second linear gradient that is applied shortly after this excitation for a fixed duration of time along an orthogonal direction will encode a specific phase offset that depends both on the strength of the gradient and the spin-packet's location in space along the axis of this *phase-encoding* gradient. Finally, a third linear gradient applied in the remaining orthogonal direction during signal detection will cause the Larmor frequency of the spin-packets to change according to their location in space along the axis of this final, *read-out* gradient. In single slice imaging, this process is repeated with incremented strengths of the phase encoding gradient and a composite of FIDs is collected and used to populate a 2D matrix (k-space) that can be Fourier transformed in both the X and Y directions to reconstruct a 2D image corresponding to the originally excited slice of sample (Figure 1-1, panel c). In multislice imaging, the process is repeated for each 2D slice that is acquired, and the strategy of interleaving these acquisitions allows multiple slices to be acquired in the same time that it takes to acquire one.

The complexity of this process is most readily apparent when problems occur during the acquisition of the multiple FIDs. Figure 1-1, panel e illustrates the effect of motion on the reconstructed image, where sample displacement during the acquisition of phase encoded FIDs leads to a banding effect that is present in the axis of the phase encoding gradient across the entire reconstructed image. This simplified explanation of the methods and theory of MRI is intended to highlight and provide context for the

important aspects of the imaging experiments that are described in the studies presented herein, but the reader is directed to the following literature for far more detailed treatments of NMR Spectroscopy (Fullerton and Cameron, 1988; Hallenga, 1991) and basic MRI techniques (Curry et al., 1990; Brown and Semelka, 1999; Hornak, 2002; Paschal and Morris, 2004).

Changing hemodynamics associated with changing neuronal metabolism

Despite its size, accounting for only about 2% of total human bodyweight, the brain consumes a stunning 20-25% (Squire et al., 2003; Shulman et al., 2004) of the total glucose produced and utilized by the body. Several independent studies of neuroenergetics suggest that the highest energetic costs in the brain are related to glutamate neurotransmission, and that in the awake resting state most of the energy consumed by the brain is used to maintain stasis amid a constant background of neural activity (Sibson et al., 1998; Attwell and Laughlin, 2001; Shulman et al., 2004). Models suggest that the majority of the energy consumed by neurons is used to maintain ion gradients across the neuronal membrane in pre and post synaptic neurons, and that only 5-10% of the glucose consumed is relegated to neurotransmitter cycling, and a small amount is consumed for other processes within the neuron such as vesicularization (Mata et al., 1980; Pellerin and Magistretti, 1994; Sibson et al., 1998; Magistretti et al., 1999). Studies comparing glial, GABAergic, and glutamatergic glucose consumption suggest that only 10-15% of the glucose consumed by cortical tissue is used to support glial processes, while the remaining energy consumption supports glutamatergic and

GABAergic neurons (Rothman et al., 1999; Shulman et al., 2004), further supporting the dogma that neuronal activity and glucose metabolism are tightly coupled.

It is not surprising that an organ with an associated energy cost as large as that of the brain is highly specialized so that it may operate efficiently, nor is it surprising that, internally, localized changes in the demand for energy are satisfied with a dynamic and localized response, rather than a change in supply to the entire organ. Indeed, it was observed more than 115 years ago that sensory stimulation increases blood flow selectively to the parietal cortex in animals (Roy and Sherrington, 1890), prompting the ongoing investigation of the mechanisms by which neuronal activity alters the cerebral vasculature to change the supply of oxygen and nutrients on a local scale.

Neurogenic mechanisms hold promise as mediators of vascular dynamics; observations that microvessels within the brain are richly innervated and the finding that functional receptors for some neurotransmitters exist on the vessels themselves (Riad et al., 1998; Cohen et al., 1999) has been exploited for the clinical treatment of migraine headaches with sumatriptan succinate, a 5-HT_{1D} receptor agonist (GlaxoSmithKline, 2003), and supports the notion of a neural mechanism for regulating local blood flow. Other neurotransmitters and neuropeptides are also potential candidates, including noradrenaline, serotonin, acetylcholine, neuropeptide Y, and substance P (Squire et al., 2003). Other chemicals are known to affect the cerebral vasculature, and are produced locally by neurons as byproducts of metabolism. Importantly, CO₂ and NO are known to elicit a potent vasodilatory response, and are likely to play significant, if partial, roles in

the localized increase in cerebral blood flow (CBF) that quickly follows an increase in neural activity.

Coupling between localized changes in neural activity and local vascular parameters such as cerebral blood flow (CBF) and cerebral blood volume (CBV), as well as local metabolic parameters such as cerebral metabolic rate of glucose (CMR_{glu}) and cerebral metabolic rate of oxygen (CMRO₂), remains an active area of research. Although the proposed relationships between these parameters that account for steady state and dynamic observations of changing hemodynamics and metabolism associated with changes in neural activity are still the subject of debate (Roland et al., 1987; Fox et al., 1988; Hyder et al., 1996; Buxton et al., 2004; Liu et al., 2004), there is good agreement that changes in neural activity, especially increases in rates of neuronal membrane depolarization, evoke a reliable response from the cerebral vasculature that can be exploited to localize changes in neural activity within the brain.

The BOLD signal and functional MRI

While fully oxygenated hemoglobin is diamagnetic, deoxygenated hemoglobin is paramagnetic and its presence creates microscopic distortions in the magnetic field surrounding erythrocytes as well as macroscopic distortions in the field surrounding vessels containing blood with a low level of oxygen saturation (Thulborn et al., 1982; Buxton, 2002). The interaction of water molecules with these field distortions causes an increase in the transverse relaxation rate of blood (decrease in T₂) that is dependent on the concentration of deoxyhemoglobin (Thulborn et al., 1982), and also causes an

increase in the transverse relaxation rate of the tissue surrounding vessels containing deoxygenated blood, due to macroscopic field inhomogeneities caused by the presence of paramagnetic deoxyhemoglobin in the vessels themselves (decreasing the $T2^*$ of this tissue) (Ogawa et al., 1990; Ogawa et al., 1992; Buxton, 2002). Due to the sensitivity of gradient echo (GE) sequences to $T2^*$ contrast (often considered to be a problem due to signal drop out in many regions of the brain) Seiji Ogawa and others reported in 1990 that a GE imaging sequence revealed contrast surrounding cerebral vessels that was sensitive to the level of de-oxygenation of the blood they contained (Ogawa et al., 1990). Vessels containing high concentrations of deoxyhemoglobin, and the tissue immediately surrounding them appeared darker than tissue distal from these vessels, owing to the rapid relaxation (decreased $T2^*$) in these areas (Ogawa et al., 1990).

Within two years of the initial report by Ogawa et al., sequences sensitive to small changes in magnetic susceptibility (generating $T2^*$ weighted images) and sequences sensitive to changes in blood flow (generating perfusion weighted images) were used in functional brain mapping applications with promising results; Kwong et al. observed a stimulus coupled change in $T2^*$ and perfusion weighted image contrast that could be elicited by a pharmacological stimulus (CO_2), visual stimulus (light presentation), and sensory-motor task (hand squeezing) (Kwong et al., 1992). Within weeks, Ogawa et al. reported similar results of $T2^*$ changes in the visual cortex in response to a visual stimulus, and coined this signal as blood-oxygenation-level-dependent (BOLD) contrast, laying the foundation for the future applications of MRI to functional brain mapping (Ogawa et al., 1992).

Due to the complex relationship between changes in cerebral hemodynamics in response to changes in neural activity, the effect on BOLD contrast due to neural stimulation is somewhat surprising. Earlier work using positron emission tomography (PET) had revealed that as the increase in neural activity induces cerebral vasodilation, the quantity of arterial blood recruited to the area consistently overcompensates for the increase in oxidative metabolism (Fox et al., 1988). This overcompensation may have evolved as a protective mechanism, guarding the neuropil against oxidative stress and ischemic damage (Squire et al., 2003), but it forms the basis of most fMRI imaging performed currently. The process of vascular changes in response to increased neural activity is illustrated in Figure 1 – 2.

Noninvasive Measurement of Cerebral Blood Flow using MRI

In addition to changes in the BOLD signal, other hemodynamic surrogates of neural activity can be measured non-invasively using MRI. Cerebral blood flow (CBF) describes the volume of blood that perfuses a given volume of cerebral tissue in a given period of time, and determines the supply of oxygen available to the tissue. In the clinic, perfusion MRI methods are increasingly used to assess CBF for the purposes of localizing areas affected by arterial occlusions, assessing the volume of the tissue that has been subjected to ischemic stress following infarction, and predicting the recovery of infarcted and penumbral tissue following reperfusion after a stroke (Warach et al., 1996; Duyn et al., 2005), assessing traumatic brain injury (Cunningham et al., 2005), and more

recently, for grading CNS neoplasms based on physiological parameters (Wolf et al., 2005).

Noninvasive measurement of CBF by MRI proceeds by manipulating the magnetic spins of water molecules in arterial blood within a specific location. These manipulated (*labeled* or *tagged*) spins are then used as an endogenous tracer and their influx or efflux within a given tissue volume are measured over time to determine the local perfusion. Figure 1-3, panel a illustrates the continuous arterial spin labeling (CASL) technique, in which spins are continuously inverted at the location of the carotid arteries for a period of several seconds. As these labeled spins travel to and diffuse into the tissue within the brain, a steady state of altered magnetization is developed that can be detected by MRI.

The process of quantifying blood flow from the steady state contrast between labeled and unlabeled images using CASL is an important aspect of the research to follow. A simple model which assumes that water is a freely diffusible tracer can be used to quantify the relationship between changes in magnetization and blood flow according to a modified Bloch equation (Detre et al., 1995; Barbier et al., 2001). This is shown in Equation 1.01, where M_b = z -magnetization (i.e. magnetization in direction of B_0) per unit volume of brain tissue, M_{b0} = the value of M_b under fully relaxed conditions, M_a = the z -magnetization per unit volume of arterial blood, M_v = the z -magnetization per unit volume of venous blood, T_1 = the spin-lattice relaxation time of brain water, and f = blood flow to the tissue in ml per g·s. An assumption is made that the water in the tissue volume of interest exists in a well mixed compartment and consequently, the efflux of water magnetization from this compartment (M_v) can be described in terms of the total

blood magnetization influx and by the respective ratio of water concentrations between the brain and the vascular compartments, denoted by the brain/blood partition coefficient (λ) (Equation 1.02).

The labeling process is imperfect, and we must make a correction with an assumption of constant labeling efficiency, ranging between 0 – 100% (α); in the case of arterial spin inversion, this correction factor for the magnetization of arterial blood is incorporated by Equation 1.03. If we assume that transit times from the point of inversion to the location of exchange with brain water molecules is short with respect to the T_1 relaxation time of the water molecules themselves (i.e. $M_{a0} = M_a$), we can substitute the value of M_a in equation 1.03 into equation 1.01, obtaining equation 1.04. During the initial conditions, we observe that inflowing magnetization is equal to magnetization outflow (i.e. $M_a = M_v$ in equation 1.02), and introducing the factor $(1-2\alpha)f$ to the equality yields an expression (Equation 1.04) that can be substituted into Equation 1.01 to yield a linear ordinary differential equation (Equation 1.05), with a discrete solution (Equation 1.06). Under steady state conditions, we can assume that $t=\infty$ and Equation 1.06 can be reduced to the solution for CBF (f) indicated by Equation 1.07.

$$\frac{dM_b}{dt} = \frac{M_b^0 - M_b}{T_1} + fM_a - fM_v \quad (1.01)$$

$$M_v = \frac{M_b}{\lambda} \quad (1.02)$$

$$M_a = (1 - 2\alpha) M_a^0 \quad (1.03)$$

$$(1 - 2\alpha) f M_a^0 = \frac{(1 - 2\alpha) f M_b^0}{\lambda} = f M_a \quad (1.04)$$

$$\begin{aligned} \frac{dM_b}{dt} &= \frac{M_b^0 - M_b}{T_1} + \frac{(1 - 2\alpha) f M_b^0}{\lambda} - \frac{f M_b}{\lambda} \\ &= -M_b \left(\frac{1}{T} + \frac{f}{\lambda} \right) + M_b^0 \left(\frac{1}{T} + \frac{f(1 - 2\alpha)}{\lambda} \right) \end{aligned} \quad (1.05)$$

$$e^{-t \left(\frac{1}{T_1} + \frac{f}{\lambda} \right)} = M_b^0 \left(\frac{1}{T_1} + \frac{f(1 - 2\alpha)}{\lambda} \right) - M_b \left(\frac{1}{T_1} + \frac{f}{\lambda} \right) \quad (1.06)$$

$$f = \frac{\lambda}{T_1} \cdot \frac{M_b^0 - M_b}{M_b + (2\alpha - 1) M_b^0} \quad (1.07)$$

This steady state model is widely used, and typical results of the CASL experiment are shown in Figure 1-2, panels b-e. The steady state assumptions are acceptable under most conditions, but a dynamic treatment of perfusion-induced MR contrast is supplied in Chapter IV, where slice dependent acquisition delays must be taken into account in the interpretation of results.

Antipsychotic medications

The history of antipsychotic drug development

Psychosis is a defining feature of schizophrenia (American Psychiatric Association, 1994; Breier and Berg, 1999) that can often be observed in other psychiatric diseases including bi-polar disorder (manic depression), unipolar depression, epilepsy, Alzheimer's disease and other neurodegenerative forms of dementia, brain trauma, and in some cases of acute substance abuse (e.g. cocaine and phencyclidine) (American Psychiatric Association, 1994; National Library of Medicine (US), 2005). The primary components of psychosis include formal thought disorder, delusions, and hallucinations (American Psychiatric Association, 1994) and reflect a general failure of patients to understand, or to correctly interpret the stimuli from the external world (Nestler et al., 2001). In the case of schizophrenia, these components are considered to be *positive* symptoms that are reported by patients and have been the primary focus of pharmacological treatments since the accidental discovery that the phenothiazine tranquilizer chlorpromazine ablated these symptoms. Chlorpromazine was given to patients as a preoperative anxiolytic (Laborit and Huguenard, 1951; Rothman et al., 1999), and was later found to suppress symptoms of delusion and mania in psychiatric patients when administered repeatedly in a clinical setting (Delay et al., 1952a; Delay et al., 1952b; Hamon J et al., 1952).

Following the discovery of chlorpromazine as a putative antipsychotic medication, the identification of other compounds with antipsychotic efficacy progressed in parallel

with observations that drugs having clinical efficacy for treating psychotic symptoms also exhibited serious dose-dependent motor side effects, termed extrapyramidal symptoms (EPS), including Parkinsonism, dystonia, and akathisia (Rothman et al., 1999; Kapur and Mamo, 2003). More than two decades elapsed before the relationship between dopamine receptor blockade and antipsychotic efficacy was firmly established (Seeman and Lee, 1975; Creese et al., 1976; Seeman et al., 1976). Selective blockade of the dopamine D₂ receptor is the defining characteristic of the first generation of antipsychotic medications, generally known as *typical* antipsychotic drugs (Nestler, 2002), and all effective antipsychotic drugs currently in clinical use exhibit some degree of D₂ receptor antagonism. The prevalence of EPS and other problems associated with treatment with first generation antipsychotic drugs (neuroleptics), as well as the lack of an effect on the *negative* symptoms of schizophrenia that include apathy, flattened affect, and social withdrawal (American Psychiatric Association, 1994; National Library of Medicine (US), 2005) prompted the search for alternative compounds with improved clinical benefits, and with a reduced liability for serious side effects (Rothman et al., 1999; Kapur and Mamo, 2003). Among the drugs discovered was clozapine in 1958 by Schmutz and colleagues at Wander Pharmaceutical (Schmutz and Eichenberger, 1982). Clozapine exhibits a dramatically reduced liability for EPS (Kapur and Mamo, 2003) and has a radically different spectrum of receptor blockade than traditional (typical) antipsychotic drugs (Nestler et al., 2001; Katzung, 2004). Clozapine's affinity for receptors other than D₂ prompted its classification as an *atypical* antipsychotic drug, a class of drugs that now includes several other effective antipsychotic medications that were discovered

subsequently. A study of treatment-resistant schizophrenic patients in 1988 rejuvenated interest in atypical antipsychotic drugs, when these patients were found to respond to clozapine, but not to multiple traditional antipsychotics, such as haloperidol (Kane et al., 1988). The successful treatment of these patients ultimately led to clozapine's approval for the treatment of refractory (treatment-resistant) schizophrenia in 1990.

Although the incidence of EPS is not a primary concern with clozapine treatment (Katzung, 2004), other serious and potentially fatal side effects (e.g. agranulocytosis in ~1.3% of patients) (Novartis Pharmaceutical Corporation, 2005) are factors that limit its use in the clinic. In recent years several additional atypical antipsychotic medications have been discovered which demonstrate superiority over haloperidol for the treatment of psychotic symptoms with a reduced liability for EPS and other side effects, including olanzapine (Zyprexa), risperidone (Risperdal), quetiapine (Seroquel) (Sharma, 2001), Amisulpride (Solian) (Curran and Perry, 2001), and possibly aripiprazole (Abilify) pending the outcome of ongoing investigations (Katzung, 2004). The high cost of atypical antipsychotics, combined with the presence of drug-specific side effects other than EPS, as well as impractical administration protocols for some drugs have prevented this new class of medication from completely supplanting the typical antipsychotic drugs as the first line of treatment for psychosis (Katzung, 2004). Research to identify a safe, effective, and practical alternative to the currently marketed atypical antipsychotics is ongoing.

Receptor affinity and the enduring mystery of therapeutic action

The atypical antipsychotic drugs that are currently available for treatment are antagonists at a broad spectrum of receptors with varying affinity, and appear to be similar only in the respect that they share a relatively lower affinity for the D₂ receptor than typical antipsychotic medications (Nestler et al., 2001). Table 1 – 1 illustrates the principal receptor affinities for some marketed antipsychotic medications in comparison to haloperidol (Bymaster et al., 1997; Casey, 1997; Nestler et al., 2001; Trevor et al., 2002; Katzung, 2004) and reflects a prevalence of antagonism at serotonergic, adrenergic, muscarinic, and histaminergic receptor subtypes. The significance of these receptors in the pathophysiology of psychosis (and schizophrenia in particular) is unknown, as is the role that antagonism (or partial agonism) of these receptors plays in the therapeutic efficacy observed after sustained treatment with atypical antipsychotic drugs. Of practical value is the fact the therapeutic window between the onset of clinical benefit and the onset of EPS is dramatically widened for atypical antipsychotics with respect to typical antipsychotics (Casey, 1997), supporting the theory that neuroplastic changes mediated by action at receptors other than the D₂ receptor can affect positive clinical changes in psychotic patients.

There is considerable debate as to which receptors, other than D₂, are important mediators of the clinical benefits of treatment with atypical antipsychotics. Antagonism of the 5-HT_{2a} receptor as well as agonism of the 5-HT₁ receptor has been postulated as an important feature for atypical efficacy (Meltzer, 1999), but the selective 5-HT_{2a} receptor antagonists M100907 and SR46349B failed to show antipsychotic efficacy that exceeded that of haloperidol (Shipley, 1998; Meltzer et al., 2004). Selective antagonism of the D₄

receptor (Seeman et al., 1997) has also been investigated for therapeutic benefit, but the drug candidate sonopipirozole failed to demonstrate an improvement in symptoms in comparison to placebo (Corrigan et al., 2004). D₃ receptor antagonism (Schwartz et al., 2000) remains a viable target and the efficacy of D₃ antagonists in the treatment of schizophrenia is currently being assessed; early results of a selective D₃ antagonist did not suggest an improvement in psychotic symptoms (Lahti et al., 1998), but more recent work suggests an adjuvant role for D₃ antagonism in the treatment of negative symptoms with supporting genetic evidence that implicates the D₃ receptor as the mediator of this effect (Lane et al., 2005). Antagonism of muscarinic or histaminergic receptors alone does not appear to improve the symptoms of psychosis (Nestler, 2002). Additionally, recent work focused on agonism of the NMDA receptor has shown considerable promise in the treatment of the negative symptoms of schizophrenia (Lindsley et al., 2006), but the limited action of existing atypical antipsychotics at the NMDA receptor suggests that this receptor does not mediate their therapeutic effects.

Alternative theories postulate that the therapeutic effects of atypical antipsychotics are still mediated by D₂ receptor antagonism. Neuroimaging studies using positron emission tomography (PET) revealed >70% D₂ receptor occupancy in patients treated with atypical antipsychotics other than clozapine (Farde et al., 1988), consistent with a putative therapeutic range of 60%-70% receptor occupancy for antipsychotic effects, below the 80% occupancy rate that is associated with the onset of EPS (Farde et al., 1992). It has also been proposed that a distinguishing feature of atypical antipsychotic drugs is that these drugs preferentially occupy D₂ receptors that are located extrastrially

(Xiberras et al., 2001), in the thalamus and frontal and temporal cortices, possibly explaining the onset of therapeutic effects at doses that are lower than those required to induce EPS, and explaining the wider therapeutic window of atypical versus typical antipsychotics that are thought to occupy the D₂ receptor equally within and outside of striatal regions (Kapur and Mamo, 2003). However, recent data indicates that some atypical antipsychotic drugs also occupy extrastriatal D₂ receptors at consistently lower rates (35% less) than typical antipsychotic drugs at therapeutically relevant doses (Kessler et al., 2006), supporting a role for receptors other than D₂ in the therapeutic effects of treatment with these medications.

Activation of neural networks and their visualization by fMRI

Functional MRI has been used extensively to visualize concomitant activation of regions participating in signaling networks within the brain related to sensory and cognitive processing. In the studies described in the following chapters, changes in fMRI measures are reported after sensory and nociceptive stimulation, among conscious rats resisting the MRI restraint apparatus, amid the constant background of auditory stimulation from the scanner, and following a dopaminergic challenge intended to stimulate dopaminergic transmission throughout the brain. A brief introduction to the neural networks implicated under these conditions follows, and some examples of fMRI research related to the detection of changes in neural activity within these networks are provided.

The spinothalamic tracts within the anterolateral system mediate sensations of pain and simple touch, and ascend from the dorsal roots of the spinal cord to the brain stem where they supply inputs to the reticular formation, superior colliculus, and several thalamic nuclei. Thalamic nuclei, in turn, stimulate and respond to regions of the sensory cortex through thalamocortical and corticothalamic fibers, in a largely parallel processing of sensory information (Gilman and Newman, 2003). A recent fMRI study performed at high resolution and high field (11.7T) demonstrated detection of this network following electrical forelimb sensory stimulation in anesthetized rats, noting significant activation of the primary and secondary somatosensory cortices, the thalamus, and the cerebellum, wherein it was proposed that projections from the medulla and pons to the cerebellum are responsible for observations of changing neural activity there (Keilholz et al., 2004).

The basal ganglia is a collection of interconnected nuclei of critical importance in motor function, and is best described by the dual action of the competitive and simple circuits, the *direct* and *indirect* loops. In the direct loop, dopaminergic transmission from the substantia nigra pars compacta (SNpc) stimulates the striatum via D₁ receptors, which inhibits the medial or internal portion of globus pallidus, disinhibiting the thalamus, and stimulating sections of the cerebral cortex, which, in turn, stimulate the striatum in a process of positive feedback. In the indirect loop, dopaminergic transmission from the SNpc inhibits the striatum via D₂ receptors, inhibiting the lateral or external portion of the globus pallidus (LGP), disinhibiting the subthalamic nucleus, which stimulates the internal globus pallidus, inhibiting the thalamus, ultimately inhibiting the cortex and striatum in a process of negative feedback (Gilman and

Newman, 2003). The competitive balance of these circuits is necessary for effective motor control, and activation of basal ganglia circuitry has been resolved by fMRI in humans executing voluntary and involuntary motor tasks (Taniwaki et al., 2006), and observed to be disrupted among patients suffering from Parkinson's disease (Holden et al., 2006).

Recent work, much of which was completed by a member of this examination committee and his colleagues, has elucidated networks activated in nociception in humans by fMRI that include elements of the reward and aversion pathways in addition to classic spinothalamic pain circuitry (Becerra et al., 2001; Becerra et al., 2004). Animal fMRI studies of neural substrates activated by painful stimuli have revealed a simpler pattern, consisting mainly of the primary and secondary somatosensory regions, the cingulate, thalamus, and hypothalamus with some differences in other regions reported between studies (Chang and Shyu, 2001; Malisza and Docherty, 2001; Hess et al., 2006). These animal studies were conducted in anesthetized rats, however, and a direct comparison to studies in conscious humans, where pain has emotional valence, is difficult.

Visual stimulus paradigms were some of the first used in the early development of fMRI and readily reveal neural activation in the visual cortex of both animals (Koyama et al., 2004; Van Camp et al., 2006) and humans (Belliveau et al., 1992; Blamire et al., 1992; Kwong et al., 1992; Ogawa et al., 1992). The activation of the visual cortex among conscious rats has not been examined by fMRI, but changing visual perception due to eye movement and auditory perception of the noise of the scanner during experiments with

conscious rats may contribute to observations of changing fMRI signals in visual and auditory cortical regions.

The principal dopaminergic neurons in the brain can be considered to belong to one of three groups of pathways. The nigrostriatal pathway extends from the substantia nigra to the caudate putamen, and is the pathway primarily associated with motor control and Parkinson's disease (Nestler et al., 2001; Marsden, 2006). The mesolimbic pathway extends from the ventral tegmental area (VTA) to the limbic areas including the nucleus accumbens and amygdala, and the mesocortical pathway extends from the VTA to several cortical regions including the medial, prefrontal, cingulate, and entorhinal cortices. These pathways are implicated in the processing of rewarding stimuli, as well as in more general cognitive and emotional functions (Nestler et al., 2001; Marsden, 2006). An additional dopamine pathway, the tuberoinfundibular dopamine system, connects the arcuate and periventricular nuclei of the hypothalamus to the pituitary where it inhibits the production of prolactin (Nestler et al., 2001; Marsden, 2006). The extensive innervation of much of the brain by the mesocortical and mesolimbic dopamine neurons makes elucidation of these pathways by fMRI difficult, while reports of nigrostriatal circuitry involvement in the basal ganglia have been discussed previously.

Figure 1-1

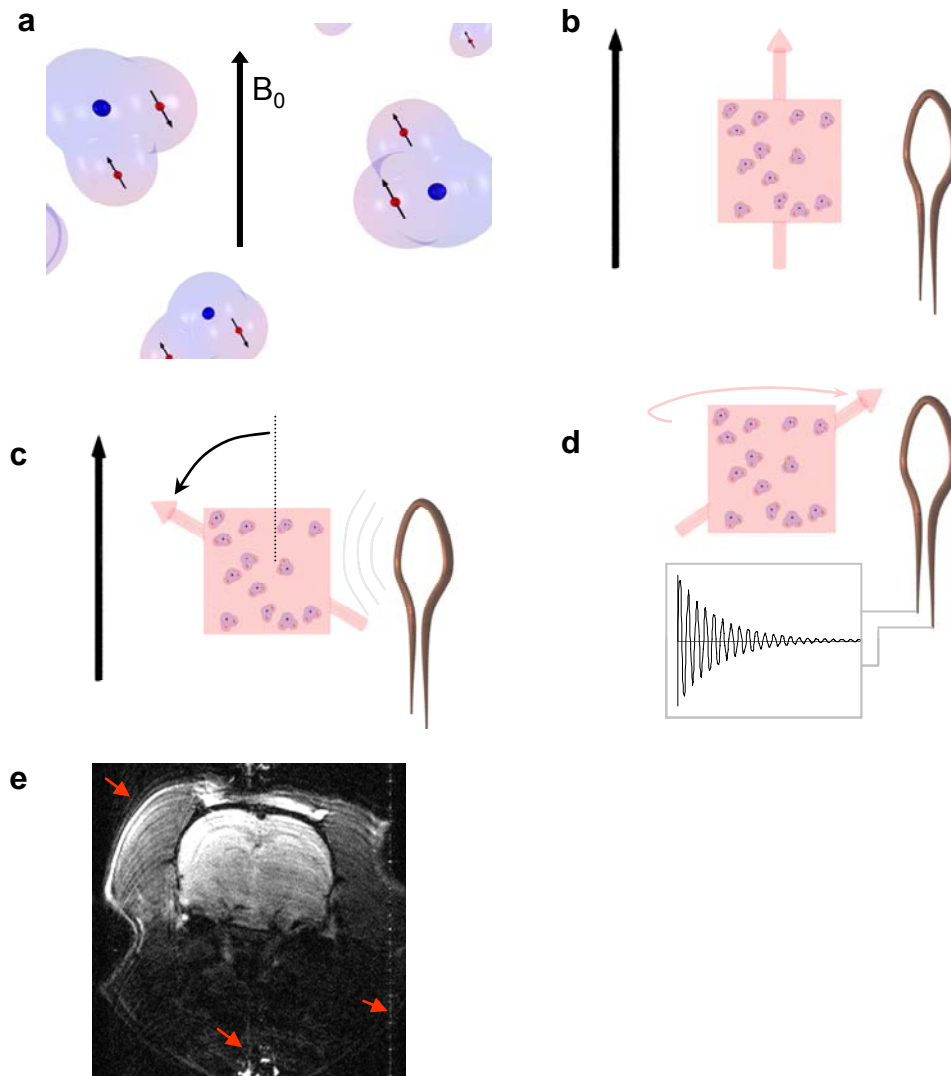


Figure 1 – 1: MRI of the ^1H Nucleus

(a-d) Illustration of the origin of the nuclear magnetic resonance signal in clinical proton imaging. (a) Hydrogen nuclei of atoms bound in water molecules have intrinsic magnetic moments which nearly align or nearly counteralign with a strong external magnetic field, B_0 . (b) A large population of these spins exhibits a net magnetization that is aligned with the external magnetic field. (c) Irradiating the sample with RF radiation at the Larmor frequency causes an alteration of this net magnetization which is analogous to tipping the magnetization vector out of alignment with the external magnetic field, where it will precess about the external magnetic field (d), emitting the detected nuclear magnetic resonance signal, or free induction decay (FID). (e) Animal or sample motion during acquisition causes artifacts in the reconstructed images that manifest themselves as banding in the phase encoding direction (arrows), and are a significant issue in fMRI of conscious animals.

Table 1-1

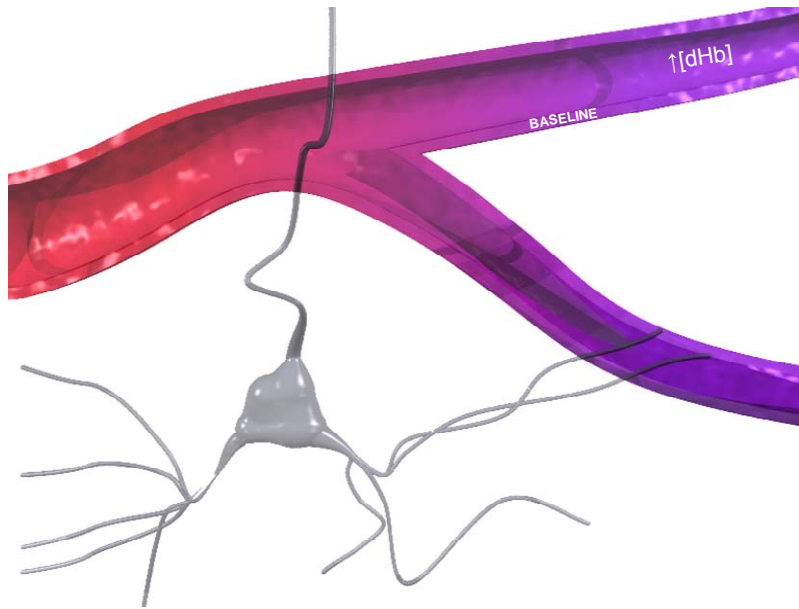
Drug	D₁	D₂	D₃	D₄	α₁	5-HT₂	M	H₁
Haloperidol	+	+++			++			
Clozapine		+	++	+	++	++	++	+
Quetiapine	++	+			+	++	+	+
Risperidone		+			+	+++	+	+
Sertindole		++			+	+++		
Olanzapine		+			+	++	++	+

Table 1 – 1: Profiles of receptor blockade among atypical antipsychotic medications and haloperidol

Drugs that are effective at treating the symptoms of psychosis exhibit a broad spectrum of affinity for different receptor types. The effective blockade of different receptor types is shown for the typical antipsychotic drug, haloperidol, and several atypical drugs which exhibit a broader spectrum of receptor antagonism. The degree of blockade is shown by “+” signs, where a larger number indicates a more potent antagonism of the receptor subtype. See text for citations regarding the specificity of these compounds.

Figure 1-2

a



b

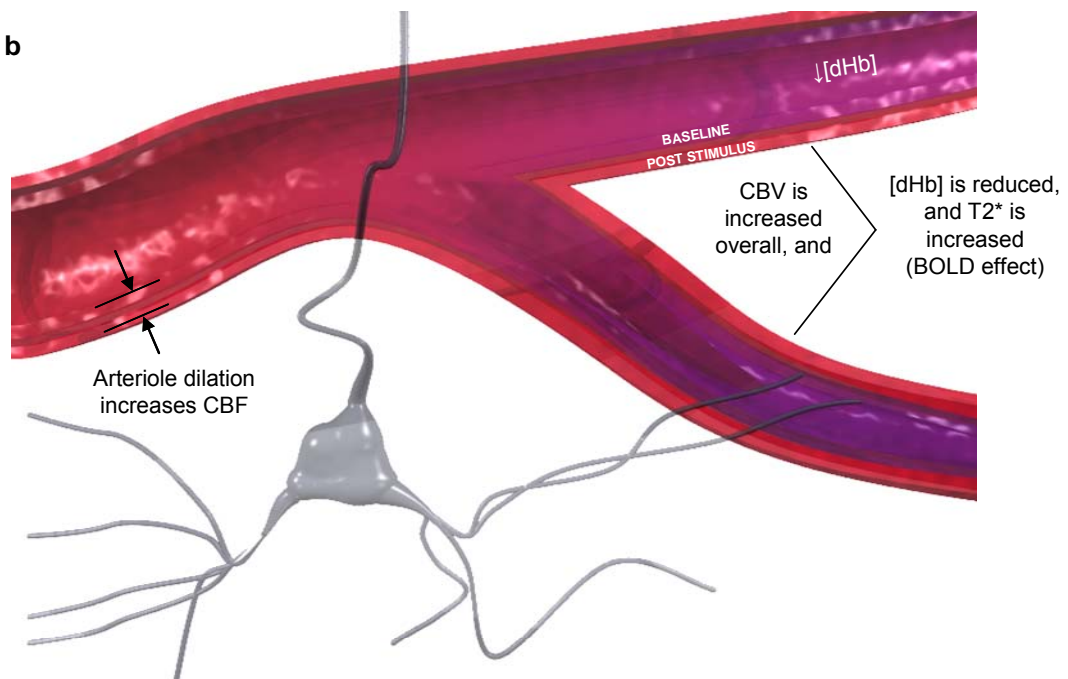


Figure 1 – 2: Hemodynamic changes following increased neural activation.

The hemodynamic changes that result from increased neural stimulation are shown in schematic form. Following increased rates of neuronal membrane depolarization, vasoactive metabolites and putative neurogenic mechanisms cause the arterioles in the microvasculature to dilate with respect to baseline conditions (a). (b) Illustrates the increase in microvessel diameter with arrows, and the increase in cerebral blood flow (CBF) and cerebral blood volume (CBV) with respect to the baseline state, following increased neural stimulation. The resulting increase in blood flow and concomitant oxygen supply to the region reliably overcompensates for the increase in metabolic demand, and a decrease in deoxyhemoglobin concentration ($[dHb]$) (b) can be observed by MRI.

Figure 1-3

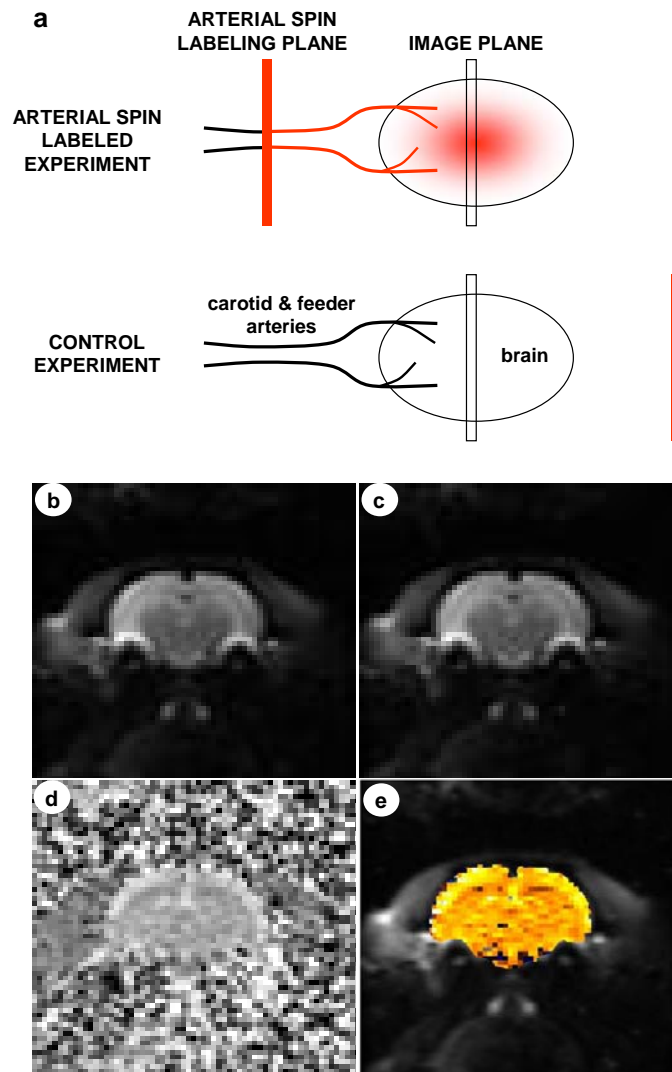


Figure 1 – 3: Continuous Arterial Spin Labeling (CASL)

(a) Schematic of the arterial spin labeling and control experiments performed in CASL to assess blood flow. In the labeling experiment, the magnetization of arterial water spins is inverted with respect to the external magnetic field at the location of the carotid arteries, and used as an endogenous tracer. In a separate control experiment, the same inversion pulse is applied, but in a location outside of the animal, where it fails to invert any of the spins in the arterial blood. (b-c) The images acquired from these two experiments exhibit small differences that can be visualized when the images are combined (subtracted and normalized) (c), providing a measure of cerebral blood flow in the imaging planes. (e) This perfusion calculation is typically visualized in false color overlay on the original anatomical images. Figure reproduced from (Ferris et al., 2006).

CHAPTER II

MEASURING ΔCMRO_2 BY MULTI-MODAL IMAGING IN THE ANESTHETIZED RAT

The work presented in this chapter is reproduced with changes in text from (Liu et al., 2004). Zhaohui Liu and Dr. Timothy Q. Duong were the primary contributors to this work, and it is with great gratitude to them and to other authors that I reproduce these results in this dissertation to introduce the technique which motivated much of the remaining research and on which much of it is based. My involvement in these studies was under the direction of Dr. Duong, where my contributions consisted of participation in a portion of the animal experiments, generating the tools enabling the group analysis of multisubject data, and the execution of the Monte Carlo simulation of the calculated results.

Introduction

The complex relationship between changes in cerebral hemodynamics and changes in neural activity warrants careful interpretation of the BOLD signal, and it would be beneficial to add the capability to make a more direct measurement of local tissue metabolism. In this study, a technique for the non-invasive measurement of changes in the cerebral metabolic rate of oxygen (CMRO₂) was applied to the anesthetized animal, and used to measure localized changes in oxygen metabolism that resulted from an electrical sensory stimulus. Under conditions of sensory stimulation, the relationship between changes in neural activity and changes in BOLD contrast has been investigated with concomitant electrophysiological recordings (Logothetis, 2002). Here we test the hypothesis that changes in CMRO₂ can also be measured as a surrogate of changing neural activity, and that the measured changes in CMRO₂ are consistent with those reported by others and are a valid measure that can be used in pharmacological studies.

Theory

Changes in the BOLD signal, as well as changes in CBF can be measured simultaneously using an arterial spin labeling sequence in which the control images are BOLD weighted (Silva et al., 1999; Duong et al., 2000). In 1998, Davis and others illustrated that CBF and BOLD measurements could be combined with mass conservation principles and a biophysical model of changes in T2* that are related to

changes in deoxyhemoglobin concentration in order to calculate changes in oxygen consumption within the tissue (CMRO_2) (Ogawa et al., 1993; Yablonskiy and Haacke, 1994; Boxerman et al., 1995a; Davis et al., 1998). Subsequently, Hoge and others re-derived this relationship to produce an algorithmically simpler form that is now used to enable MRI based assessment of changes in CMRO_2 (Hoge et al., 1999b). By acquiring BOLD and CBF changes simultaneously, the addition of a hypercapnic calibration experiment before the stimulus being investigated permits the measurement of changes in CMRO_2 with the same temporal resolution as the original BOLD and CBF measurements.

This methodology for determining ΔCMRO_2 via MRI is based upon several assumptions that are important considerations in the interpretation of the results of this measurement. The relationship between the $R2^*$ relaxivity ($1/T2^*$) of tissue has been shown to be related to the concentration of deoxyhemoglobin, local blood volume, and a proportionality constant that depends partially on field strength, by Equation 2.1 (Boxerman et al., 1995a). We assume that the signal change that we are measuring is a result of changing venous deoxyhemoglobin (Equation 2.2) (Boxerman et al., 1995a; Hoge et al., 1999b). Assuming mass conservation (i.e. Fick's law) (Katzung, 2004) we can calculate the oxidative metabolism of the tissue as a function of the concentration of deoxygenated hemoglobin in the venous outflow (Equation 2.3), where the factor of $\frac{1}{4}$ accounts for the stoichiometry of oxygen and hemoglobin binding (Alberts et al., 2002). It has been established that under normal conditions the relationship between CBF and CBV is highly predictable, and that these two values are tightly coupled (Equation 2.4)

(Grubb et al., 1974). Substituting this relationship into Equation 2.2, a change in BOLD contrast is related to a change in R_2^* due to changing deoxyhemoglobin concentration and blood flow by Equations 2.5 and 2.6, providing us with the basis for the solution that follows.

$$R_2^*|_{dHB} = A \cdot CBV ([dHb]_v)^\beta \quad (2.1)$$

$$\Delta R_2^* = A \cdot CBF^\alpha ([dHb]_v)^\beta - A \cdot CBF_0^\alpha ([dHb]_{v0})^\beta \quad (2.2)$$

$$CMRO_2 = 4 \cdot CBF ([dHb]_v) \quad (2.3)$$

$$CBV = CBF^\alpha \quad (2.4)$$

$$\frac{\Delta BOLD}{BOLD} = e^{-TE \cdot \Delta R_2^*} - 1 \quad (2.5)$$

$$\ln \left(\frac{\Delta BOLD}{BOLD} + 1 \right) = -TE \cdot A \cdot \left[CBF^\alpha ([dHb]_v)^\beta - CBF_0^\alpha ([dHb]_{v0})^\beta \right] \quad (2.6)$$

$$[dHb]_v = \frac{CMRO_2}{8 \cdot CBF} \quad (2.7)$$

$$\ln \left(\frac{\Delta BOLD}{BOLD} + 1 \right) = \frac{TE \cdot A \cdot}{CBF_0^\alpha [dHb]_{v0}^\beta} \left[1 - \left(\frac{CBF}{CBF_0} \right)^\alpha \left(\frac{CMRO_2}{4 \cdot CBF} \right)^\beta \right] \quad (2.8)$$

$$\ln \left(\frac{\Delta BOLD}{BOLD} + 1 \right) = \frac{TE \cdot A \cdot}{CBF_0^\alpha [dHb]_{v0}^\beta} \left[1 - \left(\frac{CBF}{CBF_0} \right)^{\alpha-\beta} \left(\frac{CMRO_2}{CMRO_{20}} \right)^\beta \right] \quad (2.9)$$

$$\text{Approximate: } \ln \left(\frac{\Delta BOLD}{BOLD} + 1 \right) \cong \left(\frac{\Delta BOLD}{BOLD} + 1 - 1 \right) + \dots$$

$$\text{and define: } M \equiv \frac{TE \cdot A \cdot}{CBF_0^\alpha [dHb]_{v0}^\beta}$$

yielding:

$$\frac{\Delta BOLD}{BOLD} = M \left[1 - \left(\frac{CBF}{CBF_0} \right)^{\alpha-\beta} \left(\frac{CMRO_2}{CMRO_{20}} \right)^\beta \right] \quad (2.10)$$

$$\text{Under isometabolic conditions: } M = \frac{\frac{\Delta BOLD}{BOLD}}{1 - \left(\frac{CBF}{CBF_0} \right)^{\alpha-\beta}} \quad (2.11)$$

The parameter M is constant and represents the maximal BOLD signal change that can be expected from a particular tissue volume given a particular set of baseline parameters (Eq. 2.10); it is the scaling factor describing the sensitivity of the BOLD

signal to changes in blood flow and oxygen metabolism. Determination of the parameter M is possible if both BOLD and CBF are changed and measured while CMRO₂ is held constant. A hypercapnic challenge has been shown to have little impact on the metabolism of local tissue (Horvath et al., 1994; Yang and Krasney, 1995), and we can assume that CMRO₂ is held constant under mildly hypercapnic conditions while BOLD and CBF are modulated from baseline values, permitting determination of the parameter M.

Materials and methods

Animal Preparation

Six male Sprague Dawley rats, weighing between 300-375 g, were investigated. Rats were anesthetized with 2% isoflurane for surgery and placement into an MR compatible stereotaxic headset to prevent motion during the imaging experiments. A femoral artery was catheterized using PE-50 tubing, and needle electrodes were inserted beneath the skin of the forepaws. The rats breathed spontaneously during the MR experiments, without mechanical ventilation. Anesthesia was reduced to 1.2% isoflurane during the imaging experiments, and temperature was stabilized to $37 \pm 0.5^{\circ}$ C using a warm water heating pad with feedback from a rectal temperature monitor. Blood pressure (BP) was monitored at 5 ms intervals via the arterial catheter using a BioPak digital acquisition system (Santa Barbara, CA), and respiration rate (RR) and heart rate (HR) were derived from frequency analysis of the BP signal.

During the hypercapnic challenge experiments, rats breathed normal air during the baseline period, then breathed a prepared mixture containing air and CO₂ at 5% concentration. During forepaw stimulation experiments, graded stimulation currents of 4 mA, 6 mA, and 8 mA with a 0.3 ms pulse duration at 3 Hz were used. In four of the six rats, pairs of electrodes were configured to permit selective stimulation of individual forepaws. In the remaining two rats, both paws were stimulated simultaneously.

MRI experiments

The MRI experiments were performed using a 4.7-T/40-cm bore magnet (Oxford, UK) equipped with a Biospec console (Bruker Biospin, Billerica, MA), and a 20-G/cm gradient insert with a 12cm inner diameter (ID) that is capable of a 120 μ s rise time. A custom surface coil with a 2.3 cm ID was used for imaging, and a second coil located below the carotid arteries of the animal was used for arterial spin labeling (Silva et al., 1999; Duong et al., 2000). The coils were electronically decoupled during the imaging experiments with a switch box that interfaced with the console (Insight Neuroimaging Systems, Worcester, MA). High resolution anatomical images were acquired using a fast spin-echo pulse sequence (RARE) with the following parameters: TR = 2 s, flip angle = 90°, RARE factor = 16, effective TE = 104ms, matrix = 128 x 128, FOV = 2.56 x 2.56 cm, averages = 16, thk = 1.5 mm, and eight slices were acquired.

Functional images were acquired using the continuous arterial spin labeling (CASL) technique (Silva et al., 1999; Duong et al., 2000), allowing simultaneous measurement of BOLD and CBF changes. Images were acquired using a single shot

gradient echo (GE) echo planar imaging (EPI) imaging sequence, with the following parameters: matrix = 64 x 64, FOV = 2.56 x 2.56 cm, TE = 15ms, TR = 2s, flip angle = 90°, thk = 1.5 mm, and eight slices were acquired, consistent with the geometry of the anatomical images. During arterial labeling, a 1.78 s square radiofrequency pulse was applied to the labeling coil in the presence of a 1.0 G/cm gradient along the direction of blood flow, satisfying the adiabatic inversion condition (Dixon et al., 1986; Williams et al., 1992). During control images, the frequency of the labeling pulse was offset and corresponded to a location outside of the anterior end of the animal, in a location symmetrically opposed to the center of the imaging planes. Labeled and control images were acquired sequentially, and 31 pairs of images were acquired during the baseline period and an additional 31 pairs were acquired during the hypercapnic challenge or forepaw stimulation epochs.

Data analysis

Data were analyzed using Stimulate (Strupp, 1996) and Matlab (MathWorks, Inc. Natick, MA) software packages, and repeated BOLD and CBF measurements within the same animal were averaged during the baseline and stimulation epochs. BOLD images were obtained from the control (unlabeled) images from the functional image sequence, and a CBF image time series was created by calculating the voxelwise CBF using equation 1.07, with the following values: $T_1 = 1.54$ s, $\lambda = 0.9$, $\alpha = 0.7$. Cross-correlation analysis was performed on the BOLD, VBF and CMRO₂ data sets to obtain percent-change activation maps. For the calculation of CMRO₂ maps, equation 2.12 was used,

and the value of the parameter M was determined for each voxel using the hypercapnic challenge data and equation 2.11. The values of the parameters in equations 2.11 and 2.12 were: $\alpha = 0.38$ (Mandeville et al., 1999) and $\beta = 1.5$ (Boxerman et al., 1995b; Davis et al., 1998).

$$\frac{CMRO_2}{CMRO_{20}} = \left[\left(\frac{CBF}{CBF_0} \right)^{\beta - \alpha} \left(1 - \frac{1}{M} \frac{\Delta BOLD}{BOLD} \right) \right]^{\frac{1}{\beta}} \quad (2.12)$$

Regions of interest (ROI) were analyzed by defining the areas containing the primary and secondary somatosensory regions on the anatomical images using a rat brain atlas (Paxinos and Watson, 1998), and by transferring these areas to calculated maps to extract the mean changes in BOLD, CBF, $CMRO_2$ for the average and timecourse measurements reported herein. The effects of noise on the parameter M and the change in $CMRO_2$ measurements were analyzed using Monte Carlo simulation and custom software written in the Java programming language (Sun Microsystems, Inc., San Jose, CA). Data from 1 and 9 voxel ROIs in the somatosensory region were used as inputs to the simulation. The input parameters for the simulation were as follows: For hypercapnia using the 1 voxel ROI, $\Delta BOLD = 3.6\% \pm 0.9\%$ and $\Delta CBF = 208\% \pm 55\%$. For hypercapnia using the 9 voxel ROI, $\Delta BOLD = 4.7\% \pm 0.4\%$ and $\Delta CBF = 189\% \pm 24\%$. For 6 mA stimulation using the 1 voxel ROI, $\Delta BOLD = 0.9\% \pm 0.8\%$ and $\Delta CBF = 73\% \pm 45\%$, and for 6 mA stimulation using the 9 voxel ROI, $\Delta BOLD = 3.3\% \pm 0.3\%$ and $\Delta CBF = 163\% \pm 16\%$ (mean \pm standard deviation). Simulations were also performed with an artificial increase of the standard deviation of measurements from the 9 voxel ROI by a factor of 3.

Raw EPI image data sets from all subjects were manually aligned and averaged together using custom software (Schmidt et al., 2004), and BOLD, CBF, M , and $CMRO_2$ maps were calculated from coregistered datasets. Activation maps following unilateral stimulation revealed a bilateral response and, consequently, equal numbers of right paw stimulation ($N = 2$), left paw stimulation ($N = 2$), and both paw stimulation ($N = 2$) data sets were averaged together to produce the group average activation maps shown in Figure 2 – 2.

Results

Following stimulation at 4 mA, there were no statistically significant changes in mean arterial blood pressure (MABP), HR, or RR relative to baseline. At 6 mA, there were small and transient changes in HR ($P = 0.06$) and MABP ($P = 0.01$) immediately following the onset of stimulation, but these changes became insignificant, returning to near baseline levels, during the sustained stimulation period. At 8 mA, there was a large transient increase in HR ($P < 0.01$) and MABP ($P < 0.01$) and both measurements remained elevated during the stimulation period. Table 2-1 indicates the magnitude of changes observed during the stimulation period, in comparison to the baseline period before the onset of stimulation.

Figure 2-1 illustrates anatomical images, CBF maps, M maps, and $\Delta BOLD$, ΔCBF , and $\Delta CMRO_2$ activation maps for a single subject in which both forepaws were simultaneously stimulated. The value of the parameter M was heterogeneous throughout the brain, with larger values of M observed near the ventricles, cortical surface, and

around large draining veins. The average value of M in the primary somatosensory cortices was 0.05 ± 0.01 (mean \pm standard deviation, $N = 6$). The ΔBOLD , ΔCBF , and ΔCMRO_2 activation maps show a bilateral activation in the primary and secondary somatosensory cortices. This bilateral activation is clearly visible in the averaged, coregistered maps (Figure 2-2), where the primary and secondary somatosensory cortices are clearly delineated as the most significantly active structures. While the ΔBOLD activation map shows enhanced activation near the cortical surface of the somatosensory cortices (Figure 2-2), the more uniform activation shown in these regions in the ΔCBF and ΔCMRO_2 activation maps reflects a reduced sensitivity of the CBF measurement to the effects of cortical surface vessels. There were no statistically significant negative changes observed in BOLD, CBF, or CMRO_2 activation maps of the individual or group averaged data.

Figure 2-3, panel a illustrates the dynamic changes in BOLD and CMRO_2 that accompany stimulation at various currents, measured from the somatosensory regions of a representative subject. Changes in BOLD and CMRO_2 increased with increasing stimulation amplitude in a manner that was consistent between animals. Figure 2-3, panel b summarizes the group average changes in BOLD ($0.5\% \pm 0.2\%$ at 4 mA, $1.4\% \pm 0.3\%$ at 6 mA, and $2.0\% \pm 0.3\%$ at 8 mA), CBF ($23\% \pm 6\%$ at 4 mA, $58\% \pm 9\%$ at 6 mA, and $87\% \pm 14\%$ at 8 mA), and CMRO_2 ($14\% \pm 4\%$ at 4 mA, $24\% \pm 6\%$ at 6 mA, and $43\% \pm 11\%$ at 8 mA). The group average baseline measure of CBF was 0.91 ± 0.13 ml/g/min, consistent with previously reported values for the rat brain under 1.2% isoflurane anesthesia (Duong et al., 2001).

BOLD changes vs. CBF changes and CMRO₂ changes vs. CBF changes were linearly correlated across the ranges observed for all stimulation amplitudes (Figure 2-4). Changes in CBF vs. changes in CMRO₂ were linear with a proportionality of 2.2:1, and changes in CBF vs. changes in BOLD were linear with a proportionality of 40:1. While there was some overlap in the ranges of BOLD, CBF, and CMRO₂ changes for each stimulation amplitude among the entire group, the mean values of changes of these measures were reasonably segregated (Figure 2-4).

Monte Carlo simulation was performed to assess the propagation of noise through Equations 2.11 and 2.12 to assess the shape of the error distribution in measured changes in CMRO₂, in order to investigate possible bias introduced by the nonlinear propagation of errors in Equation 2.12. The results of these simulations are shown in Figure 2-5. Of note is the increasing skew of the M distribution with increasing width (SD) of the input parameters, introducing a bias toward lower M values with increasing noise in the original measurements of BOLD and CBF changes (Figure 2-5). This bias is nearly eliminated, however, with the subsequent CMRO₂ calculation (Figure 2-5), a property that was also reported in the original work reporting this model (Davis et al., 1998).

Discussion

The data presented in this investigation illustrate localized increases in CMRO₂ following sensory stimulation over a range of stimulation amplitudes that were measured non-invasively using MRI and a biophysical model of the BOLD signal. Additionally, the simultaneous measurement of changes in both BOLD and CBF using the CASL

technique permits the measurement of changes in CMRO_2 to be made with high temporal resolution, comparable to that of traditional functional MRI experiments that rely on BOLD or CBF changes alone. This technique holds promise for the investigation of metabolic changes induced by pharmacological stimuli, where additional insights into the origin of observed changes in hemodynamics may be necessary to deduce changes in underlying neural activity.

The results of these estimated changes in CMRO_2 are in general agreement with changes in CMRO_2 reported using other measurement techniques. Using PET and the Kety-Schmidt method, a 5% change in CMRO_2 was reported following visual stimulation in the human cortex (Fox et al., 1988), summarily ΔCMRO_2 values of 16% (Davis et al., 1998), 25% (Hoge et al., 1999a; 1999b), and 16% (Kim et al., 1999) were measured by calibrated MRI in the human cortex following visual stimulation, and CMRO_2 changes of 19% (Mandeville et al., 1999) reported following electrical sensory stimulation in rat measured by calibrated fMRI. An advantage of calibrated fMRI measurement of CMRO_2 changes is the direct measurement of the parameter M which contains several physiological variables that would otherwise need to be estimated (see the definition of M in equation 2.10). This may explain the general consistency of the calibrated functional MRI results in comparison to the reported value of 5% in Fox et al.'s 1988 PET study. Thalamic activation was not observed to be significant at the thresholds used for delineating sensory activation, consistent with a reduced BOLD response from these regions with respect to primary and secondary somatosensory regions (Keilholz et al., 2004).

Monte Carlo simulation of the ΔCMRO_2 measurement confirms the non-linear propagation of noise present in the original measurements (ΔBOLD and ΔCBF), highlighting the challenge to maintain adequate sensitivity in experiments measuring ΔCMRO_2 . However, skew in the probability distribution of the calculated parameter M is ablated by the subsequent calculation of ΔCMRO_2 , which appears to be normally distributed, suggesting that strategies for increasing the statistical power of the original measurements of ΔCMRO_2 (e.g. multiple subjects and ROI analysis of many voxels) will not bias final measurement.

This study demonstrates the use of calibrated functional MRI for the measurement of changes in CMRO_2 following sensory stimulation in spontaneously breathing, isoflurane anesthetized rats. The measurements of CMRO_2 changes in this study under the least intense electrical stimulation are consistent with reported changes in CMRO_2 resulting from a visual sensory stimulus in conscious humans. Changes in CMRO_2 increased with increasing stimulus intensity in a linear fashion, and changes in CMRO_2 were observed to be linearly correlated with changes in BOLD and CBF under the conditions studied. The ability to perform this measurement in a single experimental setting, by measuring BOLD and CBF changes simultaneously, suggests that the technique will be valuable in other applications, including fMRI of pharmacological challenges where the repeated administration of drug doses may be impractical.

Table 2-1

Current	RR	HR	MABP
Baseline	61 ± 15	394 ± 35	135 ± 6
4 mA	62 ± 18	386 ± 26 (387 ± 32)	136 ± 6 (136 ± 4)
6 mA	64 ± 15	405 ± 37 (406 ± 39)*	139 ± 11 (141 ± 6)**
8 mA	64 ± 18	415 ± 38** (419 ± 44)**	143 ± 6** (148 ± 8)**

Mean ± SD, N = 6. Values in parentheses are maximum changes in transient signal following stimulation onset. Statistical significance of comparisons with baseline are indicated. * P=0.06; ** P < 0.01, two tailed, paired t-test.

Table 2 – 1: Respiration rate, heart rate, and mean arterial blood pressure during baseline and electrical forepaw stimulation

Physiological measurements of respiration rate (RR, breaths per minute), heart rate (HR, beats per minute), and mean arterial blood pressure (MABP, mmHg) during baseline, 4 mA, 6 mA, and 8 mA electrical forepaw stimulation in the anesthetized rat are shown. Significant increases in HR and MABP were observed following stimulation with 6 mA or 8 mA, but no significant changes in RR were observed or in any physiological parameters following stimulation at 4 mA. Table reproduced from (Liu et al., 2004).

Figure 2-1

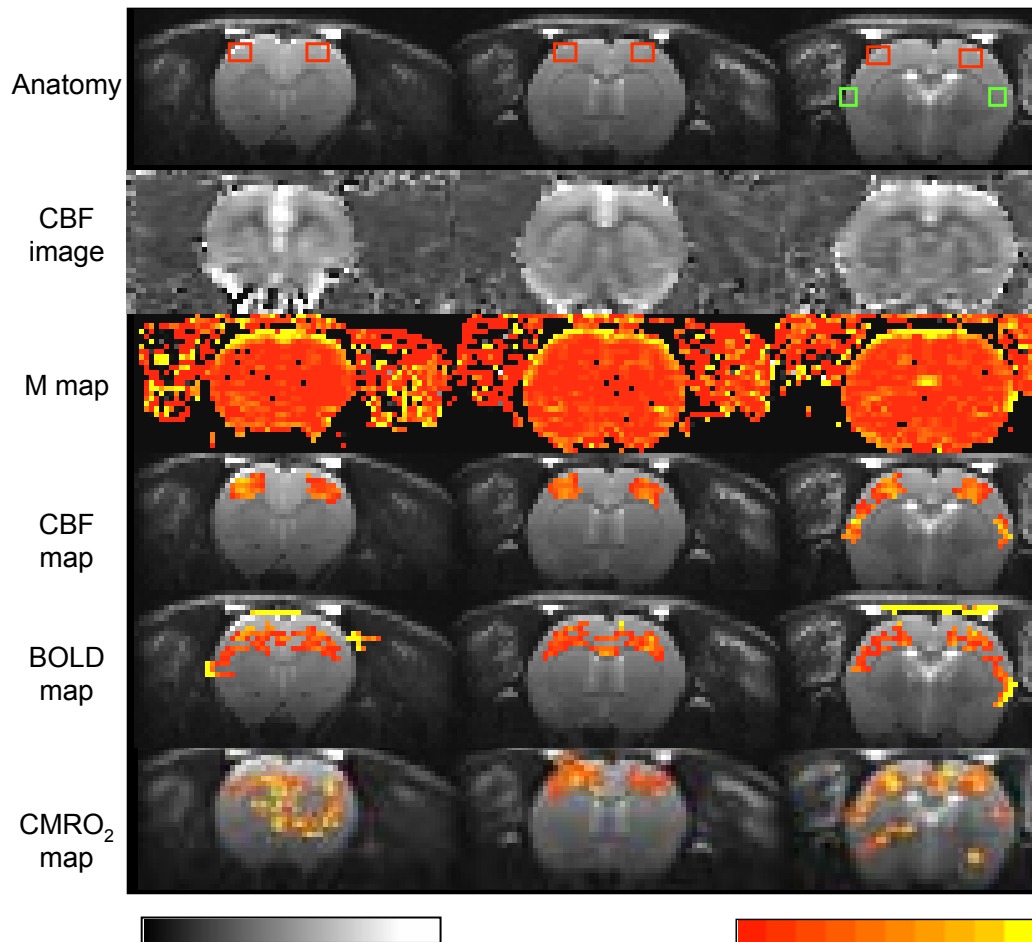


Figure 2 – 1: Anatomical images, quantitative CBF, the parameter M and changes in BOLD, CBF, and CMRO₂ following electrical forepaw stimulation from a single animal

Anatomical images at three locations from rostral (left) to caudal (right), the quantitative CBF images, the calculated parameter M, and changes in CBF, BOLD, and CMRO₂ following 6 mA electrical forepaw stimulation in a single animal are shown. Changes are mapped on a voxelwise basis, and reflect activation in areas consistent with those expected from electrical forepaw stimulation (i.e. primary and secondary somatosensory regions). Statistical thresholds were used to eliminate background effects and insignificant activation. Gray scale: CBF values 0–3 ml/g/min. Color scale: M 1–20%, CBF 80–200%, BOLD 2–10%, CMRO₂ 20–100%. Boxes indicate the regions measured and reported in Figure 2-3. Figure reproduced from (Liu et al., 2004).

Figure 2-2

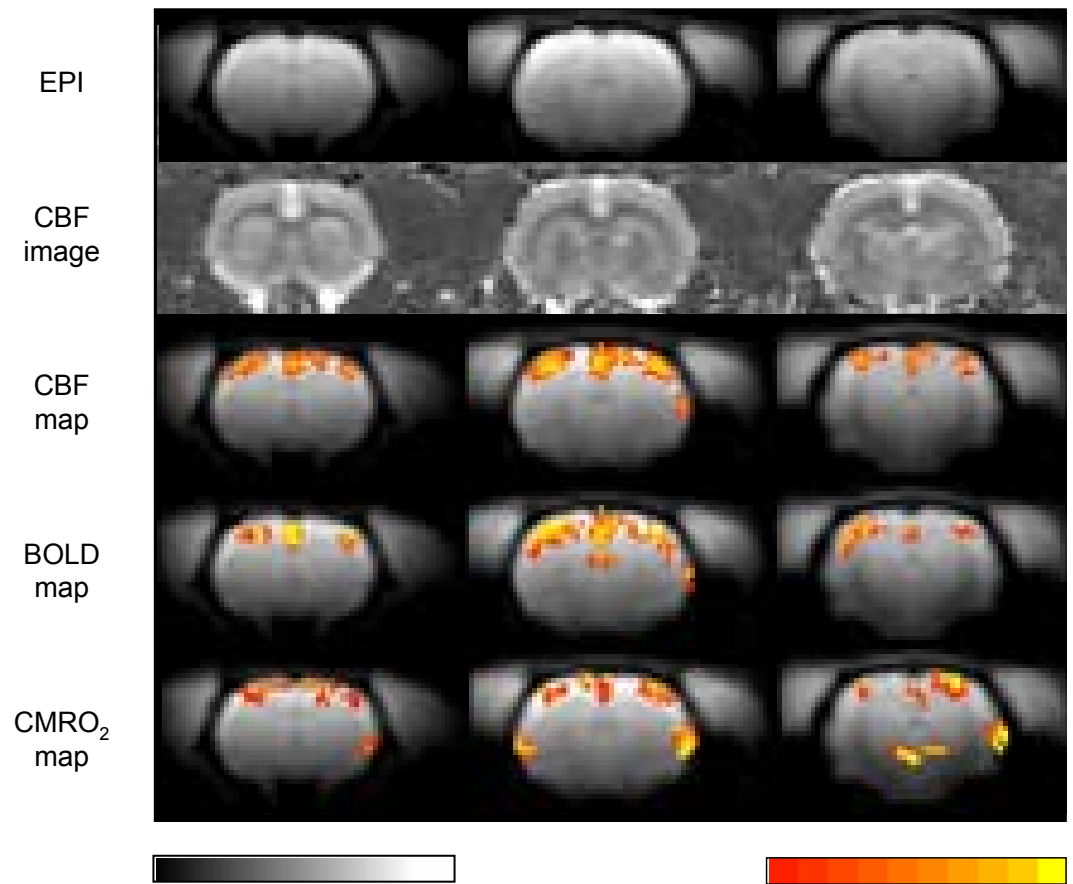


Figure 2 – 2: Group average EPI images, quantitative CBF, and changes in CBF, BOLD and CMRO₂

Datasets were coregistered and combined to visualize effects that are significant at the group level. The result of the coregistration process is shown in the combined EPI images, and the resulting group average CBF map. The group average changes in CBF, BOLD, and CMRO₂ maps following 6 mA electrical forepaw stimulation reflect a reliable activation of the primary and secondary somatosensory regions and cingulate cortex. Statistical thresholds were used to eliminate background effects and insignificant activation. Gray scale: CBF values 0–3 ml/g/min. Color scale: M 1–20%, CBF 80–200%, BOLD 2–10%, CMRO₂ 20–100%. Figure reproduced from (Liu et al., 2004).

Figure 2-3

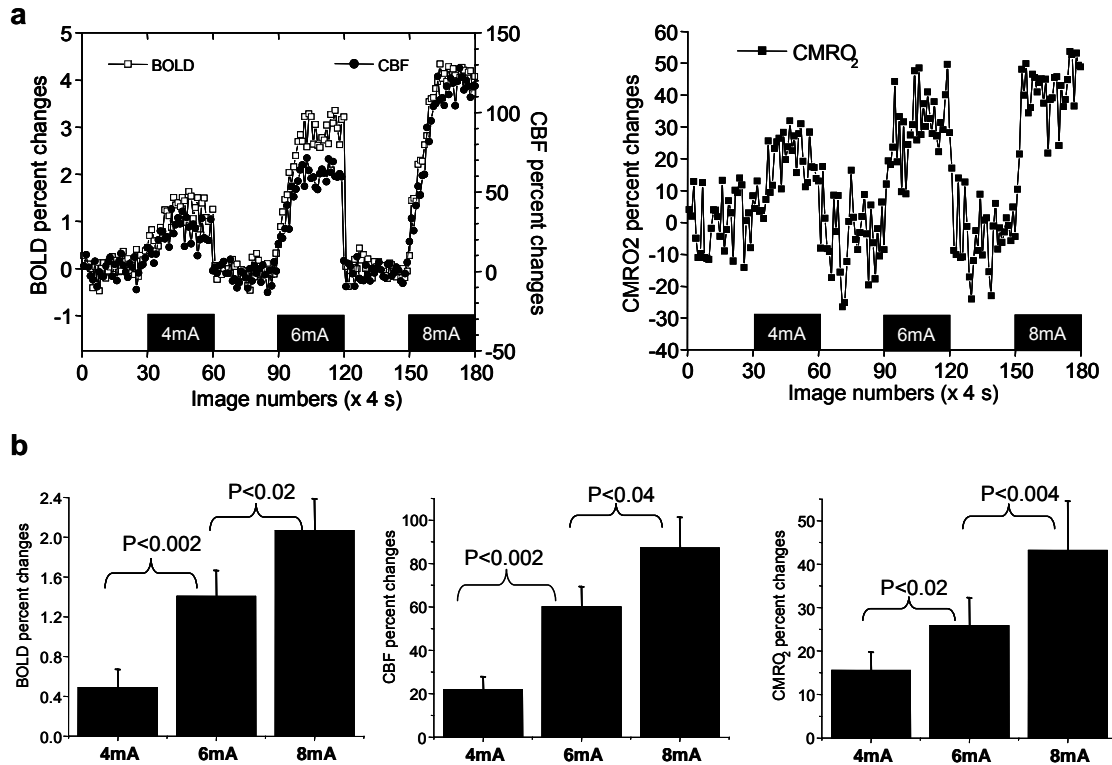


Figure 2 – 3: Dynamic changes in BOLD, CBF, and CMRO₂.

(a) Changes in time in BOLD signal contrast, CBF, and CMRO₂ were measured from the ROIs indicated in Figure 2 -1. Bilateral activation following unilateral stimulation permitted the averaging of signal changes from bilateral ROIs in all stimulus conditions. The magnitude of changes is dependent on the degree of stimulation in (a) an individual representative animal, and (b) at group level when measured from all animals. Error bars = SEM, N = 6. Significance was calculated using a two tailed t-test with a Bonferroni multiple comparisons correction. Figure adapted from (Liu et al., 2004).

Figure 2-4

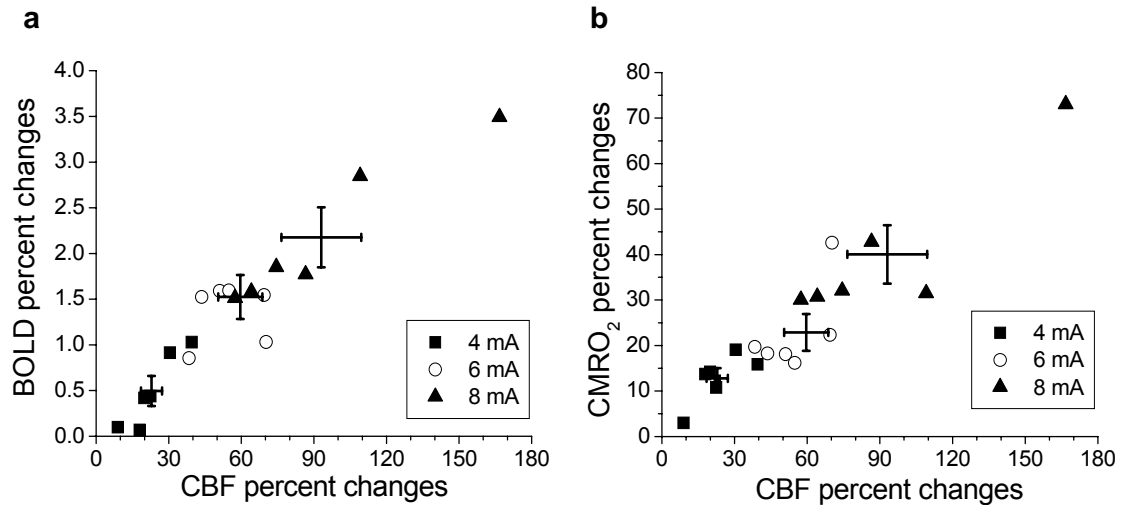


Figure 2 – 4: Changes in BOLD, CBF and CMRO₂ are correlated over the observed ranges of signal change.

Changes in BOLD, CBF, and CMRO₂ in the somatosensory cortex are linearly correlated over the ranges observed, consistent with the biophysical model. Average changes in these measures from all animals for each of the stimulation amplitudes (N = 6) are shown as crosses, bars indicate SEM. The CBF:BOLD and CMRO₂:CBF ratios were 40:1 and 2.2:1, respectively, assuming a linear relationship within the ranges observed. Figure reproduced from (Liu et al., 2004).

Figure 2-5

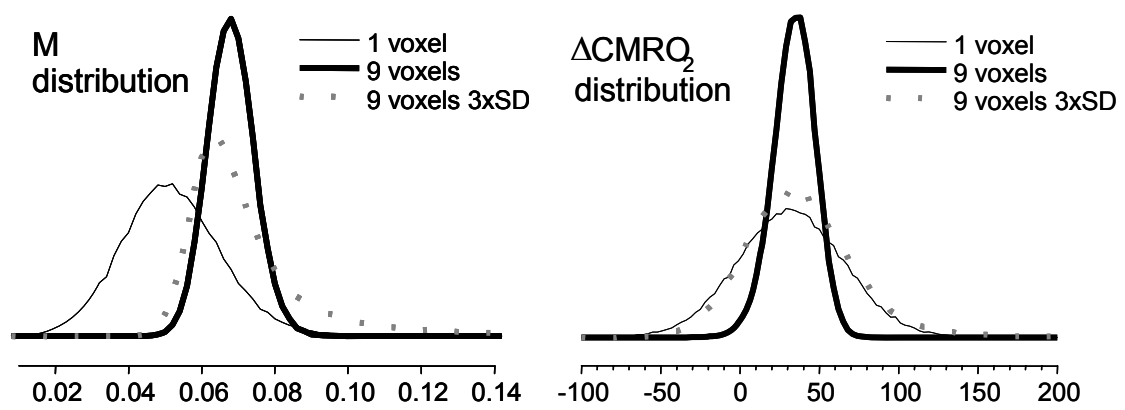


Figure 2 – 5: Monte Carlo simulation of error propagation through the biophysical model

Experimental data was used as input to a Monte Carlo simulation to determine error propagation through the biophysical model used for the measurement of changes in CMRO₂. Probability (arbitrary units) is indicated on the vertical axis, and parameter values are indicated on the horizontal axes. Δ CMRO₂ values are shown as percentages. Skew was observed in the distribution of the calculated parameter M (left panel) with increasing standard deviation (SD), with values trending toward lower than mean. This skew was summarily corrected in the calculation of changes in CMRO₂ (right panel), which appeared to be normally distributed, but increases in the variance of Δ CMRO₂ measurements are non-linear with respect to the variances of the input measurements (Δ BOLD and Δ CBF), consistent an analytical analysis of error propagation. Figure reproduced from (Liu et al., 2004).

CHAPTER III

MEASUREMENT OF CHANGES IN CMRO₂ FOLLOWING COCAINE ADMINISTRATION IN THE ANESTHETIZED RAT

The work presented in this chapter is reproduced with minor changes in text from (Schmidt et al., 2006). This work was conducted under the direction of Dr. Timothy Q. Duong, and it is with great gratitude to him and to other authors that I reproduce these results in this dissertation. My contributions to this work consisted of participation in a portion of the animal experiments, generating the tools and completing the analysis of the presented data, and synthesizing the text of the published manuscript with significant assistance and contributions from Dr. Duong and other authors.

Introduction

If changes in CMRO₂ yield a reliable surrogate of changing neural activity under conditions of sensory stimulation, does the same measurement following the administration of cocaine yield results that are consistent with cocaine's action on the nervous system? Cocaine is a psychostimulant that is frequently abused and has reinforcing characteristics that can establish a state of addiction characterized by motivated drug-seeking behavior and by a loss of the ability to control use (American Psychiatric Association, 1994). Cocaine-mediated activation of the mesolimbic dopamine system has been observed using a variety of techniques (Porrino et al., 1988; Stein and Fuller, 1992; Marota et al., 2000), and these and other studies have illustrated the complexity of the brain's response to cocaine, whereby activation occurs in many brain regions beyond the dopaminergic reward pathway (Bardo, 1998; Nestler, 2002; Kelley, 2004). The successful development of therapies to treat addiction to psychostimulants such as cocaine and methamphetamine may require detailed information about the changes in neural activity that these drugs induce in other large-scale neural networks throughout the brain (O'Brien, 2003), and the acquisition of this information may be facilitated by experimental techniques that are able to observe changes in neural activity *in vivo* following administration.

Functional MRI can be used to map brain function at higher spatial and temporal resolution than other modalities such as positron emission tomography (PET). Traditional fMRI experiments infer changes in neural activity from changes in surrogate signals such

as blood-oxygenation-level-dependent (BOLD) contrast, cerebral blood flow (CBF), and cerebral blood volume (CBV). While studies based on changes in BOLD contrast comprise the majority of published fMRI research, the relationship of BOLD contrast to neural activation is complex, and the interpretation of BOLD signal changes may be complicated by the presence of pharmacological agents that could affect physiology and the cerebral vasculature independently of changes in neural activity.

The use of fMRI to investigate cocaine's effects on neural circuitry in humans and in animal models have been reported (Breiter et al., 1997; Luo et al., 2003; Honey and Bullmore, 2004). Systemic administration of cocaine and other pharmacological agents can cause significant changes in cardiovascular physiology (Pitts et al., 1987) and changes in vascular tone, potentially modulating the fMRI signals independently of changes in neuronal activity (Gollub et al., 1998; Marota et al., 2000; Kaufman et al., 2001; Stein, 2001).

In addition to conventional BOLD fMRI, changes in cerebral metabolic rate of oxygen ($CMRO_2$) could also be estimated to serve as a metabolic marker for changes in neural activity (Hyder, 2004). Stimulus-evoked changes in $CMRO_2$ can be estimated from BOLD and CBF measurements using a biophysical model of the BOLD signal (See Chapter II) and a brief hypercapnic challenge that does not alter neural metabolism but does modulate CBF and BOLD contrast (Kety and Schmidt, 1948; Hafkenshiel and Friedland, 1952), revealing the regionally specific coupling of changes in CBF to changes in BOLD under isometabolic conditions. By combining the measured proportionality of changes in CBF to changes in BOLD contrast, the change in $CMRO_2$ can be estimated.

This non-invasive technique offers several advantages over PET-based measurements by eliminating the need for a radioactive tracer and by enabling the measurement of dynamic changes in CMRO₂, and has been used to estimate changes in CMRO₂ following sensory stimulation in humans (Ogawa et al., 1993; Davis et al., 1998; Hoge et al., 1999b; Kim et al., 1999) and in animal models (Mandeville et al., 1999; Liu et al., 2004).

In this study, we used the CMRO₂ technique to monitor changes in neural metabolism following the administration of cocaine, to test the hypothesis that changes in CMRO₂ can be measured as a surrogate of changing neural activity following a pharmacological challenge. Changes in CBF and BOLD contrast were measured simultaneously (Silva et al., 1999; Duong et al., 2000), requiring only a single administration of cocaine to enable estimation of changes in CMRO₂. This may be an important feature in pharmacological investigations where drug challenges can not be administered repeatedly within the same animal, due to slow rates of drug clearance, sensitization or desensitization, or other physiological adaptations that make the response irreproducible over time

Materials and methods

Animal Preparation.

Eleven male Sprague-Dawley rats weighing 300-375g that had not previously been exposed to cocaine were investigated. Rats were anesthetized with 2.5% gaseous isoflurane (Phoenix Pharmaceutical, St. Joseph, MO) during surgery and placed into a stereotaxic headset for immobilization during scanning. Isoflurane was reduced to 1.2%

during imaging experiments. Catheters were inserted into the left femoral vein and artery for the administration of cocaine and saline, and for monitoring physiology, respectively. Heart rate (HR), mean arterial blood pressure (MABP), and respiration rate (RR) were measured continuously during the MR experiment and recorded using a digital data acquisition system (Biopak Systems, Inc. Santa Barbara, CA). The MABP signal was analyzed for high and low frequency oscillations to determine HR and RR, respectively. Prior to the cocaine challenge experiments, a hypercapnic (5% CO₂) challenge experiment was performed for the derivation of the calibration parameter (M) map (Davis et al., 1998). During the cocaine challenge experiments, a dose of 1.0 mg/kg in a 1.0 ml/kg saline vehicle was administered intravenously over a period of approximately 10s.

MRI Experiments.

BOLD and CBF measurements were made on a 4.7T/40cm bore magnet (Oxford, UK), Bruker Biospec console (Bruker BioSpin, Billerica, MA), using a 20-G/cm gradient insert with a 12cm inner diameter (ID), capable of a 120- μ s rise time. A 2.3cm ID surface coil was used for brain imaging and a separate neck coil for arterial spin labeling as previously described (Silva et al., 1999; Duong et al., 2000; Liu et al., 2004). Functional images were acquired with a single shot, gradient echo, echo-planar imaging (EPI) sequence in the presence (labeled images) and absence (control images) of arterial spin inversion. Arterial spin inversion was accomplished with a 1.7s hard radio frequency pulse (square pulse) applied to the neck coil in the presence of a 1.0 G/cm gradient along the direction of blood flow, in order to satisfy the adiabatic inversion condition (Williams et al., 1992). The frequency offset of the hard pulse was determined to excite arterial

spins within the carotid arteries. During the acquisition of control images, the sign of the frequency offset of the hard pulse was reversed (corresponding to a location outside of the animal) to control for magnetization transfer contrast unrelated to arterial spin labeling (Detre et al., 1992; Williams et al., 1992). Pairs of control and labeled images were acquired continuously throughout each experiment. Sequence parameters were: data matrix=64 x 64, field of view (FOV)=2.3 cm x 2.3 cm, eight 1.5 mm thick slices, TE=15ms, and TR=2s. During the hypercapnic challenge experiments, 30 pairs of images were acquired during baseline and an additional 30 pairs of images were acquired following the administration of 5% CO₂. During the cocaine challenge experiments, 50 pairs of images were acquired during baseline, and an additional 160 pairs acquired following the administration of cocaine. Anatomical images were acquired at higher resolution (128 x 128) using a RARE sequence, and used for co-registration of the functional images to a digital atlas (Paxinos and Watson, 1998).

Data analysis.

Custom software was developed in the Java programming language (Sun Microsystems, Inc., San Jose, CA) for data analysis. A BOLD image time series was derived from the control images, and a CBF image time series was generated by calculating CBF on a voxel by voxel basis as previously described (Silva et al., 1999). BOLD and CBF time series were analyzed for each voxel using a generalized linear model approach (Worsley and Friston, 1995) with a single step boxcar model as the input function for both the hypercapnic and cocaine challenge experiments. P values reflecting the likelihood of observing the timecourse correlation with the model among random data

were generated for each voxel, and used as thresholds. Percent change maps of BOLD and CBF changes following CO₂ or cocaine administration were generated from voxels with P values less than 0.001, and all other voxels were set to zero percent change to reduce artifacts caused by noise in the calculated CMRO₂ maps. In Fig. 3 – 2, BOLD and CBF timecourses from a single subject were normalized by division with the average BOLD or CBF value from the 40 baseline repetitions, and Δ CMRO₂ were calculated independently for each repetition.

The biophysical model of the BOLD signal described in chapter II was used in conjunction with the hypercapnic calibration scans and M map to calculate Δ CMRO₂ maps (Davis et al., 1998; Hoge et al., 1999a) . Equations 2.10 and 2.11 recapitulate the formulae used in this calculation, and the variables α and β were assigned the values 0.38 (Ueki et al., 1988) and 1.5 (Madsen et al., 1998), respectively. In the calculation of the M map, voxels which contained physiologically meaningless M values (imaginary values, negative values, and infinite values) were identified and excluded from subsequent map and ROI calculations.

Each slice was manually co-registered to an atlas (Paxinos and Watson, 1998) using custom software (Schmidt et al., 2004) and the following degrees of freedom: x and y translation, independent x and y scaling, and rotation about the z axis. The original images were resampled in the transformation to the atlas coordinate system, and a new set of images that was anatomically coincident with the atlas were created. Regions of interest were defined and used to measure average values from the Δ CBF, Δ BOLD, Δ CMRO₂, and M maps of each subject for the measurements presented in Table 3 – 1.

The ROIs analyzed using this method were: periaqueductal gray (PAG), substantia nigra (SN), ventral tegmental area (VTA), hippocampus (HIP), primary somatosensory cortex (S1), ventral posterolateral thalamic nucleus (VPL), lateral globus pallidus (LGP), cingulate cortex (CG), nucleus accumbens (NAc), and striatum. In Figure 3 – 1, calculated maps co-registered to the atlas coordinate space were averaged together on a voxel by voxel basis for visualization.

Results

Mean arterial blood pressure (MABP) increased from 113 ± 14 mmHg (mean \pm standard deviation, $N = 8$) to 137 ± 33 mmHg ($p < 0.05$) following the injection of cocaine, and remained elevated at 119 ± 15 mmHg for up to 2 minutes thereafter ($P < 0.05$). Respiration rate increased from the baseline level of 81 ± 7 to 89 ± 8 breaths per minute (bpm) during the injection, and summarily increased to 103 ± 16 bpm 1 to 2 min after the injection. Within 5 minutes following the injection, MABP, RR, and HR returned to baseline levels.

Figure 3-1 illustrates group average changes observed in BOLD, CBF, and calculated $CMRO_2$, and the group average value of the parameter M , overlaid on top of co-registered anatomical images; areas outside of the brain were masked. The parameter M , representing the maximum expected BOLD response from the tissue volume, varied between 8% and 17% throughout the regions investigated, consistent with previously conducted studies under similar experimental conditions (Liu et al., 2004). Due to the significant extravascular contribution to the $T2^*$ BOLD signal by large veins, the

parameter M was observed to be considerably higher in the vicinity of large diameter cortical draining veins, consistent with observations in humans (Davis et al., 1998) and rats at 4.7T (Liu et al., 2004) and 11.7T (Keilholz et al., 2006) field strengths. The spatial distribution of the parameter M did not vary significantly between subjects, hence, an average M map was calculated for nine subjects (Figure 3-1, panel M, Table 3-1). S1 and CG exhibited larger increases than midbrain nuclei, and only a moderate increase was observed in the hippocampus. Modest, but significant increases in CBF within the VTA and SN must be interpreted cautiously because of low signal to noise, susceptibility artifacts, and partial volume effects in these regions. Changes in CMRO₂ after cocaine administration were positive in all regions of the brain studied, ranging from 17% to 38% (Table 3-1 and Figure 3-1, panel Δ CMRO₂). Along the cortical surface a decrease in BOLD was often observed while CBF and calculated CMRO₂ changes were observed to be positive, suggesting that the negative BOLD signal change within these cortical areas is not the result of image or motion artifacts (Figure 3-1, red box). The time courses of BOLD, CBF, and CMRO₂ changes for a representative subject (Figure 3-2) illustrate the rapid and sustained increases in BOLD and CBF within S1, while the increases in these measures were considerable smaller in the NAc.

The parameter M relates changes in CBF and BOLD to changes in oxidative metabolism, and the BOLD and CBF changes observed for several ROIs with M values of 0.10 ± 0.02 are indicated in Figure 3-3. Iso-contour lines in Figure 3-3, panel a illustrate the expected changes in BOLD and CBF for given changes in CMRO₂ within a region having an M value of 0.10 and illustrate that negative changes in BOLD may be

observed in regions experiencing dramatically increased oxidative metabolism, potentially leading to erroneous inferences made from BOLD measurements alone. Changes in CBF and CMRO₂ were linearly correlated by a ratio of approximately 2.8:1 (Pearson's $r = 0.92$) (Figure 3-3, panel b), and BOLD and CMRO₂ were also linearly correlated ($r = 0.79$) (Figure 3-3, panel c). Two regions, the VTA and PAG, exhibited a negative and near-zero BOLD response but showed a significant increase in CBF, corresponding to an increase in CMRO₂ (Figure 3-3, panel c). One region, the SN, deviated significantly from the correlative relationship observed between changes in BOLD, CBF, and CMRO₂ exhibited by the other regions investigated, suggesting that the large increase in BOLD observed in this ROI may be an artifact.

Discussion

This study demonstrates the use of BOLD, CBF, and CMRO₂ functional MRI after intravenous cocaine administration in the anesthetized rat with concomitant physiological measurements (MABP, HR, and RR). Cocaine evoked significant and heterogeneous changes in BOLD, CBF, and CMRO₂ within the mesocortical limbic pathway and throughout other regions of the brain. With the exception of negative BOLD changes in some cortical surface areas, and within the VTA, BOLD, CBF, and CMRO₂ changes were positive. Brain regions exhibiting increases in CMRO₂ are consistent with regions identified as having increased metabolism of glucose in 2-deoxyglucose autoradiography studies reported previously (Porrino et al., 1988), and the changes in CBF that were observed are consistent with previously reported results (Stein and Fuller, 1992).

BOLD fMRI of cocaine using similar doses has been previously reported in rats (Chen et al., 2001; Mandeville et al., 2001; Luo et al., 2003), although the magnitude and sign of the BOLD responses varied between labs. Negative BOLD near the surface of the cortex (but not in the subcortical structures) associated with cocaine challenge was consistently observed in the present study. Such negative BOLD could be due to a marked cocaine-evoked increase in deoxyhemoglobin concentration in the large draining veins on the cortical surface (Krings et al., 1999). The susceptibility effects of high deoxyhemoglobin concentration in these veins would be enhanced at higher field strength, such as the 4.7T field strength used in this study. Spin-echo BOLD experiments which are less sensitive to macrovascular contributions (Duong et al., 2003) could be used to further investigate the origin of this negative BOLD signal, and may improve the estimation of changes in $CMRO_2$ by suppressing macrovascular contributions, and preventing a possible overestimation of changing $CMRO_2$ in these regions.

While others have reported scattered negative BOLD responses throughout the brain (Luo et al., 2003), our previous work with forepaw stimulation under similar experimental conditions (Liu et al., 2004) did not show negative BOLD changes on the cortical surface. This suggests that the negative BOLD effect observed here is biological in origin and related to the effects of systemic cocaine challenge. Mandeville and others (Mandeville et al., 2001) did not observe significant negative BOLD changes at 2T. These differences may be due to differences in experimental conditions (e.g. anesthetics and ventilation protocols) and possibly may be due to magnetic field dependent effects. Anesthesia, in particular has been shown to impact the measured BOLD signal (Sicard et

al., 2003). Additionally, variations in the reported values of BOLD signal changes between labs may suggest that BOLD fMRI is more susceptible to non-neural physiological phenomena and the precise experimental conditions, than to changes in neural activity alone. For example, BOLD signal change is strongly dependent on baseline CBF and blood oxygenation (Sicard et al., 2003; Uludag et al., 2004). Vasoconstriction has been reported following cocaine administration (Kaufman et al., 2001; Luo et al., 2003) and has been shown to cause negative changes in BOLD and CBF (Gollub et al., 1998). This explanation of the negative BOLD observed in this study is difficult to reconcile with the consistent observation of increased CBF in pertinent regions.

In contrast to changes in BOLD, reported changes in CBF following cocaine administration are reasonable consistent between laboratories, despite differences in experimental conditions, anesthetics, and measurement techniques. Positive CBF increases were observed throughout the brain and were particularly pronounced in the neocortices. Our results are in good agreement with increases in CBF after cocaine administration measured by using [^{14}C]iodoantipyrine in awake rats (Stein and Fuller, 1992). Our estimated CBV changes, obtained from CBF changes and the Grubb et al.'s relation (Grubb et al., 1974) in the cingulate gyrus (CG), nucleus accumbens (NAc), motor cortex (S1), dorsal thalamus (VPL), and striatum are linearly correlated ($r = 0.96$) with the CBV changes measured using a monocrystalline iron oxide nanocolloid (MION) contrast agent (Marota et al., 2000), although our estimated CBV changes were consistently larger (Figure 3-4).

Non-invasive CMRO₂ fMRI offers a valuable surrogate measure of neural activation. Increased neural activity has been shown to be correlated with an increased rate of glucose metabolism (CMRGlu) (Kennedy et al., 1976; Sokoloff et al., 1977) and CBF (Jones et al., 2004), however, the magnitude of stimulus-evoked changes in CMRO₂ remains controversial. Original work using PET revealed a lower than expected change in CMRO₂ with increasing neural activity (Fox et al., 1988), while other reports have indicated a potent (200% - 400%) increase in CMRO₂ following increased neural activity (Hyder et al., 1996), fueling the debate as to whether increases in metabolic demand within the neuropil are satisfied by aerobic or anaerobic metabolism of glucose. A recent investigation of this question suggests that neural metabolism during stimulation is primarily oxidative, and that anaerobic processes within the astrocytes primarily function to supply neurons with lactate for oxidative degradation to ATP (Kasischke et al., 2004), lending credence to the viability of CMRO₂ as a marker for neural activity. Although CMRO₂ changes associated with cocaine administration have not been reported previously for comparison, the magnitudes of CMRO₂ changes reported herein were consistent with those reported using various sensory stimuli.

Figure 3-1

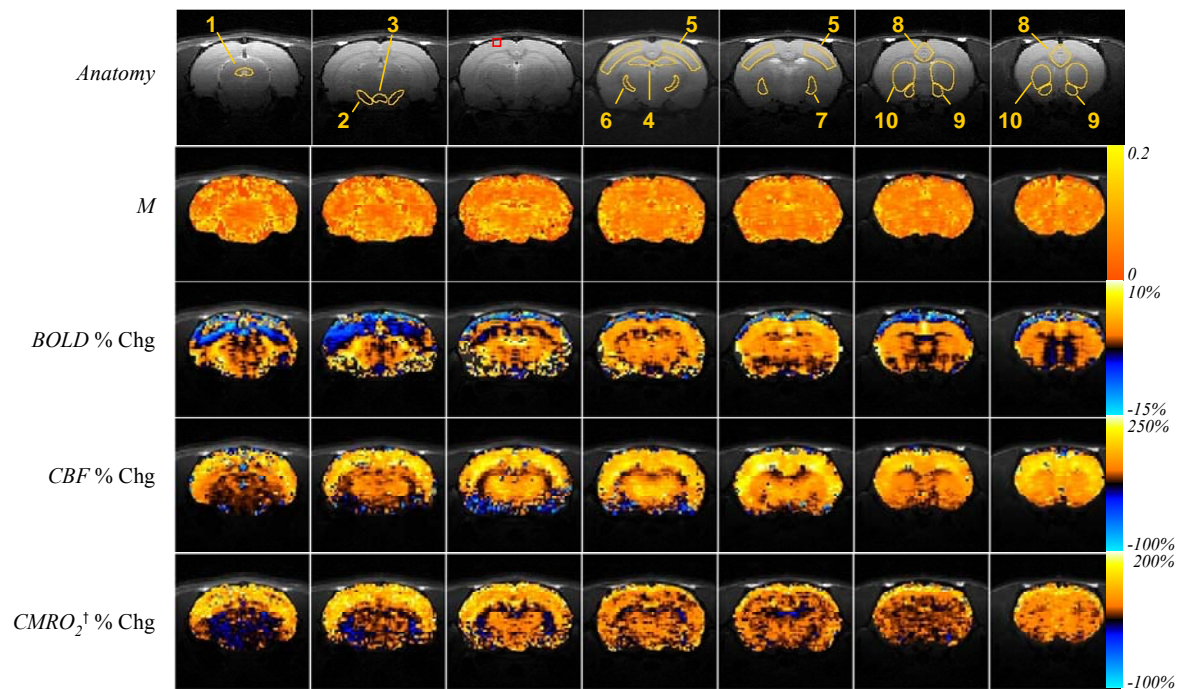


Figure 3 – 1: Group average changes in BOLD, CBF, estimated CMRO₂.

BOLD, CBF, and CMRO₂ changes are shown for all subjects (N = 11) and the mean calibration parameter M (N = 9) in the anesthetized rat brain following intravenous administration of 1.0 mg/kg cocaine. Color scales to the right indicate the extent of positive and negative changes, or the value of the parameter M. ROIs used in the quantitative analysis reported in Table 3 – 1 are indicated on the anatomical images. 1—Periaqueductal gray (PAG); 2—substantia nigra (SN); 3—ventral tegmental area (VTA); 4—hippocampus (Hip); 5—primary somatosensory cortex (S1); 6—ventral posterolateral thalamic nucleus (VPL); 7—lateral globus pallidus (LGP); 8—cingulate cortex (CG); 9—nucleus accumbens (NAc); 10—striatum. A cortical ROI which exhibited negative changes in BOLD but positive changes in CBF and CMRO₂ is indicated by a red box. Figure reproduced from (Schmidt et al., 2006).

Table 3-1

	$M_{N=9}$	$\Delta BOLD_{N=11}$	$\Delta CBF_{N=11}$	$est. \Delta CBV^{\dagger}_{N=11}$	$\Delta CMRO_2^{\dagger}_{N=11}$
<i>PAG</i>	0.05 ± 0.005	0.1 ± 0.2*	16 ± 1	5 ± 0	10 ± 3
<i>SN</i>	0.17 ± 0.01	5.4 ± 1.0	25 ± 5	5 ± 1	12 ± 3
<i>VTA</i>	0.16 ± 0.02	-1.2 ± 0.5	14 ± 3	4 ± 1	14 ± 2
<i>Hip</i>	0.11 ± 0.005	1.5 ± 0.2	52 ± 4	16 ± 1	24 ± 3
<i>S1</i>	0.12 ± 0.01	3.7 ± 0.2	150 ± 9	39 ± 1	46 ± 3
<i>VPL</i>	0.11 ± 0.01	2.5 ± 0.2	80 ± 6	21 ± 1	24 ± 4
<i>LGP</i>	0.08 ± 0.01	1.4 ± 0.1	49 ± 3	15 ± 1	17 ± 2
<i>CG</i>	0.18 ± 0.01	3.6 ± 0.4	128 ± 9	33 ± 2	55 ± 5
<i>NAC</i>	0.09 ± 0.01	0.6 ± 0.2*	64 ± 7	15 ± 1	34 ± 5
<i>Striatum</i>	0.11 ± 0.01	1.6 ± 0.2	80 ± 6	21 ± 1	33 ± 3

[‡] Percent change in CBV maps are calculated according to: $1 + CBV \% \text{ change} = (1 + CBF \% \text{ change})^{0.38}$

$P > 0.01$ *

[†] Percent change maps calculated using a single *M* map combined from 9 subjects

PAG = periaqueductal gray; *SN* = substantia nigra, *VTA* = ventral tegmental area; *HIP* = hippocampus;

S1 = primary somatosensory cortex; *VPL* = ventral posterolateral thalamic nucleus; *LGP* = lateral globus pallidus;

CG = cingulate cortex; *NAC* = nucleus accumbens

Table 3 – 1: Quantitative changes in BOLD, CBF, estimated CMRO₂ and the parameter *M* in various regions of interest following intravenous administration of 1.0 mg/kg cocaine.

Significance was determined against baseline using a two tailed t-test without a multiple comparisons correction. Table reproduced from (Schmidt et al., 2006).

Figure 3-2

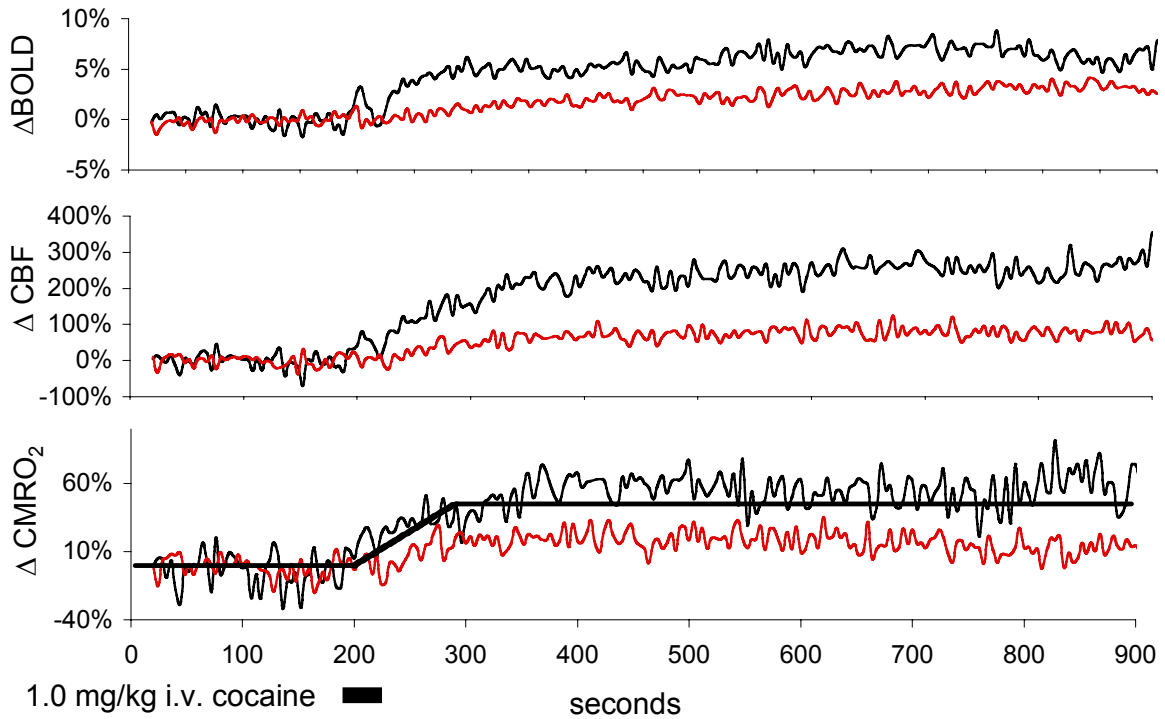


Figure 3 – 2: Time dependent changes in BOLD, CBF, and CMRO₂ for a single subject

Time dependent changes measured for two regions of interest are shown: black lines represent primary somatosensory cortex (S1) and red lines represent nucleus accumbens (NAc). The black line represents the single step model used for analysis. Figure reproduced from (Schmidt et al., 2006).

Figure 3-3

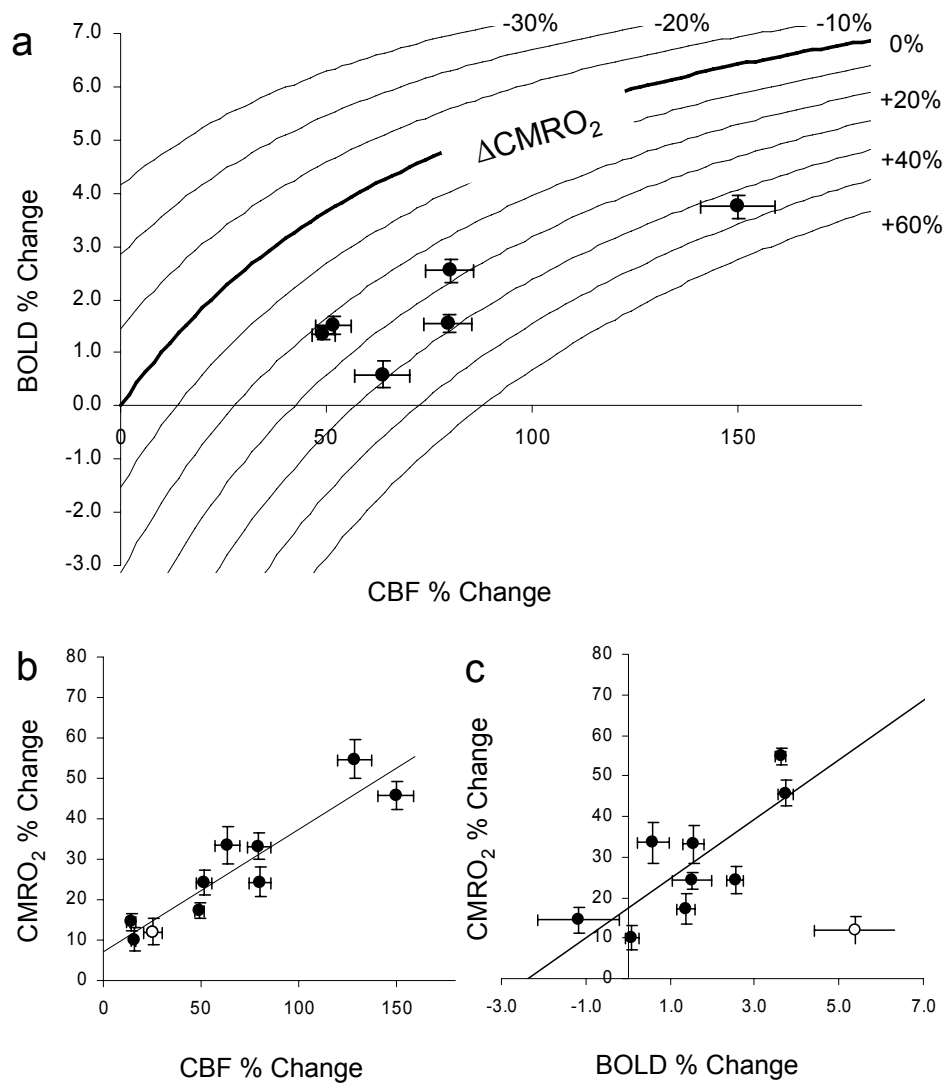


Figure 3 – 3: Relationship among CBF, BOLD, and CMRO₂ changes following intravenous administration of 1.0 mg/kg cocaine obtained from different brain regions.

(Mean values, error bars illustrate SEM, N = 11). (a) CBF and BOLD changes for the regions of similar M value (Hip, S1, VPL, LGP, NAc, and striatum). Iso-countour lines indicate the expected coupling of changes in CBF and changes in BOLD under conditions of increased or decreased CMRO₂ (M = 0.1). (b, c) Changes in CMRO₂ as a function of CBF and BOLD changes. Lines indicate the least square linear regressions for data point that are indicated by closed circles (Pearson's r: b: 0.92, c: 0.79). The substantia nigra (open circle) was excluded from the analysis in (b) and (c). Figure reproduced from (Schmidt et al., 2006).

Figure 3-4

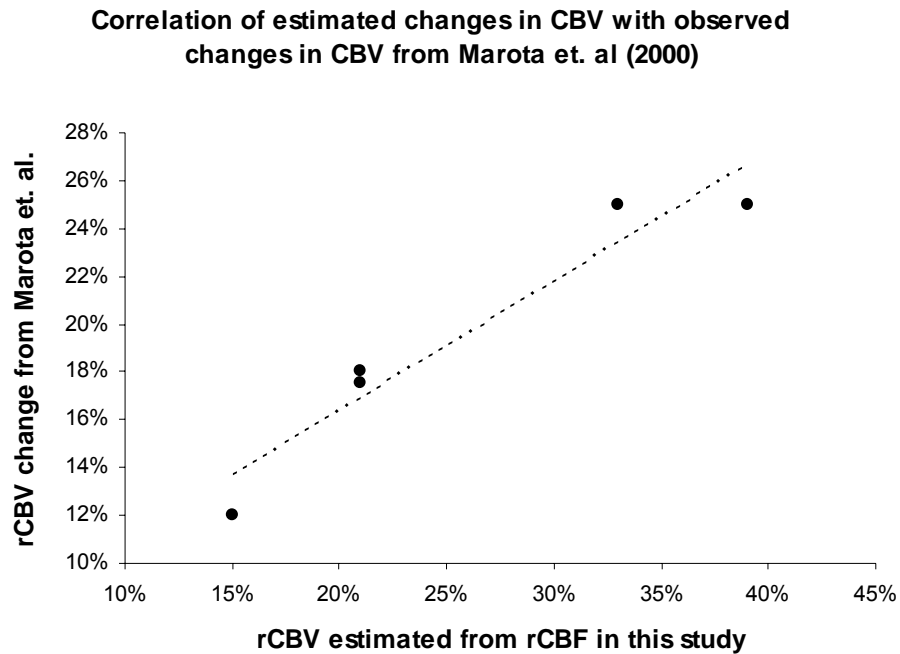


Figure 3 – 4: Estimates of changes in CBV from this study are correlated with reported changes in CBV following a similar dose of cocaine that were measured using MION contrast agent

Estimates of changes in CBV derived from measurements of CBF (Grubb et al., 1974) made in this study are correlated (Pearson's $r = 0.96$) with direct measurements of changes in CBV using MION, but estimated changes in CBV from this study were consistently larger than those reported by (Marota et al., 2000).

CHAPTER IV

WHOLE BRAIN ANALYSIS OF MULTIPLE SUBJECTS MANDATES SPIN ECHO MRI ACQUISITION: DEVELOPMENT OF A 3 COIL SYSTEM FOR MULTI-MODAL IMAGING IN CONSCIOUS ANIMALS

The work presented in this chapter is reproduced with minor changes in text from a manuscript in revision to the Journal of Neuroscience Methods described on the copyright page. This work was conducted under the direction of Dr. Craig Ferris, with significant contributions from Dr. Rostislav Lemdiasov, Mathew Brevard, and other authors. It is with great gratitude to Drs. Ferris and Lemdiasov, and to other authors that I reproduce these results in this dissertation. My contributions to this work consisted of the execution of animal experiments and required modification of MRI protocols, data analysis, synthesis of the text presented here, and in the contribution of design recommendations to Dr. Lemdiasov.

Introduction

Functional magnetic resonance imaging (fMRI) of conscious animals can be used to non-invasively map changes in neural activity within the brain with high spatial and temporal resolution (Lahti et al., 1998; Ludwig et al., 2004) and is a growing area of research with direct relevance to the fMRI research performed in humans in the clinic. The investigation of drugs, sensory perception, and cognition within the conscious animal using fMRI techniques has the potential to eliminate the confounding effects of anesthetics and to enable the observation of cognitive processes which are unobservable in the anesthetized state, such as arousal and reward (Ferris et al., 2001; Ferris et al., 2005). The use of integrated coil and restraint systems to perform fMRI in the conscious animal has been previously demonstrated using a variety of imaging techniques (Lahti et al., 1998; Khubchandani et al., 2003; Ludwig et al., 2004), but continued progress in this emerging field depends upon the development and application of improved imaging capabilities to fully realize the potential of fMRI in the conscious animal.

Blood-oxygen-level-dependent (BOLD) imaging is used extensively in fMRI to assess neural activation, where localized changes in blood deoxyhemoglobin concentration and changes in blood volume due to increased metabolism in the surrounding neuropil contribute to detectable changes in image intensity (Ogawa et al., 1993; Boxerman et al., 1995b; Nair, 2005). BOLD contrast can be measured using gradient-echo (GE) acquisition which is sensitive to local changes in $R2^*$ relaxivity, or it can be measured using spin-echo (SE) acquisition which is sensitive to changes in $R2$

relaxivity. Images acquired with GE sequences suffer from susceptibility artifacts in regions containing magnetic field inhomogeneities that cause tissue to undergo rapid $R2^*$ relaxation, and these artifacts confound the investigation of neural activation in many areas of the brain. In contrast, SE acquisition provides superior coverage of these brain regions by reducing susceptibility artifacts, and SE BOLD contrast, while reduced in magnitude with respect to GE BOLD contrast, has been shown to suppress the contribution from large draining veins, providing a more localized signal originating from changes in deoxyhemoglobin concentration and blood volume within the microvasculature (Boxerman et al., 1995b; Bauer et al., 1999; Silvennoinen et al., 2003; Jochimsen et al., 2004; Hulvershorn et al., 2005). Additionally, SE acquisition requires that all tissue within the brain experience uniform 90° and 180° excitations, indicating the use of transmission coils whose field geometries are uniform across all areas of the brain. Consequently, optimal conditions for fMRI using SE acquisition typically entail a two-coil configuration where uniform excitation is achieved through the use of a volume resonator, and an electronically decoupled surface coil is used for detection of the emitted nuclear magnetic resonance signal.

Detection of localized changes in cerebral blood flow (CBF) is an additional fMRI measurement that can be used to infer changes in neural activity (Colebatch et al., 1991; Madsen et al., 1991; Hoge et al., 1999b; Kim et al., 1999; Mandeville et al., 1999) and various techniques for measuring CBF by MRI are reviewed in (Barbier et al., 2001). Arterial spin labeling fMRI protocols are able to detect changes in CBF and use water molecules within the blood as an endogenous tracer, eliminating the need for exogenous

contrast agents. The reduced contrast to noise ratio of CBF measurements made using arterial spin labeling techniques with respect to changes in the BOLD signal (Lu et al., 2003) often precludes the use of CBF measurements alone in fMRI experiments. However, when changes in BOLD and CBF are monitored simultaneously it is possible to use redundancy between the two measures to identify image artifacts due to non-neural phenomenon, and it is also possible to make quantitative inferences of metabolic changes in the underlying tissue (Davis et al., 1998; Hoge et al., 1999b; Kim et al., 1999). Continuous arterial spin labeling (CASL) is a technique which is commonly used to acquire simultaneous measurements of BOLD contrast and CBF, and requires, in the case of multi-slice imaging experiments, that an additional coil be placed near the neck of the animal for arterial spin inversion (Silva et al., 1995; Zhang et al., 1995).

It was the goal of this study to explore the feasibility of simultaneously measuring changes in SE BOLD and CBF in the conscious rat. A novel three coil system and integrated restraint was developed which uses a volume coil for uniform excitation of all tissue within the brain, a surface coil located above the brain for improved detection of the emitted signal, and a small surface coil located below the neck of the animal for arterial spin inversion. Longer acquisition times associated with SE BOLD weighted images revealed arterial spin labeling contrast dynamics predicted by kinetic models (Buxton et al., 1998) and illustrate an intrinsic limitation of the multislice CASL imaging technique. Functional activation was observed using electrical hindpaw stimulation, and illustrates the potential of this coil configuration to measure changes in SE BOLD and CBF within the conscious animal in a single experimental setting.

Materials and Methods

MRI experiments were carried out on a 4.7T/40cm magnet (Oxford, UK), Bruker Biospec console (Bruker BioSpin Corp., Billerica, MA), and a 20 G/cm gradient with 12 cm inner diameter and 120 μ s rise time. Three actively decoupled coils were used for imaging: a 10 cm microstrip resonator volume coil was used for excitation, a 2.5 cm surface coil was used for detection, and a butterfly coil located beneath the neck of the rat was used for arterial spin labeling (Insight Neuroimaging LLC., Worcester, MA). Images were acquired using the pseudo-continuous arterial spin labeling (pseudo-CASL) technique with a single shot spin echo echo-planar-imaging (SE EPI) sequence. Arterial spin labeling was accomplished with a square radiofrequency pulse of varying duration (1 s – 4 s) in the presence of a 1.0 G/cm gradient along the direction of blood flow in the carotid arteries, satisfying the adiabatic fast passage inversion condition. The frequency offset of the labeling pulse was reversed with respect to the center of the imaging geometry during control image acquisition. Acquisition parameters were: data matrix = 64 x 64, FOV = 3.0 cm x 3.0 cm, nine 1.5 mm thick slices, TE = 54 ms, and TR = 2.7 s for the experiments illustrated in Figures 4 – 2a, 4 – 3 and 4 – 4. Data were analyzed using AFNI and custom software developed in the Java programming language (Sun Microsystems, Inc.) (Schmidt et al., 2004).

Male Sprague-Dawley rats weighing 400-450 g were studied. Rats were anesthetized with 1.2% isoflurane and placed into an integrated coil and head restraint system. Anesthesia was subsequently discontinued, and rats were allowed to fully recover consciousness before being placed in the magnet for imaging experiments. Air or air with

10% CO₂ concentration was continually supplied to the internal cavity of the coil and restraint system at a flow rate of 2.0 L/min. During electrical hindpaw stimulation experiments, electrodes were placed subcutaneously in both hind paws, and an electrical pulse of 0.33 ms duration and 1.5 mA was delivered at 3 Hz for a period of 130 s.

Results

The three coil imaging and restraint system that was developed is illustrated in Figure 4 – 1. Based upon an existing coil and restraint system (Insight Neuroimaging, LLC.) a third coil for arterial spin labeling was positioned below the carotid arteries of the rat. The third coil contains a figure 8 loop with crossover which is 1 cm in width and 5 mm in length, and field simulations of this coil geometry (Figure 4 – 2, panel a) predicted uniform coverage of the carotid arteries. Tuning, matching and decoupling circuitry was located 20cm from the neck coil to remove the animal from contact with electrical components. A coaxial cable with minimal impedance connected the neck coil loop to electronic tuning and matching circuitry that was designed using the Advanced Design System software (Agilent Technologies, Inc. Palo Alto, CA).

The field distribution of the neck coil (ASL coil) was optimized with a custom software application (Lemdiasov, 2004) capable of predicting the magnetic flux density beneath the neck of the rat. A multi-channel decoupling circuit (Figure 4 – 2, panel b) was implemented at the interface between the MR system and the three RF coils, and the volume transmit and surface receive coils were detuned during the application of the arterial labeling pulse. This circuit uses a control signal implemented in the pulse

sequence to switch the active coil during arterial labeling, excitation, and signal detection via p-type, intrinsic, n-type (PIN) diodes implemented in the three coils. The quality factor of the dedicated arterial spin labeling coil loaded with a conscious 400g rat ranged between 3 and 4. Due to the location of the surface coil used for signal detection, and the limited detection sensitivity of the volume coil used for excitation, direct measurements of arterial spin inversion efficiency by examination of the carotid arteries were not made. However, estimates of labeling efficiency made by comparison of ASL contrast to contrast obtained with other coils with known efficiency and an estimate by non-linear regression to a dynamic model of ASL contrast (Figure 4 – 3, panel b) suggest inversion efficiency values between 75 and 80 percent.

Spin echo BOLD contrast is measured simultaneously with appropriate T2 weighting of the control image that is acquired during the CASL experiment. Figure 4 – 3 (panel a) illustrates the change in ASL contrast and BOLD contrast as measured in a whole brain region of interest during an experiment in which a 10% CO₂ challenge was applied after baseline signal collection. Contrast between the labeled and control experiments (ASL contrast) is visible as the difference in signal intensity between sequential images, and the change in BOLD contrast following the CO₂ challenge is apparent as the change in signal intensity of the control images only. In this manner, consistent sampling of changes in CBF and BOLD contrast are acquired throughout the duration of the experiment, and concomitant increases in both CBF (as revealed by increased ASL contrast) and BOLD contrast following CO₂ administration are apparent.

The CASL technique applies an arterial label for a duration sufficient to establish the maximum contrast between control and labeled images, typically requiring a label duration of more than three seconds. However, in practice, it is common to abbreviate the label duration (i.e. pseudo-CASL) in order to increase the number of acquired images and, hence, the signal-to-noise ratio of data collected in a fixed length experiment. Dynamics that describe the approach to maximal contrast between the control and labeled images during the label application period, and the decline in contrast following the termination of the label have been previously described (Equation 4.1), and observed in arterial spin labeling experiments in humans (Buxton et al., 1998). In this equation, f is rate of cerebral blood flow, $\Delta M(t)$ is the change in magnetization within a voxel at time t , Δt is the transit time for blood from the label location to the voxel, τ is the label duration, α is the inversion efficiency, M_{OB} is the initial magnetization of blood in the voxel, T_{1B} is the T_1 of the blood in the voxel, and T_1' is the apparent T_1 of the tissue and blood in the voxel. These theorized dynamics accurately predict the rise and fall of ASL contrast in pseudo-CASL experiments observed in the conscious animal under 10% CO_2 administration using SE echo-planar-imaging (EPI) acquisition (Figure 4 – 3, panel b). Model parameters for the regression displayed in Figure 4 – 3 (panel b – solid lines) were determined by non-linear regression of Equation 4.1 to observed data using supplied parameters for CBF (200 mL/100mg-min under 10% CO_2), T_1 of blood at 4.7T and 37°C (1.9s), label duration (1.75s), and transit time (150ms). The apparent T_1 of tissue and labeling efficiency were determined to be 1.16s and 0.79, respectively.

$$f = \frac{\Delta M(t) e^{(t-\Delta t-\tau)/T_1'}}{2M_{OB}T_1'\alpha e^{-\Delta t/T_{1B}} (1 - e^{-\tau/T_1'})} \quad (4.1)$$

Of particular interest in simultaneous SE BOLD and CBF acquisition is the time dependent drop in ASL contrast following termination of the labeling pulse (Figure 4 – 3, panel b, grey line). Longer echo times associated with SE BOLD weighting prolong slice acquisition time and prolong the total acquisition time in multi-slice imaging experiments with respect to GE BOLD weighted acquisitions. Changes in contrast due to post-labeling acquisition delays introduce systematic errors that must be accounted for in quantitative calculations of CBF, and, although these contrast changes are self correcting in measurements of relative CBF change for images acquired with the same post labeling delay, the corresponding change in the contrast to noise ratio of the relative CBF measurements impacts the effect size of relative changes in CBF ($t_{\Delta f}$) in a manner dependent on the post-label delay duration (Equation 4.2).

$$t_{\Delta f} = \frac{\Delta f}{\sigma_M e^{(t-\Delta t-\tau)/T_1'}} \quad (4.2)$$

This change in effect size affects analyses that apply a uniform statistical threshold to all slices, as is the practice in many software analysis packages, and Figure 4 – 4 illustrates statistical parametric map artifacts that result from different post-label delays associated with each slice in a multi-slice SE BOLD CASL experiment. Following a 10% CO₂ challenge, both BOLD and CBF are increased throughout the brain, BOLD signal increases of up to 10% and CBF increases of more than 100% were observed. Applying a uniform statistical threshold to maps of relative changes in BOLD and CBF reveals a

deficit of voxels containing significantly increased CBF in slices acquired with increasing post labeling delays (Figure 4 – 4).

Despite these limitations, it is possible to use the pseudo-CASL technique to simultaneously measure SE BOLD and CBF changes resulting from electrical hindpaw stimulation in the conscious rat. Dramatically increased signal variance due to motion artifacts requires that ROI analyses of data from multiple animals be used as a reliable measure of activation. Figure 4 – 5 illustrates the change in BOLD and CBF measured in the hindpaw somatosensory region. Median values of changes in SE BOLD and CBF for 7 animals reflect a rapid increase in both measures following the start of electrical stimulation, and these changes are sustained for a period following the termination of stimulation. Mean values of Δ BOLD and Δ CBF for all animals during the initial baseline and stimulation epochs reflect increases in BOLD and CBF (1.2% and 49%, respectively) which are significant ($p < 0.05$) at the group level only, a result of the large variance in these signals as measured in the conscious animal.

In this study, the use of a novel 3 coil imaging and restraint system has been demonstrated to simultaneously measure changes in SE BOLD and ASL contrast in the conscious rat. Changes in SE BOLD and ASL contrast following a 10% CO₂ challenge reflect increases which are consistent with observations using alternate image acquisition protocols in anesthetized animals (Sicard et al., 2003). Dynamic changes in ASL contrast are accentuated by the longer acquisition times associated with SE BOLD contrast, and must be taken into account in the statistical analysis of combined SE BOLD and ASL imaging protocols based on the pseudo-CASL technique. Despite this confound in the

specific case of SE BOLD weighted pseudo CASL protocols, the novel hardware configuration presented herein permits the combined use of ASL and SE imaging protocols in the conscious animal within the same setting, and is expected to have broad application in the fMRI research.

Discussion

The three coil imaging and restraint system developed in this study presents a novel capability enabling two coil SE imaging and ASL measurement of perfusion within the same experimental setting, and this work is the first demonstration of simultaneous SE BOLD and ASL acquisition in the conscious animal using three radiofrequency coils. With sufficient improvements in sensitivity, the signal to noise ratio of this technique will be adequate to make metabolic inferences with a calibration experiment, in conscious or anesthetized animals. Currently, this system enables ASL experiments to be conducted in conjunction with traditional two-coil imaging experiments in conscious or anesthetized animals, without requiring a reconfiguration of the imaging coils or removal of the animal from the magnet.

The large variance of the BOLD and CBF measurements is an impediment to imaging experiments using conscious animals. While immobilization of the skull can be achieved using stereotactically positioned ear bars and a bite bar, contractions of the jaw and facial muscles can contribute to phase encoding artifacts that contaminate voxels within the brain, deleteriously affecting measurements of both BOLD and CBF. Additionally, sub-voxel motion (less than 400 μm in rat studies) can cause partial volume

effects that confound statistical parametric mapping algorithms that examine each voxel independently (Turner et al., 1998). These artifacts are less severe following acclimation (King et al., 2005) and in functional imaging experiments that use non-aversive stimuli, such as neutral scents or anxiolytic and sedative drugs. Additionally, the ASL signal is sensitive not only to changes in signal intensity caused by these artifacts, but it is also sensitive to potential changes in arterial spin labeling efficiency caused by animal motion in the region of the neck coil.

Dynamics of ASL contrast are a limiting factor in multi-slice imaging experiments designed to measure CBF where the acquisition time is long. Quantitative CBF measurements from CASL and pseudo-CASL protocols are particularly susceptible to these dynamics and require a correction to compensate for post-labeling delays. Although the loss of ASL signal does not affect measurements of relative CBF change as calculated from slices acquired with the same post-labeling delay, the loss of ASL contrast with increasing post-labeling delay directly impacts statistical parametric mapping algorithms commonly used to delineate areas of activation. Multi-slice experiments require that a slice-specific statistical threshold be used to create a uniform representation of activated regions.

Future studies are planned to improve the stability of the ASL signal and increase the sensitivity of CBF measurements made within the conscious animal. These improvements may be accomplished by improving arterial inversion efficiency and reducing the susceptibility of inversion efficiency to animal motion on the neck coil, a suspected source of the variability observed in our measurements. Modified neck coil

geometries that increase the volume of the homogeneous B1 field surrounding the carotid arteries may be an effective strategy to address this challenge. Alternatively, ASL sequences using trains of hyperbolic secant adiabatic inversion pulses of shorter duration than the block pulse used in adiabatic fast passage may reduce the probability that spurious animal motion adversely affects inversion efficiency. The use of less aversive stimuli than the noxious electrical hindpaw stimulation used in this study also reduces animal motion and improves ASL stability, an effect that is visible in the clear patterns of increased CBF following a benign CO₂ challenge. Improvements in the stability of concurrently measured ASL and BOLD signals would be a valuable advance, as a growing volume of research uses these measurements to map metabolic changes in neural tissue with the use of calibrated biophysical models.

Overall, the ability to perform arterial spin labeling in the conscious animal using a three coil imaging system represents a significant advance in fMRI research capabilities. In continuous ASL experiments measuring only CBF, it is possible to increase the label duration sufficiently to achieve the maximal contrast of the steady state condition, with gains in sensitivity with respect to the multi-modal pseudo-CASL approach used here. Such measurements can be made prior to, and following, a two coil BOLD fMRI experiment to control for perturbations in baseline CBF. These control measurements of CBF may be particularly valuable in pharmacological studies, where the drug under investigation may directly or indirectly interact with the cerebral vasculature, causing changes in the BOLD signal that are not the result of modulated neural activity. Anticipating future improvements in stability and sensitivity, three coil configurations

may enable novel multi-parameter functional imaging studies to investigate pharmacological mechanisms, cognition, and perception in the conscious animal. Additionally, the similarity of this configuration to perfusion imaging techniques used in the clinic suggest that this tool will be especially applicable to investigations using animal models of stroke, where there is direct translation between the MRI endpoints obtained in conscious animals to conscious humans in the clinic.

Figure 4-1

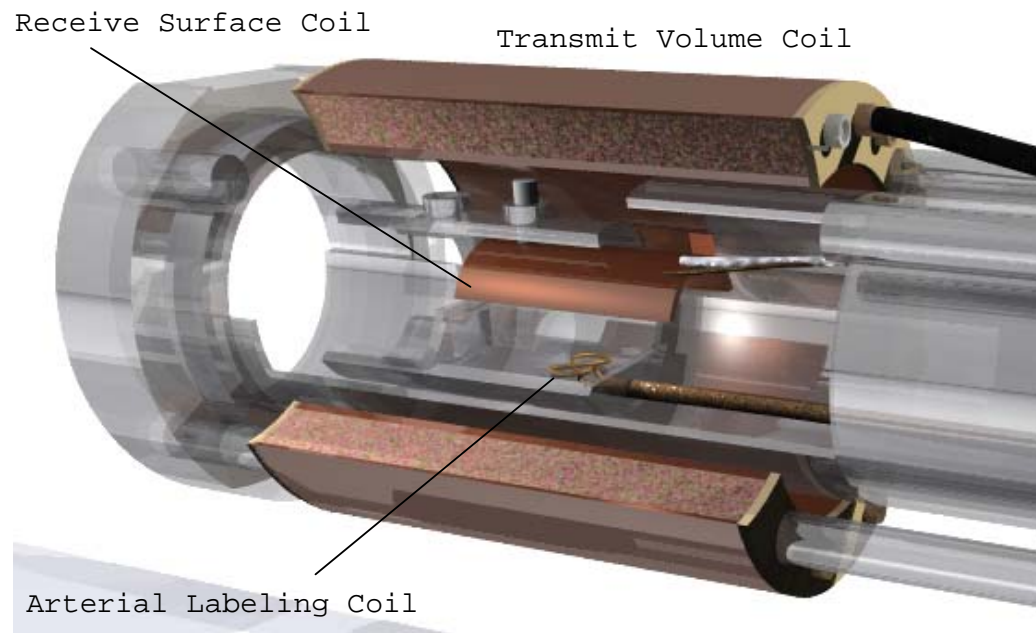


Figure 4 – 1: Three coil imaging and integrated restraint system.

A schematic of the system developed is illustrated. A micro-strip resonator volume coil is used for sample excitation, a concave surface coil located directly above the head of the rat is used for signal detection, and a butterfly (figure 8 geometry) coil located below the neck of the rat is used for arterial spin labeling. The three coils are integrated into a cylindrical animal restraint with a rigid bite bar, nose clamp, and ear bars to minimize animal motion (nose clamp and ear bars are not shown). Figure reproduced from manuscript in revision for Journal of Neuroscience Methods.

Figure 4-2

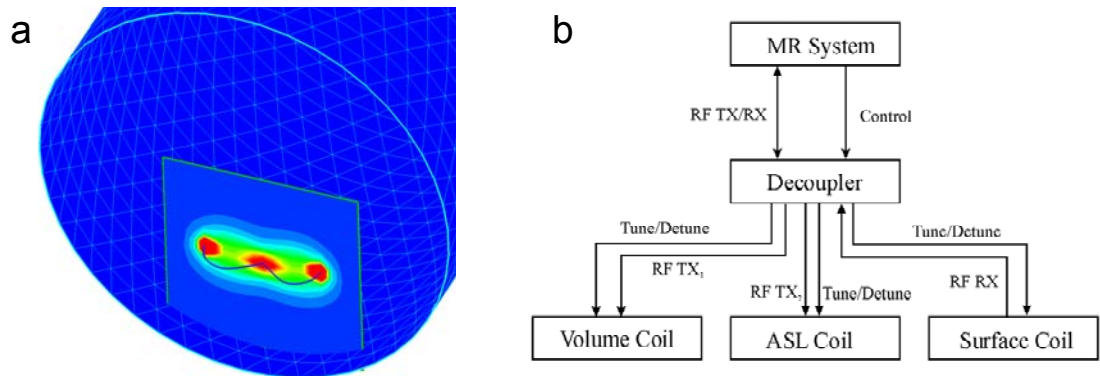


Figure 4 – 2: Simulated B1 field strength near the arterial labeling coil and active decoupling electronics.

(a) A simulation of the B1 field generated by the neck coil illustrates a homogeneous field in the region of the carotid arteries, and low field strength outside of this region, minimizing saturation effects in tissue of interest. (b) Schematic of the active decoupling circuitry implemented to switch the active coil during arterial labeling, excitation, and signal detection. Figure reproduced from manuscript in revision for Journal of Neuroscience Methods. Figure and legend produced by Rosti Lemdiasov.

Figure 4-3

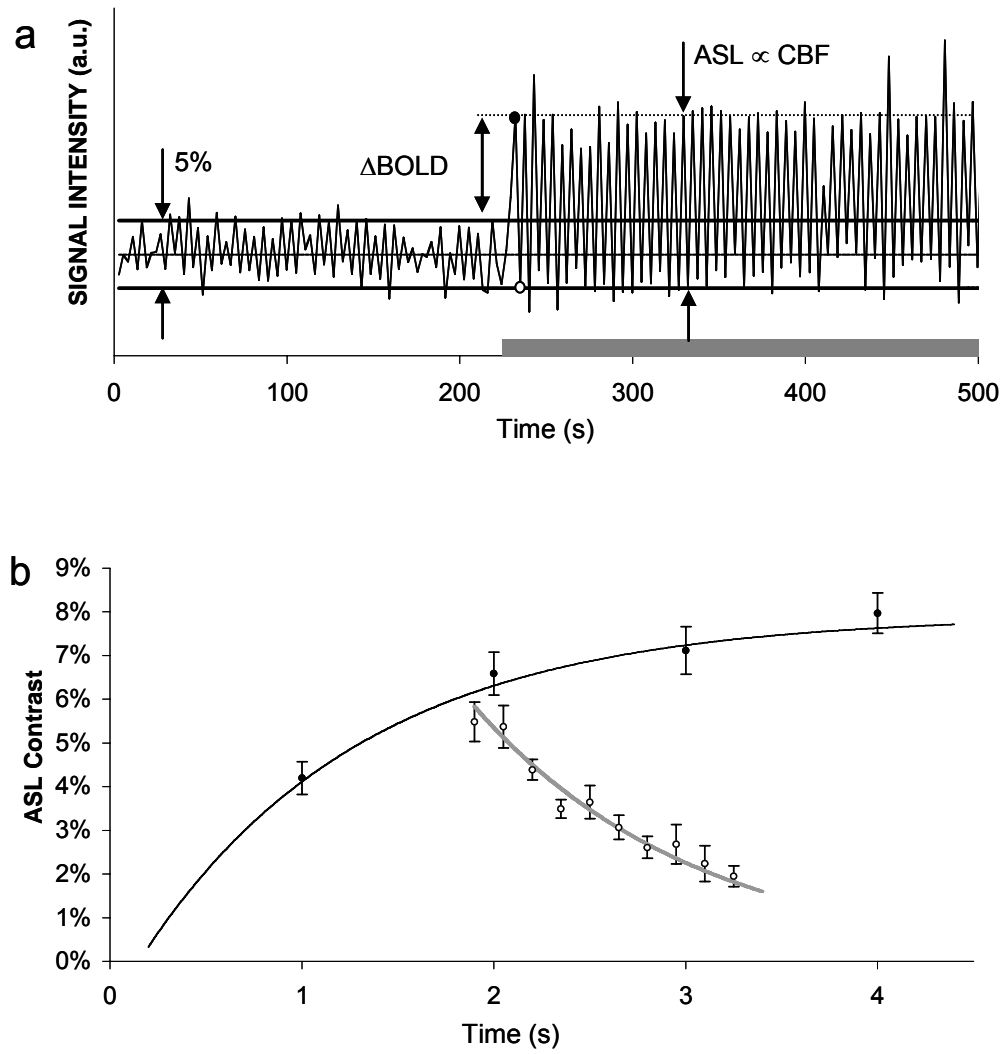


Figure 4 – 3: Arterial spin labeling contrast in pseudo-CASL with SE BOLD weighted acquisition

(a) Signal intensity measured from a single subject within a whole brain ROI during a 100 repetition pseudo-CASL experiment in which a CO₂ challenge was introduced after 220 s (grey bar), and sustained for the remainder of the experiment. Changes in CBF are assessed by the change in contrast between sequential control (high values, filled circle) and labeled (low values, open circle) signal intensities, and changes in BOLD are assessed by changes in the signal intensity obtained from control images only. (b) Arterial spin labeling contrast is accurately predicted by a kinetic model of arterial spin labeling contrast (Equation 4.1). Within whole brain regions of interest under continuous 10% CO₂ administration, contrast increases with increasing label duration (closed circles, N=6), and contrast declines to nominal levels following termination of the labeling pulse at 1.75s (open circles, N=12) in a manner consistent with the model (solid lines) using the following parameters: CBF = 200 mL/100mg-min, T₁ blood = 1.9s, T₁ apparent = 1.15s, labeling efficiency = 0.79, transit time = 150 ms. Error bars = SEM. Figure reproduced from manuscript in revision for Journal of Neuroscience Methods.

Figure 4-4

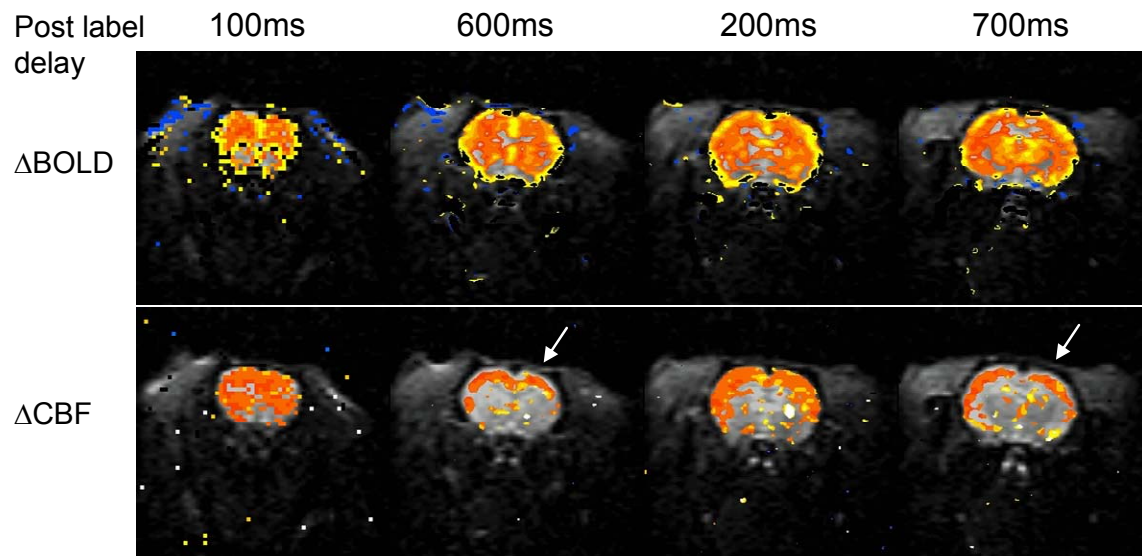


Figure 4 – 4: Effect size artifacts are visible in activation maps using statistical thresholds.

Four rostral slices from a representative subject acquired in an interleaved, 9 slice acquisition illustrate the effect size artifact resulting from varying post-label delays corresponding to the acquisition time for each slice (top). BOLD increases are seen globally throughout the brain (top row) and are equally significant in all slices. CBF changes are seen globally throughout the brain but fewer voxels contain significant increases with increasing post-labeling delay (white arrows). Color scale reflects 0-10% for BOLD maps, and 0-150% for CBF maps. Colored voxels illustrating BOLD changes were thresholded to significance greater than $P = 0.001$, and CBF voxels were thresholded to significance greater than $P = 0.01$. Figure reproduced from manuscript in revision for Journal of Neuroscience Methods.

Figure 4-5

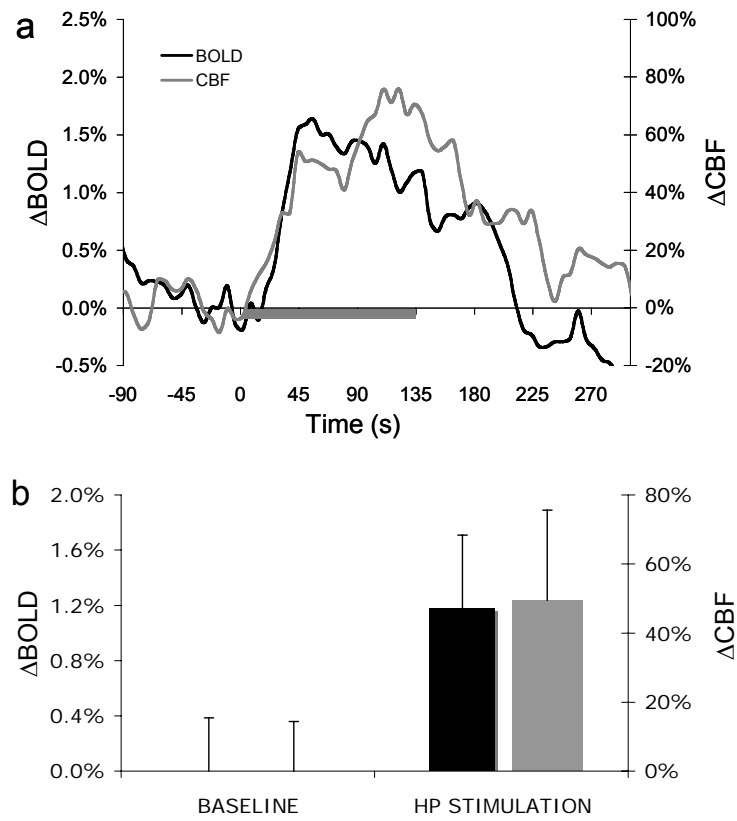


Figure 4 – 5: BOLD and CBF changes within the hindpaw primary somatosensory cortex following electrical stimulation.

(a) median changes in the BOLD and CBF signals as a function of time during a functional experiment using electrical hindpaw (HP) stimulation in the conscious rat (N = 7). Both BOLD and CBF signals increase rapidly following the onset of stimulation, and remain elevated after the termination of stimulation before returning to baseline. The BOLD signal continues to drop to a level below the initial baseline period following termination of the electrical stimulation. (b) mean changes during baseline and stimulation epochs reflect significant increases in BOLD (1.2 %, $P < 0.05$) and CBF (49%, $P < 0.05$). The large variances in these measurements reflect signal changes resulting from small amplitude motion of the animal within the restraint. (N = 7, error bars = SEM). Figure reproduced from manuscript in revision for Journal of Neuroscience Methods.

CHAPTER V

CONSCIOUS ANIMALS EXHIBIT A BOLD RESPONSE TO MORPHINE THAT DIFFERS FROM ANESTHETIZED ANIMALS

The work presented in this chapter has not yet been submitted for review. This work was conducted under the direction of Dr. Craig Ferris, where my contributions consisted of the design and execution of animal experiments, data analysis, and the synthesis of the text presented here.

Introduction

Changes in multiple functional MRI signals (e.g. CBF, CBV, and BOLD) can be readily observed following the administration of stimulants such as cocaine and amphetamine (Li and Suojanen, 1995; Marota et al., 2000; Mandeville et al., 2001; Luo et al., 2003; Schwarz et al., 2003; Schmidt et al., 2006), however, this class of drugs comprises only a fraction of the psychoactive compounds of potential interest in pharmacological fMRI investigations. The challenges of measuring changes in the fMRI signals that result from the administration of non-stimulant psychoactive compounds have not been fully resolved. Additionally, conflicting reports of both increases and decreases in BOLD signal intensity following the administration of cocaine to conscious animals (Febo et al., 2004; Mandeville et al., 2005) suggests that the cognitive status of the animal may have a profound effect on the observed changes in the fMRI signals. Although performing fMRI experiments with conscious animals requires additional technical considerations (Ludwig et al., 2004), if it is shown that pertinent differences are observed in the fMRI response from conscious vs. anesthetized animals, it is likely that this additional effort is necessary to probe the psychologically relevant actions of drugs that act on the central nervous system.

Opiates are a significant class of drugs that are used extensively for the clinical management of pain (Nestler, 2002; Katzung, 2004; Corbett et al., 2006), and that are frequently abused for their ability to induce a profound state of euphoria (American Psychiatric Association, 1994; National Institutes of Health, 1997; Katzung, 2004). The

beneficial use of opiates in clinical applications is complicated by serious side effects that emerge with sustained use including acquired tolerance and reduced analgesic effect, physical dependence, and psychological dependence as well as by acute side effects including constipation, respiratory depression, nausea, and reduced renal function (Katzung, 2004). The burden to the health care system due to opiate abuse is also significant; in 1997, the financial impact to society of the then approximately 600,000 opiate dependent addicts in the United States was estimated at greater than \$20B per year (National Institutes of Health, 1997). Presently, the number of opioid-dependent people in the US is estimated at about 750,000 (Katzung, 2004). As a result of the therapeutic interest in opiates with a reduced spectrum of adverse side effects and the need for more effective strategies to treat opiate addiction and stem illicit opiate use, the interaction of opiates with the central nervous system has been extensively studied at molecular and macroscopic scales.

Morphine is the prototype of clinical opioid analgesics, and both heroin and morphine are commonly abused by opioid addicts. Heroin is a prodrug that is metabolized to 6-monoacetylmorphine and morphine (Inturrisi et al., 1983; Corbett et al., 2006), which have high affinity for the μ opioid receptor that is distributed throughout several areas of the brain including the periaqueductal gray (PAG), nucleus accumbens and ventral tegmental area, the areas believed to mediate the effects of supraspinal analgesia and reward, respectively (Nestler et al., 2001; Squire et al., 2003). The opioid receptors μ (MOR), δ (DOR), κ (KOR) are G-protein coupled receptors that act to inhibit neurotransmitter release (Nestler et al., 2001; Williams et al., 2001; Corbett et al., 2006)

and differences in the localization of these receptors confer the differences observed in neural response to selective opioid receptor agonists. For example, agonism of the MOR causes an increase in neural activity within the PAG that is understood to result from inhibition of the GABAergic interneurons acting there (Williams et al., 2001), and it has been shown that agonists acting at MOR and other receptor subtypes can cause a reduction in glutamate, GABA, and glycine release throughout the CNS (Williams et al., 2001). Intravenously administered morphine has a half-life in the blood of approximately 1.9 h (Katzung, 2004), and users report that the euphoric, sedative, and anxiolytic effects of self-administration, a state referred to as being “on the nod”, are onset 5 – 15 minutes following administration, and maintained for a period of several hours, with diminishing effects observed on a subjective scale beginning after approximately 2 hr (Zacny et al., 1994).

Recently, fMRI was employed by several investigators to study the effects of opiates on neural activity within the rodent brain in anesthetized animals (Xu et al., 2000; Xi et al., 2002; Luo et al., 2004; Xi et al., 2004). This literature reports changes in the BOLD signal following heroin administration, and presents a valuable basis for comparison with data collected following morphine administration, an active metabolite of heroin. Of interest is the relatively short duration of BOLD signal changes reported in these studies of anesthetized rats, wherein the non-linear regressions that were used in these studies were tuned to a time scale that is relatively short, on the order of 10 min, compared to the pharmacodynamic profile of morphine.

In this study, we examined the effects of administering (0.3 mg / kg) morphine sulphate on the fMRI signals measured from conscious and anesthetized animals to investigate the potential differences between these experimental conditions. We also assessed the ability of multi-modal imaging to detect changes in BOLD and CBF following the administration of a non-stimulant, psychoactive compound. In conscious rats, this rewarding and analgesic dose of morphine reduced the frequency of struggle events, induced small and transient changes in heart and respiration rates, and induced a slow onset and regionally specific drop in the spin-echo (SE) BOLD signal that is consistent with morphine's pharmacokinetics. This response was not observed among anesthetized animals.

Materials and Methods

Animal preparation

Fourteen male Sprague Dawley rats (300 – 375 g) were studied. Vehicle (saline) or vehicle plus morphine sulphate (Sigma-Aldrich, St. Louis, MO) preparations were administered during the MRI experiments in an injection volume of 1 mL/kg and a dose of 0.3 mg/kg morphine sulphate for morphine scans. Tail veins were catheterized for vehicle or vehicle plus morphine administration under anesthesia. Rats were anesthetized with 1.2% isoflurane and placed into an MR compatible integrated coil and head restraint system (Insight Neuroimaging Systems, LLC., Worcester, MA). Anesthesia was either maintained or discontinued. For conscious scans, rats were allowed to fully recover consciousness in the restraint before imaging. Physiology was monitored by pulse

oximetry measured at the base of the tail, and recorded using a BioPak Systems data acquisition system (Santa Barbara, CA) at a sample rate of 5 ms.

MRI experiments

MRI experiments were carried out on a 4.7T/40cm magnet (Oxford, UK), Bruker console (Bruker BioSpin Corp., Billerica, MA). Concurrent measurements of changes in SE BOLD and CBF were acquired over a period of 15 minutes. Three actively decoupled coils were used for imaging: a 10 cm microstrip resonator volume coil was used for excitation, a 2.5 cm surface coil was used for detection, and a butterfly coil located beneath the neck of the rat was used for arterial spin labeling (Insight Neuroimaging LLC., Worcester, MA). Images were acquired using the continuous arterial spin labeling technique (CASL) (Silva et al., 1999) with a single shot spin echo echo-planar-imaging (SE EPI) sequence. Acquisition parameters were: data matrix = 64 x 64, FOV = 3.0 cm x 3.0 cm, nine 1.5 mm thick slices, TE = 55 ms, and TR = 2.7 s. During arterial spin labeled image acquisitions, a square radiofrequency labeling pulse of 1.75 sec duration was used for arterial spin inversion in the presence of a 10 G/cm gradient in the direction of blood flow, satisfying the adiabatic inversion condition (Williams et al., 1992). During the control image acquisitions, the frequency of the radiofrequency pulse was offset to correspond to a location outside of the anterior aspect of the animal that was equidistant from the center of the imaging planes as the labeling pulse (Silva et al., 1999). Control (unlabeled) and arterial spin labeled images were acquired sequentially, and 170 pairs of images were acquired during the experiments.

Data analysis

Data were analyzed using the software package AFNI (Cox, 1996) and custom software developed in Java (Sun Microsystems, Inc., San Jose, CA) (Schmidt et al., 2004). Small amplitude and subvoxel motion was corrected using the program 3dvolreg (Cox, 1996). BOLD measurements were derived from the control images in the acquired dataset, and quantitative CBF maps were calculated from each pair of images using equation 1.07 and the parameter values: $T1 = 1.54$ s, $\lambda = 0.9$, $\alpha = 0.7$ (Duong et al., 2000; Liu et al., 2004). BOLD and CBF image time courses were normalized to percent change on a voxel by voxel basis by division with the average value of the voxel during the baseline period preceding vehicle or morphine injection. Two scans of morphine administered to anesthetized rats, and three scans of saline administered to anesthetized rats exhibited a hardware related artifact that was removed with a low pass filter. A spectrogram was created from the pulse oximetry data for measurement of HR using a fast Fourier transform (Cooley and Tukey, 1965) implemented in Java, with a rolling aperture of 1024 samples (5.2 s). Animal motion events were derived from the pulse oximetry data by detection of rapid, large amplitude changes in excess of the physiological range of changes due to heart beats and respiration (amplitude change > 5 standard deviations of prior 200 samples). Due to artifacts in the spectrograms in some subjects as a result of animal motion, the pulse oximetry data were manually sampled with an interval of 10 s at 45 s and 200 s after the injection of morphine for the measurements displayed in Table 5-1.

To prevent co-registration errors between subjects as a result of the non-linear deformation of the SE EPI images, regions of interest (ROIs) were defined for each subject independently and average BOLD and CBF changes were measured from each ROI. Figure 5-1 illustrates the template used for the definition of ROIs (Paxinos and Watson, 1998); ROIs were defined bilaterally for the primary somatosensory cortex (S1), hippocampus, nucleus accumbens (NAc), cingulate cortex, association cortex, orbital cortex, olfactory nucleus, primary motor cortex (M1), caudate putamen (CPu), insular cortex, secondary somatosensory cortex (S2), lateral globus pallidus (LGP), piriform cortex, thalamus, hypothalamus, auditory cortex, visual cortex, periaqueductal gray (PAG), ventral tegmental area (VTA), substantia nigra (SN), pontine nuclei, and raphe nucleus. The average changes over time in BOLD and CBF with respect to baseline were determined using these ROIs and the normalized BOLD and CBF image timecourses.

Results

In anesthetized rats, a significant drop in the BOLD signal was observed in all regions investigated within 30 s following the administration of morphine (0.3 mg/kg) (Figure 5-2, panel a). Within 4 minutes, the BOLD signal returned to baseline levels. Following the administration of vehicle alone to anesthetized rats, no significant changes in the BOLD signal were observed within any of the regions investigated. The depression of the BOLD signal was correlated in time with reduced cardiac output and reduced respiratory output (Figure 5-2, panel b) that was significant at the group level in anesthetized animals (Table 5-1). Heart rate (HR) and respiratory rate (RR) were reduced

on average by $16.1\% \pm 1.3\%$ and $18.6\% \pm 4.8\%$ (% change \pm SEM, N = 6), respectively, 45 s after the administration of morphine. At 200 s following the administration of morphine HR and RR were still significantly depressed in anesthetized animals by $5.4\% \pm 2.1\%$ and $6.3\% \pm 2.4\%$, but the BOLD signal had returned to baseline levels (Figure 5-2, panel a).

In contrast to anesthetized rats, no significant changes in HR or RR were observed in conscious rats at 45 s or 200 s following the administration of morphine (Table 5-1), and SE BOLD remained at or above baseline levels for 175 s after the injection of morphine or vehicle alone (Figure 5-3, panel b). At 200-225 s after the injection of morphine, a regionally specific drop in the BOLD signal was observed in some of the ROIs investigated, and the depression in the BOLD signal was sustained for the duration of the experiment (675 s following the injection) (Figure 5-3 panel b). This late onset drop in the BOLD signal following morphine administration was regionally specific, was not observed in any regions investigated in anesthetized animals, and, when averaged over the period of 225 – 675 s following injection, was significantly different at the group level in conscious animals in comparison to vehicle controls within the association cortex, orbital cortex, olfactory nucleus, primary motor area (M1), cingulate cortex, primary somatosensory area (S1), caudate putamen (CPu), insular cortex, secondary somatosensory region (S2), lateral globus pallidus, hippocampus, auditory cortex, and visual cortex (Figure 5-4). Unexpectedly, sites mediating supraspinal analgesia (e.g. periaqueductal gray) did not exhibit significant changes in BOLD after the administration of morphine, in comparison to vehicle controls (Figure 5-4). Significant changes in

cerebral blood flow (CBF) were not observed at the group level in any of the regions investigated, suggesting that the limited sensitivity of the pseudo-CASL technique may prevent detection of small CBF reductions that should be observed in neural deactivation paradigms.

Among conscious animals, the frequency of struggle events was significantly reduced following the administration of morphine, while there was no significant change in the frequency of struggle events following the administration of saline alone (Figure 5-5).

Discussion

Transient BOLD changes observed in anesthetized vs. conscious rats

Heroin has been previously shown to elicit a transient drop in the gradient echo (GE) BOLD signal shortly after administration, in spontaneously breathing, urethane anesthetized rats (Xu et al., 2000). A similar drop in BOLD signal intensity was consistently observed in isoflurane anesthetized rats in this study, following the administration of 0.3 mg/kg morphine sulphate. Mechanical ventilation of the rats in Xu et al.'s study was shown to reduce or eliminate this drop in the BOLD signal, and implicated a systemic change in blood oxygen saturation as a source of the signal change in spontaneously breathing anesthetized animals. Our data support this observation with the correlation in time among reductions in respiration rate, heart rate, and BOLD signal intensity (Figure 5-2, Table 5-1). While tracheotomy and mechanical ventilation may also be effective for eliminating global BOLD signal changes due to the physiological

effects of morphine in the anesthetized animal, the surgical procedure cannot easily be extended to the conscious animal, and the procedure itself precludes or severely complicates the use of the same animal at a later date in longitudinal studies.

Previous studies of heroin's effects on the BOLD signal in anesthetized rats that were mechanically ventilated revealed regionally specific activations (increases in BOLD signal intensity) that included the mesolimbic system, cingulate cortex, frontal cortex, olfactory cortex, entorhinal cortex, hippocampus, and hypothalamus (Xu et al., 2000). The onset of these activations was rapid (within 2 min) and the duration of these activations was short (not longer than 10 min) relative to the half life of morphine, an ultimate metabolite of heroin. Due to the overwhelming influence of the presumed increase in deoxyhemoglobin concentration resulting from reduced cardiac and respiratory output following morphine administration in anesthetized rats, BOLD signal increases in these animals were not observed, consistent with our expectations and with previously published results (Xu et al., 2000). Surprisingly, increases in the BOLD signal were not observed in conscious animals within any of the regions investigated, despite the absence of significant effects on RR and HR (Table 5-1), and the absence of the transient drop in the BOLD signal present in anesthetized animals (Figure 5-2).

In conscious rats, and in contrast to the BOLD dynamics observed in anesthetized rats in both this and in Xu et al.'s study (Xu et al., 2000), the BOLD signal returned to or slightly (but not significantly) exceeded baseline levels within 50 seconds following administration of both vehicle and vehicle with morphine, but returned to baseline levels within 100 s (Figure 5-3, panel b) . This pattern was consistent throughout many of the

regions investigated, but in no region was the increase in BOLD due to morphine administration greater than or significantly different from the increase in BOLD due to vehicle alone. Hemodynamic factors could account for the transient increase in BOLD, including vasoconstriction due to hypertension induced by the injection, which would cause a reduction in CBV without a dramatic change in CBF or CMRO₂, thereby increasing the BOLD signal intensity (see Equation 2.1). This hemodynamic explanation is difficult to reconcile with the observations of decreasing BOLD or reduced BOLD responsivity under hypocapnic conditions, such as hyperventilation (Weckesser et al., 1999; Makiranta et al., 2004), but is supported by the observation of increased BOLD signal in some structures following a pressor challenge (Henderson et al., 2004); also, acute hypertension induced by injection would be expected to activate the baroreceptor reflex, but a significant change in HR was not observed at 45 s post injection in the pulse oximetry data (Table 5-1). Another possible explanation is that sensory stimulation from the injection alone causes changes in neural activity throughout several regions in the brain. This explanation is consistent with the nearly significant increase in BOLD observed at the group level within S1 among conscious rats (Figure 5-3).

Conscious, but not anesthetized, animals exhibit BOLD signal changes consistent with the pharmacodynamics of morphine

In conscious rats receiving morphine, a late onset drop in the BOLD signal was observed in several regions of the brain that was significant at the group level, and significantly different from group wide BOLD changes in these regions following the administration of saline (Figure 5-4). The time of onset of this drop in BOLD,

approximately 200 s after injection (Figure 5-3), is consistent with the onset of anxiolytic, analgesic, and euphoric effects reported by medicinal and recreational opioid users (Zacny et al., 1994; Katzung, 2004), and the reduction in BOLD signal intensity was maintained for the duration of the experiment, consistent with the 1.9 hr half life of morphine in the blood. Consequently, these late onset changes in the BOLD signal are better explained by the expected pharmacodynamics of morphine, than the transient changes in the BOLD signal observed during the 2 – 3 minutes immediately following the injection.

If we assume that BOLD signal changes following vehicle and morphine injection do, in fact, reflect local changes in neural activity, then the regionally specific, late onset drop in BOLD signal intensity following morphine administration is consistent with the muted sensory perception and analgesia expected from the drug. The significantly reduced rate of struggling (i.e. reduced motor activity) observed after the injection of morphine (Figure 5-5) is consistent with the fMRI observations that BOLD signal intensity is significantly reduced in M1, CPu, and LGP with respect to saline injected animals during this latter portion of the experiment (Figure 5-4). The significant reduction in BOLD with respect to saline injected animals that was observed in primary (S1) and secondary (S2) somatosensory, auditory, and visual cortices is consistent with reduced sensory stimulation due to analgesia and anxiolysis, and the drop in BOLD among frontal cortical regions is consistent with a muted state of consciousness.

Limitations of the technique

This study collected both BOLD and CBF measurements simultaneously (Silva et al., 1999; Duong et al., 2000; Schmidt et al., 2006), in an effort to validate a multi-modal imaging approach to pharmacological MRI of non-stimulant drugs. Not only were significant changes in CBF undetectable, but significant changes in the BOLD signal were detectable only in ROI based analyses at the group level. Statistical parametric maps calculated from individual subjects from the BOLD signal alone and tuned to assess the significance of the late onset drop in the BOLD signal at the individual voxel level were contaminated by artifacts due to animal motion, and unsuitable for publication.

Additionally, non-linear distortion of the EPI images prevented a coregistration approach to data analysis, and required the definition of each ROI in individual subjects. EPI distortion and inter-subject errors in ROI definition may contribute to the high variance observed in measurements made in small nuclei such as the PAG, entorhinal cortex, and VTA. Consequently, EPI based multi-modal imaging approaches may be suitable in only a subset of pharmacological studies, where changes of interest in BOLD and CBF are expected to be large in amplitude, as in the hemodynamic changes following the administration of a psychostimulant (Schmidt et al., 2006). Blood pool contrast agents used to measure changes in CBV have been shown to be effective in localizing changes in hemodynamics associated with neural activity induced by a drug (Marota et al., 2000), and the reduced sensitivity of changes in CBV to systemic changes in blood oxygenation may make CBV measurements a desirable alternate to BOLD imaging in some circumstances.

In a separate set of experiments, 10 mg / kg naloxone was administered 8 min after the administration of morphine sulfate to assess the reversibility of the late onset drop in BOLD signal among conscious rats. This dose was sufficiently aversive that animal motion immediately following naloxone administration contaminated measurements of the BOLD signal, preventing reliable detection of BOLD signal changes (data not shown). Future studies using a reduced dose of naloxone with reduced potential for aversion may reveal a partial reversal of the late onset drop in BOLD signal, further supporting the hypothesis that this change in signal is due to morphine's agonism of the MOR.

Physiological changes following morphine administration, such as decreased HR and RR, and the absence of these changes among conscious rats, suggest that autoregulatory reflexes may be intact in conscious but not anesthetized animals. These autoregulatory reflexes may induce detectable changes in neural activity within the medulla in regions that regulate respiration, but these changes were not observable in this study, due to the selection of imaging geometry that was focused on anterior cortical areas. Future fMRI and phMRI studies may reveal specific changes in BOLD or CBF measures within the vagal system in response to chemical challenge or activation of the carotid body reflex, but the technical challenges of making these observations in rats are difficult to anticipate.

Implications for pharmacological functional MRI

Despite the technical difficulty associated with imaging conscious animals, pertinent differences in the fMRI response to morphine between anesthetized and conscious rats suggests that investigations of other psychotropic drugs may also yield different results if performed in conscious vs. anesthetized animals. In anesthetized rats, transient and global reductions in SE BOLD following morphine injection are observed to dissipate within minutes, far more rapidly than morphine is cleared from tissue or plasma. In contrast, late onset changes in SE BOLD in conscious rats are consistent with the pharmacokinetics of morphine and suggest that morphine induces a complex neural response that is dominated by secondary actions in regions that are not direct substrates for opiates (Nestler, 2002). Functional MRI of the conscious rat may help to elucidate the secondary neural effects that are associated with the reward, anxiolysis, and euphoria that accompanies intravenous injection of opiates of abuse, and fMRI of conscious animals may be a difficult but important technique for determining the changes in neural activity induced by a drug under investigation.

Figure 5-1

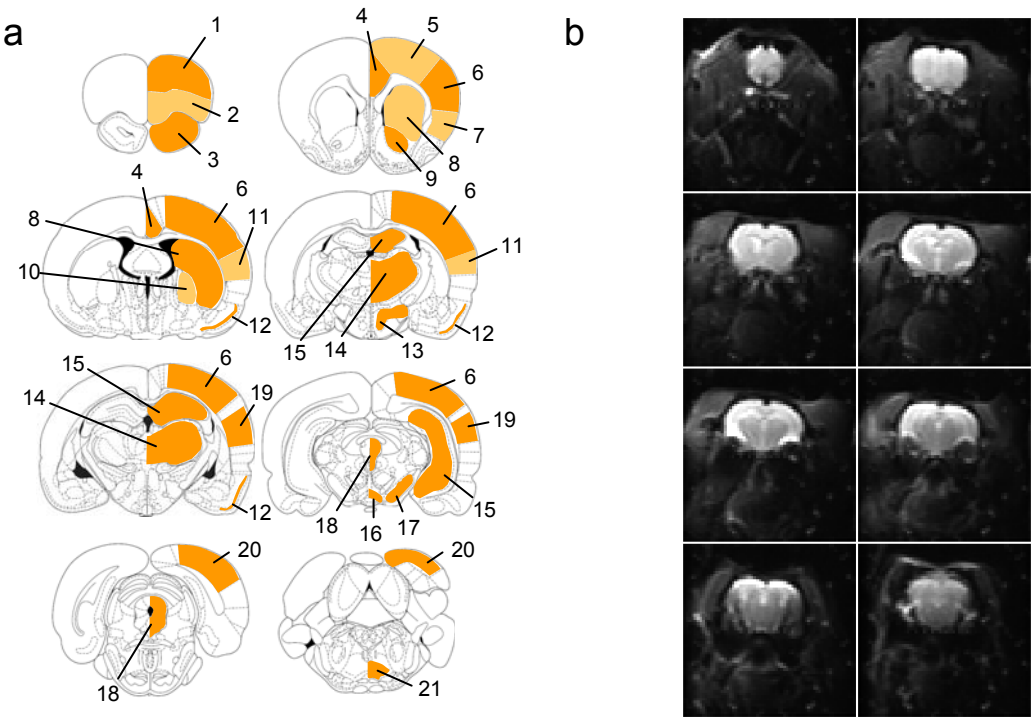


Figure 5 – 1: Regions of interest investigated.

(a) A template was used for definition of the regions of interest investigated in this study. Due to the limited resolution of the functional MRI scans, regions were aggregated in the manner shown in, and defined bi-laterally on the functional images. The figure shows only unilateral definition to illustrate the aggregation of sub regions defined in the atlas. Regions defined are: 1 – Association Ctx, 2 – Orbital Ctx, 3 – Olfactory Nucleus, 4 – Cingulate Ctx, 5 – Primary motor area (M1), 6 – Primary somatosensory cortex (S1), 7 – Insular Ctx, 8 – Caudate putamen (CPu), 9 – Nucleus accumbens (NAc), 10 – Lateral globus pallidus (LGP), 11 – Secondary somatosensory cortex (S2), 12 – Piriform Ctx, 13 – Hypothalamus, 14 – Thalamus, 15 – Hippocampus, 16 – Ventral tegmental area (VTA), 17 – Substantia nigra (SN), 18 – Periaqueductal gray (PAG), 19 – Auditory Ctx, 20 – Visual Ctx, 21 – Raphe Nucleus (b) Non-linear distortion of the functional (SE EPI) images, especially visible in ventral and lateral brain regions such as the amygdala, prevents a coregistration based approach to multi-subject analysis.

Figure 5-2

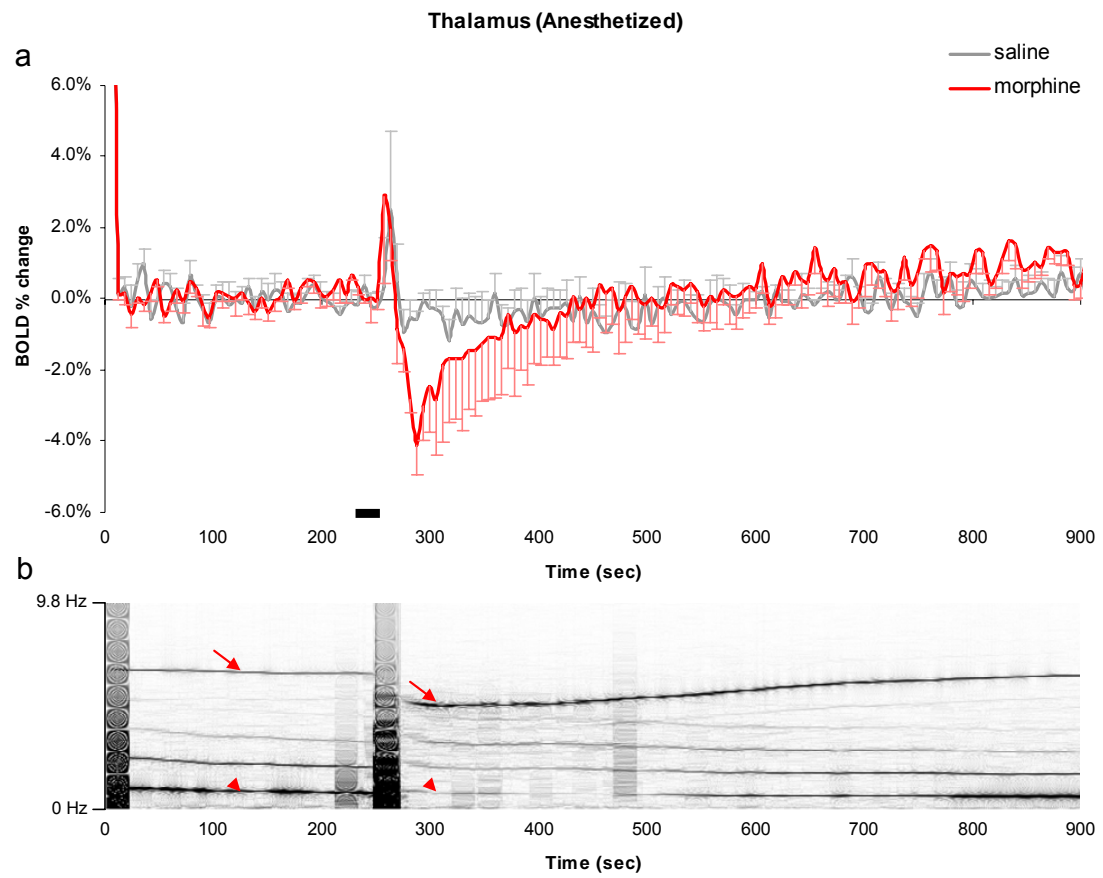


Figure 5 – 2: Changes in BOLD signal intensity in the thalamus correlate with physiological changes observed following morphine administration in anesthetized rats.

(a) Consistent with previous reports, transient decreases in SE BOLD are observed in group average time courses of anesthetized rats following morphine administration. No change in BOLD signal intensity is observed following administration of vehicle (saline). (black bar indicates injection period, N=6, error bars = SEM) (b) Spectral analysis of pulse oximetry data from a single anesthetized rat reveals a drop in heart rate (arrow) and decreased respiration (arrow head) following morphine injection that is correlated in time with the decreased BOLD signal intensity.

Table 5-1

		45 s post injection	200 s post injection
Heart Rate % chg	Conscious		
	Saline	0.7% ± 2.2%	1.9% ± 2.3%
	Morphine	4.7% ± 7.1%	-0.4% ± 5.2%
	Anesthetized		
	Saline	0.7% ± 2.9%	1.1% ± 3.4%
	Morphine	-16.1% ± 1.3%**	-5.4% ± 2.1%*
Respiration Rate % chg	Conscious		
	Saline	3.0% ± 3.1%	6.2% ± 4.1%
	Morphine	3.8% ± 10.3%	-6.3% ± 9.2%
	Anesthetized		
	Saline	4.3% ± 8.3%	-2.8% ± 5.8%
	Morphine	-18.6% ± 4.8%**	-6.3% ± 2.4%*

** $p < 0.01$

* $p < 0.05$

Table 5 – 1: Changes in heart rate (HR) and respiration rate (RR) following saline or morphine administration in conscious and anesthetized rats (N = 6).

Changes in HR and RR post injection were compared with the baseline period preceding injection of saline or morphine in conscious and anesthetized animals. Anesthetized rats exhibited a significant reduction in RR and HR at 45s and 200s following the injection of morphine. No significant changes were observed following the injection of saline in anesthetized rats, and no significant changes were observed following saline or morphine injections in conscious rats. Significance was determined using a two tailed t-test, without a correction for multiple comparisons.

Figure 5-3

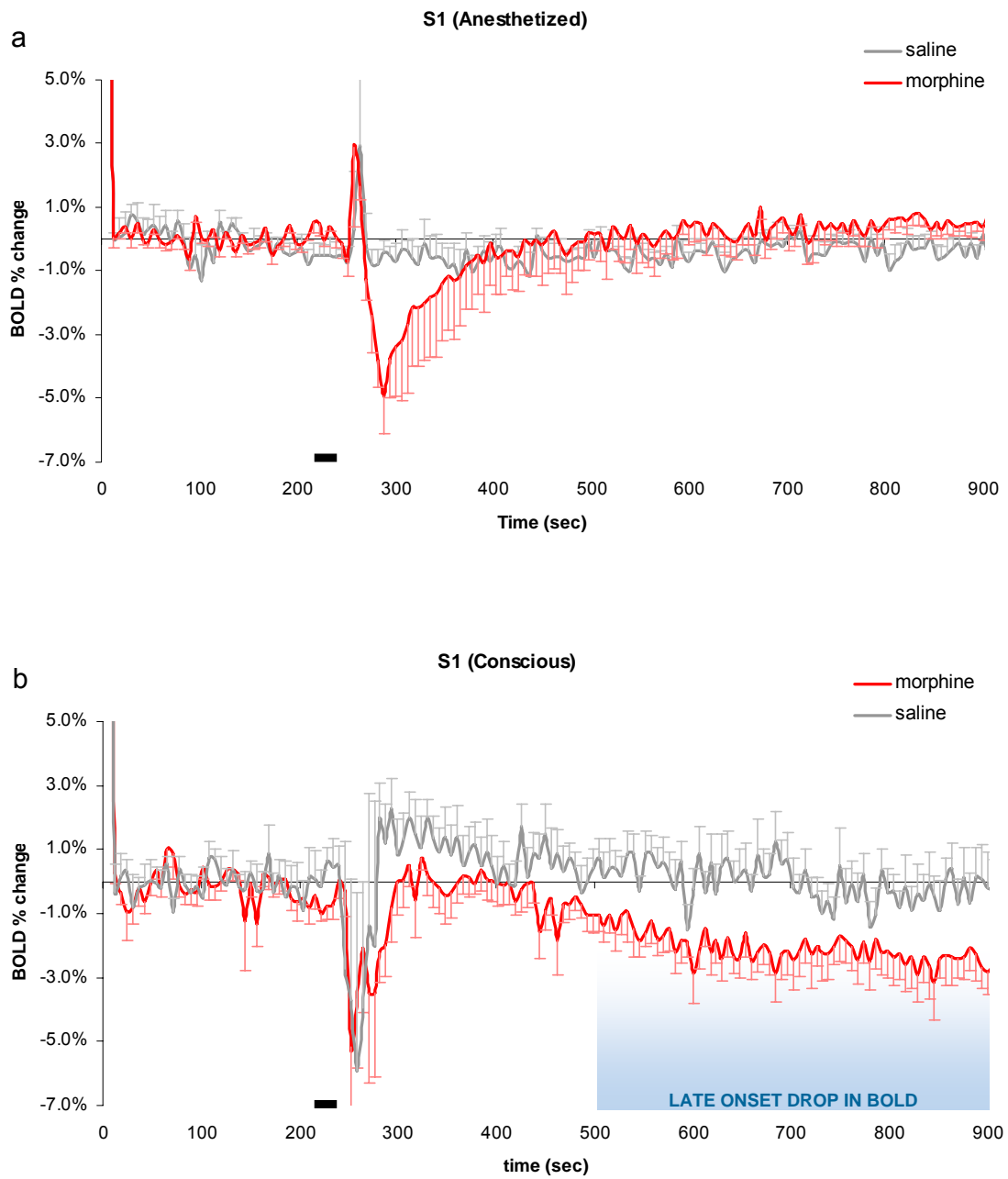


Figure 5 – 3: Group average SE BOLD signal changes within S1 in conscious and anesthetized rats following morphine or vehicle injection.

Injectons of morphine or vehicle induce transient and insignificant increases in BOLD contrast within S1 in conscious rats. In anesthetized rats a transient decrease in BOLD is observed following morphine injection and no change is observed following vehicle injection. Morphine administered to conscious rats produces a regionally specific decrease in BOLD (late onset drop in BOLD) that is observed after 4 minutes following injection. The temporal pattern of BOLD responses in conscious rats is thus more consistent with the pharmacokinetics of i.v. morphine than the BOLD response observed in anesthetized rats. (black bars indicate injection period, N = 6, error bars = SEM).

Figure S-4

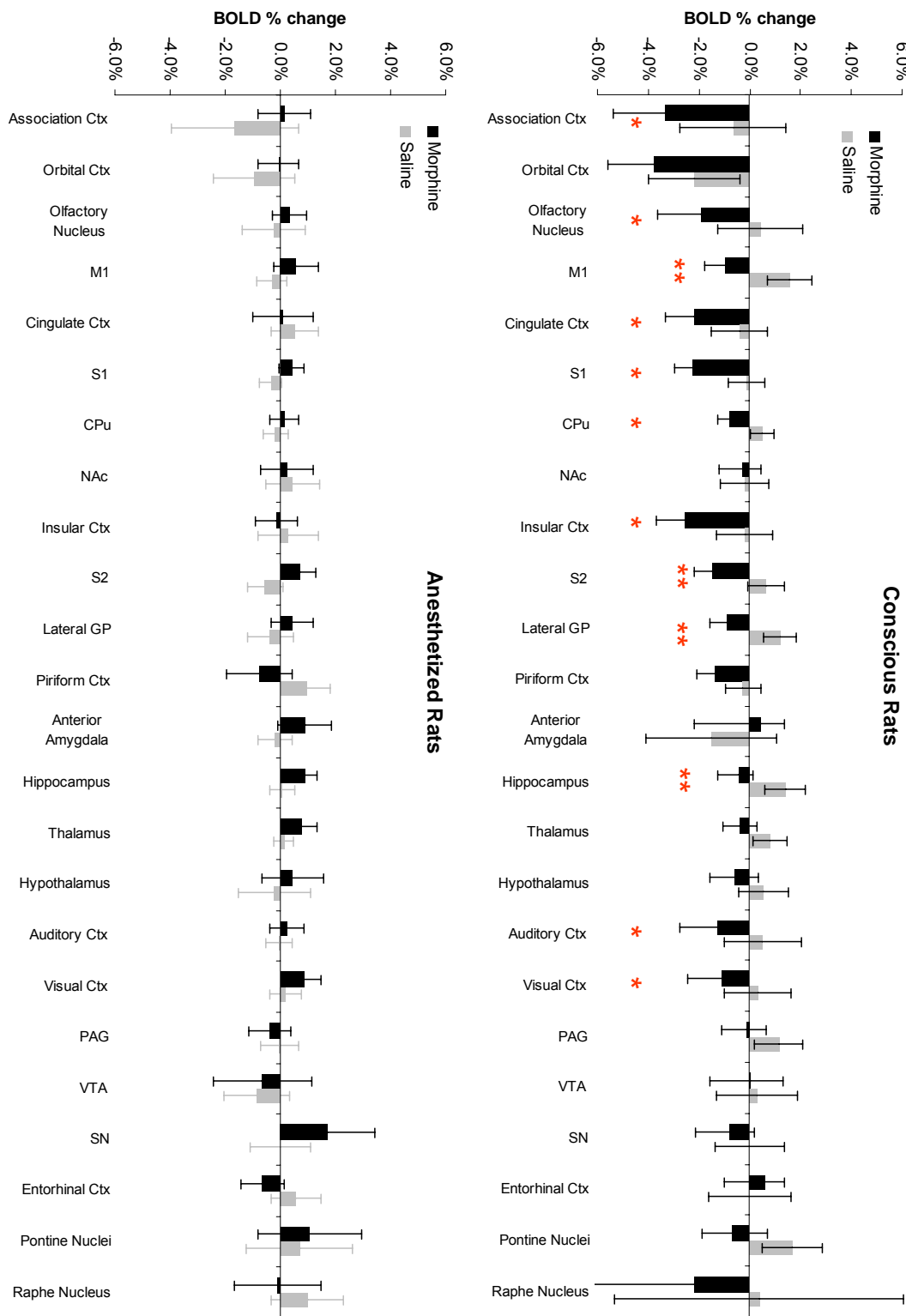


Figure 5 – 4: Late onset changes in the BOLD signal among all regions investigated in conscious and anesthetized rats.

Significant changes in BOLD contrast following morphine administration in comparison to vehicle controls were observed during the late onset period (600 – 900 s) within the Association Ctx, Orbital Ctx, Olfactory Nucleus, Primary motor area (M1), Cingulate Ctx, Primary somatosensory cortex (S1), Caudate putamen (CPu), Nucleus Accumbens (NAc), Insular Ctx, Secondary somatosensory cortex (S2), Lateral globus pallidus (Lateral GP), Piriform Ctx, Hippocampus, Auditory Ctx, and Visual Ctx. No significant changes with respect to vehicle controls were observed in anesthetized rats during this period. ** $p < 0.01$, * $p < 0.05$. Significance was determined from a two tailed t-test, without a correction for multiple comparisons. (N = 6, error bars = SEM).

Figure 5-5

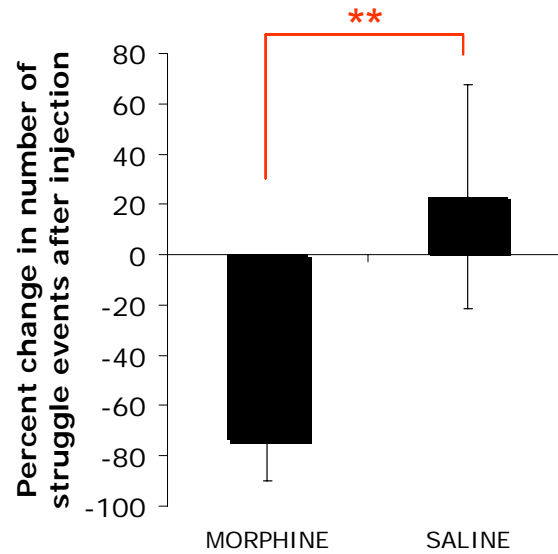


Figure 5 – 5: The frequency of struggle events decreases following morphine administration in conscious rats.

The frequency of animal struggle events among conscious rats was significantly reduced following the administration of morphine when compared to the administration of saline (** $p < 0.01$, error bars indicate SEM, $N = 6$, significance determined using a two tailed t-test).

CHAPTER VI

BOLD SIGNAL CHANGES IN RESPONSE TO INTRACEREBRAL VENTRICULAR APOMORPHINE CHALLENGE IN THE CONSCIOUS RAT ARE MODULATED BY PRETREATMENT WITH NEUROLEPTICS

The work presented in this chapter has not been submitted for review. This work was conducted under the direction of Dr. Craig Ferris, where my contributions consisted of the design and execution of animal experiments, data analysis, and the synthesis of the text presented here. Drs. Craig Ferris and Pamela Skoubis completed the animal experiments in the olanzapine pretreated group, and Tara Messenger contributed significantly to the animal experiments in the saline control group.

Introduction

Schizophrenia is a chronic and debilitating disease that ranks among the 10 most significant causes of disability, affecting approximately 1% of the population worldwide (Murray et al., 1996). Medications to treat the psychotic symptoms of schizophrenia have been available since the early 1950's (see Chapter I) and greatly improve the prognosis of most patients suffering from this disease. The benefits of treatment with older drugs (e.g. haloperidol) are tempered by the virtual guarantee of adverse side effects affecting the patient's motor control. Classified as extrapyramidal side effects (EPS), treatment with neuroleptics can induce rigidity, tremors, and infrequently the devastating neurological syndrome Tardive Dyskinesia, a potentially permanent disorder characterized by repetitive, involuntary, purposeless movements (Nestler et al., 2001). Beginning with the 1990 approval by the FDA of the atypical antipsychotic drug clozapine for the treatment of schizophrenia, a new generation of drugs have been developed to offer patients greater efficacy with reduced motor side effects, including olanzapine, quetiapine, risperidone, aripiprazole. However, patients taking these atypical antipsychotic drugs still suffer from a myriad of serious side effects, including: diabetes mellitus, seizures, weight gain, EPS, sexual dysfunction, somnolence, asthenia, nausea, hyperglycemia, and the potentially life threatening condition of agranulocytosis (Alvir et al., 1993; Nestler et al., 2001; Kinon et al., 2004).

A significant barrier hindering the development of new, atypical antipsychotic medications with reduced severity and incidence of side effects is our incomplete

understanding of the mechanisms by which typical and atypical antipsychotic drugs confer their therapeutic efficacy. In addition to not knowing which receptor or receptors, other than D2, are responsible for the therapeutic effects of atypical antipsychotic medications (see Chapter I), another fundamental question hinders the rational design of novel antipsychotic drugs. In the case of both typical and atypical antipsychotic drugs, therapeutic effects are observed only after several weeks of sustained treatment with the medication (Nestler et al., 2001; Squire et al., 2003; Katzung, 2004). It is generally believed that treatment with any of these medications causes a gradual change in neural signaling through neural plastic changes and synaptic remodeling, and that this change in signaling confers the therapeutic effects possibly by correcting abnormal communication between brain regions such as the striatum, frontal cortex and hippocampus (Horacek et al., 2006). The complex response of the intact, conscious brain to stimulation of a particular type of receptor (see Chapter V) further confounds our understanding of the neural signaling altered by treatment with antipsychotic drugs, and makes it difficult to anticipate the substrates ultimately affected by chronic treatment with antipsychotic medications.

The use of neuroimaging to investigate changes in neural signaling, with the hopes of identifying the neural substrates that are responsible for the pathogenic state and that are altered in the treated state of schizophrenic patients, has increased dramatically in recent years. A positron emission tomography (PET) study of glucose metabolism in treated schizophrenic patients that abstained from their haloperidol treatment for a period of 30 days illustrated that glucose metabolism is decreased in striatal and thalamic areas,

and increased in frontal cortical areas with respect to untreated controls (Holcomb et al., 1996), suggesting that these sites may be important mediators of therapeutic effects. In a later study, acute treatment with haloperidol was found to induce changes in neural metabolism that differed significantly between responding and non-responding patients (Bartlett et al., 1998), where non-responding patients exhibited a response to acute haloperidol challenge that was similar to haloperidol administered to healthy (non-schizophrenic) adults (Bartlett et al., 1996). Functional paradigms have been used to assess differences in brain function under task conditions among schizophrenic patients compared with healthy individuals (Holcomb et al., 2000; Lahti et al., 2001; Medoff et al., 2001), and the effects of treatment with antipsychotic medications on correcting functional abnormalities (Juckel et al., 2006) may be informative for understanding the signaling networks in the brain that are modulated by chronic antipsychotic treatment.

We investigated the effects of acute treatment with typical, atypical, and investigational antipsychotic drugs on correlated brain activation following a dopaminergic challenge (apomorphine). If acute treatment with antipsychotic drugs modulates networks of brain activation that contain nuclei beyond the dopaminergic pathways, it may be possible to develop a putative fingerprint of the effects of treatment with known antipsychotics for use in the classification and development of novel drugs, and for use in identifying patterns of signaling that are altered under chronic vs. acute treatment conditions.

Materials and methods

Animal preparation

Thirty six male Sprague Dawley (SD) rats (300-375 g) were studied. Animals were pretreated 45 min prior to scanning with i.p. injection (0.5 mL/kg) of either DMSO (Sigma Aldrich), saline, saline and haloperidol (Sigma Aldrich), saline and olanzapine (a generous gift from Dr. Gerard Fox at Abbott Laboratories, North Chicago, IL), DMSO and clozapine (Sigma Aldrich), or DMSO and SB277011 (a generous gift from Dr. Gerard Fox at Abbott Laboratories, North Chicago, IL). Animals were anesthetized with 2% gaseous isoflurane during surgery, and the anesthesia was reduced to 1.2% during placement into an MRI compatible coil and restraint system (Insight Neuroimaging Systems, LLC., Worcester, MA). During surgery, a cannula (PE-50 polyethylene tubing, Fisher Scientific) was placed into the left lateral ventricle through a small bore hole in the skull located 4mm laterally and caudally to the bregma, and inserted a distance of 5mm (Figure 6-1, panel d) for the intracerebral ventricular (ICV) administration of apomorphine (Sigma Aldrich). Apomorphine was prepared in a 0.5 mg / mL concentration and administered to the ventricle with a volume of 10 μ L (5 μ g of apomorphine). The cannula was fixed in place with adhesive and the incision in the scalp was summarily sealed. Anesthesia was discontinued after the animal was placed into the coil and restraint system, and the animal was allowed to recover consciousness before scanning.

MRI methods

MRI experiments were carried out on a 4.7T/40cm magnet (Oxford, UK), Bruker console (Bruker BioSpin Corp., Billerica, MA). Two actively decoupled coils were used for imaging: a 10 cm microstrip resonator volume coil was used for excitation, and a 2.5 cm ID surface coil was used for signal detection (Insight Neuroimaging, LLC., Worcester, MA). High resolution anatomical RARE images were acquired with the following parameters: matrix = 128 x 128, FOV = 3 cm x 3 cm, thk = 1.2, rare factor = 8, effective TE = 55 ms, TR = 3s, averages = 6, and 12 slices were acquired. Due to spatial distortion associated with SE and GE EPI methods (Figure 6-1, panels a – c), functional BOLD weighted images were acquired using a RARE sequence with the same geometry as the anatomical images and the following sequence parameters: matrix = 64 x 64, effective TE = 56 ms, TR = 1.5s, and rare factor = 16. Eighty images were recorded sequentially in the functional experiments, and apomorphine was administered via ICV at the 30th repetition (180 s).

Data analysis

Small amplitude and subvoxel motion in the timecourse data was corrected using the program 3dvolreg (Cox, 1996). Functional datasets were coregistered to a common anatomical template (Figure 6-1, panel e) using custom software developed in the Java programming language and based on the image analysis software ImageJ (Abramoff et al., 2004; Schmidt et al., 2004). Regions of interest were defined for several areas using the common anatomical template (Figure 6-1, panel e), and changes in BOLD signal intensity were measured from within these regions for each functional dataset independently. ROIs were defined bilaterally for the amygdala, auditory cortex, cingulate

cortex, caudate putamen (CPu), entorhinal cortex, frontal cortex, hippocampus, hypothalamus, insular cortex, lateral globus pallidus (LGP), primary motor cortex (M1), periaqueductal gray (PAG), prelimbic area, primary somatosensory cortex (S1), secondary somatosensory cortex (S2), substantia nigra (SN), thalamus, visual cortex, and ventral tegmental area (VTA).

$$\rho_{ij} = \frac{\sum (\bar{S}_{ROI_i} - \langle \bar{S}_{ROI_i} \rangle) (\bar{S}_{ROI_j} - \langle \bar{S}_{ROI_j} \rangle)}{N \cdot \sigma_{S_i} \sigma_{S_j}} \quad (6.1)$$

$$t = \frac{\rho \sqrt{n-2}}{\sqrt{1-\rho^2}} \quad (6.2)$$

Correlation matrices were created for each animal, and averaged together to form single correlation matrix representative of the group. Matrices were shaded to illustrate correlations greater than 0.28 (significant at the individual test level at $p < 0.005$) and, correlation coefficients exceeding 0.75 (individual $p < 10^{-16}$) are shaded in the darkest color. These thresholds were selected to discriminate correlations among known networks of information processing within the brain (see Appendix A, Figures A – 4 through A – 7 for additional illustrations of resolved networks). Due to the large number of comparisons the family-wise error rate (FWER) among drug treatment groups is 0.85 (Bonferroni correction), but the expected rate of false positive detection (FDR) among shaded correlations in Figures 6 – 3 through 6 – 8 is below 0.05 in all cases (Benjamini

and Hochberg, 1995). The standard error of the mean of the average correlation matrices are shown in Figures A - 1 through A - 3 in the appendix. Equation 6.1 illustrates the calculation used to generate the Pearson's R correlation coefficient, where subscripts i and j indicate the ROI being compared, and subscripts S_i and S_j indicate the standard deviation of the signal measured from within the respective ROI; \bar{S} indicates the average BOLD signal measured from within the ROI, and N indicates the number of repetitions from which signal was measured. Statistical significance was determined from inference for correlation (Equation 6.2), and p values were determined from a two-tailed evaluation of Student's t -distribution. Correlation analysis was performed using the software package Excel (Microsoft, Inc., Redmond, WA).

Results

Intracerebral ventricular administration of apomorphine (5 μ g, 10 μ L injection volume) to conscious animals induces temporally complex changes in BOLD signal contrast that vary regionally and between animals (Figure 6-2). In order to detect coincident activation of brain areas, a marker of functional connectivity, correlation analysis was performed by comparing the BOLD signal changes between regions of interest at each time point. Regions of interest were defined on high resolution anatomical images, and used to measure average BOLD signal changes over time from functional datasets of each animal that had been co-registered to the anatomical dataset (Figure 6-1, panel e).

For comparison, BOLD signal changes from anesthetized rats experiencing electrical forepaw stimulation (see Chapter 2 for methods) were subjected to the correlation analysis. BOLD signal changes in the primary somatosensory cortex (S1) were highly correlated with BOLD signal changes in the secondary somatosensory cortex (S2) in a single subject (Figure 6-3, panel a) while BOLD signal changes measured from a background ROI were not correlated with BOLD signal changes measured from S1 from this subject. Among all animals undergoing electrical forepaw stimulation ($N = 6$), the average correlation coefficient observed between various regions of interest is illustrated in Figure 6-3, panel c, and revealed a general correlation among all areas investigated except for the visual cortex and thalamus. BOLD signal changes in the thalamus did, however, correlate significantly with BOLD signal changes in the primary motor area across all animals. Highly significant correlations were observed between primary and secondary somatosensory regions, primary motor areas, and areas within the basal ganglia such as the lateral globus pallidus, suggesting the detection of functional connectivity between these areas. BOLD signal changes from a background ROI did not correlate with BOLD signal changes from any of the regions investigated, at the group level.

Correlation analysis of BOLD signal changes among animals receiving pretreatment with either saline or DMSO vehicles revealed similar patterns of correlative BOLD response following the administration of apomorphine (Figure 6-4). Elements of the basal ganglia such as the CPu, thalamus, and lateral globus pallidus (LGP) exhibited a correlated response. BOLD signal changes in the thalamus were also correlated with

those in S2, while a lack of correlation in S1 may reflect the significant aggregation of sensory areas in this ROI. The hippocampus exhibited little correlation with other regions, and the frontal cortex and cingulate cortex exhibited heterogeneous correlations with other areas that differed between saline and DMSO pretreatments.

Pretreatment with 1.0 mg / kg haloperidol altered the pattern of correlation when compared with the correlation observed during apomorphine challenge among rats pretreated with vehicle (saline) alone. Figure 6-5 panel a illustrates the correlations observed among animals pretreated with haloperidol, and Figure 6-5, panel b illustrates the correlations that are disrupted by pretreatment with haloperidol (red) and the correlations that were observed in haloperidol pretreated animals, but not in vehicle controls (blue). Correlation was disrupted between several (more than 2) ROIs and the amygdala, auditory cortex, frontal cortex, hypothalamus, insular cortex, LGP, S2 and SN, and selectively disrupted in the cingulate, CPu, PAG, S1, Thalamus, and visual cortex. New patterns of correlation were observed between several ROIs and the hippocampus, LGP, PAG, and visual cortex. Correlations were selectively (two or one) disrupted between regions and the cingulate cortex, CPu, entorhinal cortex, PAG, S1, thalamus, and visual cortex, while new correlations were selectively observed between regions and the auditory cortex, cingulate cortex, CPu, frontal cortex, hypothalamus, insular cortex, and prelimbic area.

Figure 6 – 6 illustrates the results of pretreatment with 20 mg / kg clozapine in comparison to pretreatment with vehicle (DMSO) alone. Correlation was disrupted between several ROIs and the amygdala, auditory cortex, cingulate, CPu, entorhinal

cortex, hypothalamus, insular cortex, PAG, prelimbic area, S2, SN, and the thalamus, while new correlations were observed between several regions and the frontal cortex, hippocampus, LGP, and PAG. Correlations were selectively disrupted in the LGP, and new correlations were selectively observed in the amygdala, auditory cortex, M1, and VTA.

The results of pretreatment with 3 mg / kg olanzapine are illustrated in Figure 6 – 7 with comparison of pretreatment with vehicle alone. Correlation was disrupted between multiple ROIs and the auditory cortex, cingulate cortex, CPu, frontal cortex, LGP, prelimbic area, and S2, while new correlations were observed between multiple areas and the entorhinal cortex, LGP, PAG, S1, and SN. Correlations were selectively disrupted between various areas and the amygdala, hypothalamus thalamus, and visual cortex, while new correlations were selectively observed between various areas and the amygdala, cingulate cortex, frontal cortex, hypothalamus insular cortex, visual cortex, and VTA.

Figure 6 – 8 illustrates the results of pretreatment with 10 mg / kg of the selective D3 receptor antagonist SB277011 in comparison to animals pretreated with vehicle (DMSO) alone. Markedly less disruption of correlations was observed in animals pretreated with SB277011 than animals treated with the typical antipsychotic haloperidol, or the atypical antipsychotics clozapine and olanzapine. Correlations were disrupted between several regions and the auditory cortex, CPu, hypothalamus, insular cortex, PAG and thalamus, while new correlations were observed between several regions and the CPu, frontal cortex, LGP, M1, and SN. Correlations were selectively disrupted between

regions and the amygdala, cingulate, hippocampus, LGP, prelimbic area, S2, and SN, while new correlations were selectively observed between regions and the amygdala, cingulate, entorhinal cortex, hypothalamus, insular cortex, S1, and S2.

Discussion

ICV administration of apomorphine in the conscious animal

Apomorphine has been shown to induce systemic changes in blood pressure and hemodynamics that have been linked to a global reduction in BOLD signal intensity that obscures BOLD signal changes due to neural activation in the anesthetized animal (Kalisch et al., 2005). Concurrent with Kalish et al.'s publication of their study, we observed similar BOLD signal changes in the conscious animal that precluded the systemic administration of apomorphine in this study. ICV has been demonstrated as an effective route for the administration of cocaine in conscious rat studies (Febo et al., 2004) and it was thus used in this study to ablate the physiological effects of apomorphine that would otherwise contaminate the BOLD signal.

Regional correlation among animals pretreated with vehicles alone

Pretreatment with either saline or DMSO resulted in similar patterns of correlated BOLD signal changes following an apomorphine challenge administered ICV (Figure 6 – 4). Many nuclei outside of the dopaminergic pathways exhibited correlated responses in a manner that is consistent with the functional circuitry of the brain. Correlations between

the cingulate cortex and S2, and M1 are consistent with our observations that these areas are concomitantly activated following electrical forepaw stimulation (Figure 2 – 1, Figure 6 – 2, panel c), and supported by correlation between the cingulate and CPu in both vehicle controls. In saline pretreated animals, correlations throughout the basal ganglia are prominent (CPu, LGP, and Thalamus), although correlation between the CPu and S2 is stronger than correlation between the CPu and M1 in these animals. In DMSO pretreated animals, the CPu exhibited reduced correlation with the LGP, but retained correlation with other elements of the basal ganglia observed in saline pretreated animals. The anesthetic effects of DMSO (Jacob and Herschler, 1986) may be a factor causing reduced motor and sensory stimulation. Frontal cortical and CPu correlation was also disrupted in animals pretreated with DMSO as was correlation between the frontal cortex and M1, PAG, and prelimbic areas, while correlation between the frontal cortex and cingulate and S2 was apparent in both groups.

Interestingly, S1 and the hippocampus exhibited little correlation with other regions investigated. The large ROIs used for these measurements may be a confounding factor in correlation analysis. Also, the number of correlations disrupted in animals pretreated with DMSO (14) was equal to the number of correlations observed in these animals that were not observed in saline pretreated animals, suggesting that this may reflect a general limit of the specificity of this analysis. In Appendix A, Figures A – 4 through A – 7 illustrate the comparison of observed correlations to known dopaminergic, motor, and sensory networks within the brain.

Effects of pretreatment with haloperidol, clozapine, olanzapine and the selective D3 antagonist SB277011

Pretreatment with haloperidol, clozapine, and olanzapine disrupted a number of correlations observed in the vehicle controls consistent with the action of these drugs as antagonists; several (haloperidol - 23, clozapine - 37, and olanzapine - 25) distinct correlations that were observed in control animals pretreated with vehicle alone were not observed in animals that were pretreated with antipsychotic medications. In contrast, the number of new correlations observed in pretreated animals was consistent with the variance observed between vehicle controls (haloperidol - 16, clozapine - 13, and olanzapine - 17). Figure 6 – 9 panel a, illustrates the features common between haloperidol, clozapine, and olanzapine, and indicates disruption of observed correlations between the CPu, amygdala and auditory cortex, disruption of correlations between the insular and cingulate cortices, and disruption of correlations observed between the LGP and hypothalamus.

In clozapine and olanzapine pretreated animals, a marked disruption in correlation between the CPu and other regions was observed; common among both groups were disruptions in correlation between the CPu and amygdala, auditory cortex, cingulate cortex, prelimbic area, S2, and thalamus (Figure 6 – 9, panel b). Also common among these two groups was the disruption of correlations between S2 and the cingulate cortex. These disruptions were not apparent in animals pretreated with haloperidol or the D3 antagonist SB277011, and are consistent with the broader spectrum of antagonism of

these drugs (Table 1 – 1), and also include several regions that are innervated by 5-HT afferents.

In contrast to clozapine and olanzapine pretreated animals, haloperidol pretreated animals exhibited disruption in correlations observed in vehicle controls between the LGP and S2, the frontal cortex and S2, and between the amygdala and auditory cortex with several other regions. Surprisingly, the correlation of BOLD signal changes within the CPu and other regions was relatively unaffected by pretreatment with haloperidol.

Consistent with the atypical antipsychotics clozapine and olanzapine, and in contrast to the typical antipsychotic haloperidol, pretreatment with the selective D₃ receptor antagonist SB277011 (Figure 6 – 9, panels c – d) disrupted correlation between the CPu, Thalamus, and insular cortex, while correlations were observed between the CPu and other regions including M1, LGP, PAG, and SN that were not observed in vehicle controls. It is possible that extrastriatal actions of the atypical antipsychotics and SB277011 are the primary contributors to the correlations observed between the CPu and other structures. SB277011 has 100 fold higher selectivity for the D₃ receptor (Reavill et al., 2000) than for the D₂ receptor, and D₃ receptors are distributed focally throughout limbic areas of the brain, (Shafer and Levant, 1998; Gurevich and Joyce, 1999) and in thalamic nuclei and the cerebral cortex (Stanwood et al., 2000). Similarly, olanzapine and clozapine have reduced affinity for the D₂ in comparison to haloperidol, but high affinity for several other receptors that are located extrastriatally.

Implications for the characterization of known and novel antipsychotic drugs

This study examines the correlative BOLD response in the conscious rat to an apomorphine challenge delivered directly to the brain, and compares this response to that observed when animals are pretreated with drugs known to have antipsychotic effects. The approach presented herein is unprecedented and technical challenges confound the interpretation of our results; however, the data presented in this study may provide a valuable basis for the development of a *fingerprint* of antipsychotic drug actions on the intact and conscious brain.

Figure 6-1

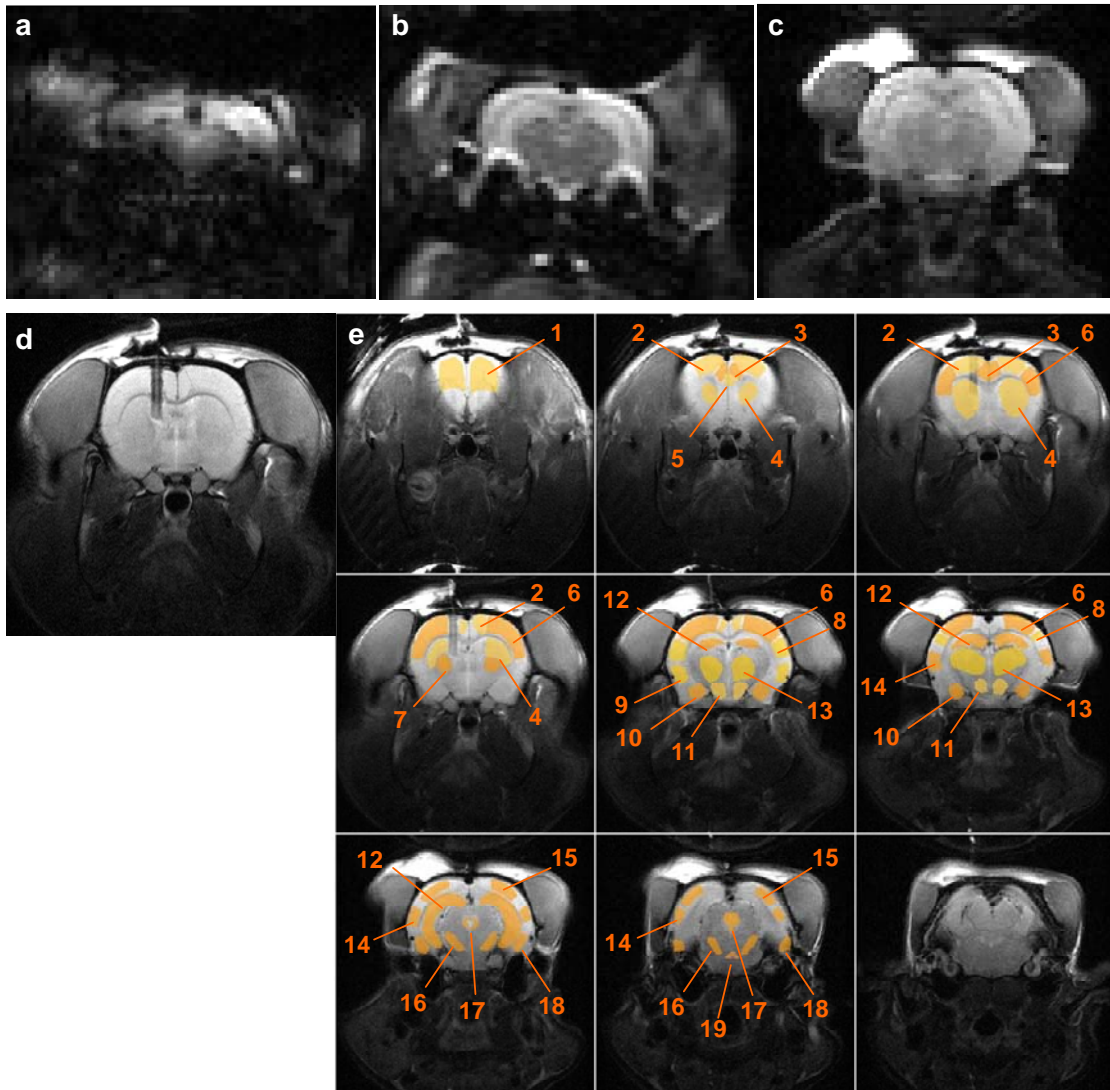


Figure 6 – 1: Criteria for selection of functional imaging protocol, location of the intracerebral ventricular cannula, and regions of interest defined.

(a-c) Representative images from functional datasets illustrate the differences in distortion and signal dropout due to susceptibility artifacts in BOLD weighted sequences acquiring (a) single shot gradient echo EPI, (b) single shot spin echo EPI, and (c) the fast spin echo (FSE) used in this study. (d) A representative anatomical image illustrating the placement of the cannula for apomorphine infusion in the left cerebral ventricle. (e) Illustration of the regions of interest measured. 1 – frontal cortex, 2 – primary motor area (M1), 3 – cingulate cortex, 4 – caudate putamen (CPu), 5 – prelimbic area, 6 – primary somatosensory region (S1), 7 – lateral globus pallidus (LGP), 8 – secondary somatosensory region (S2), 9 – insular cortex, 10 – amygdala, 11 – hypothalamus, 12 – hippocampus, 13 – thalamus, 14 – auditory cortex, 15 – visual cortex, 16 – substantia nigra (SN), 17 – periaqueductal gray (PAG), 18 – entorhinal cortex, 19 – ventral tegmental area (VTA).

Figure 6-2

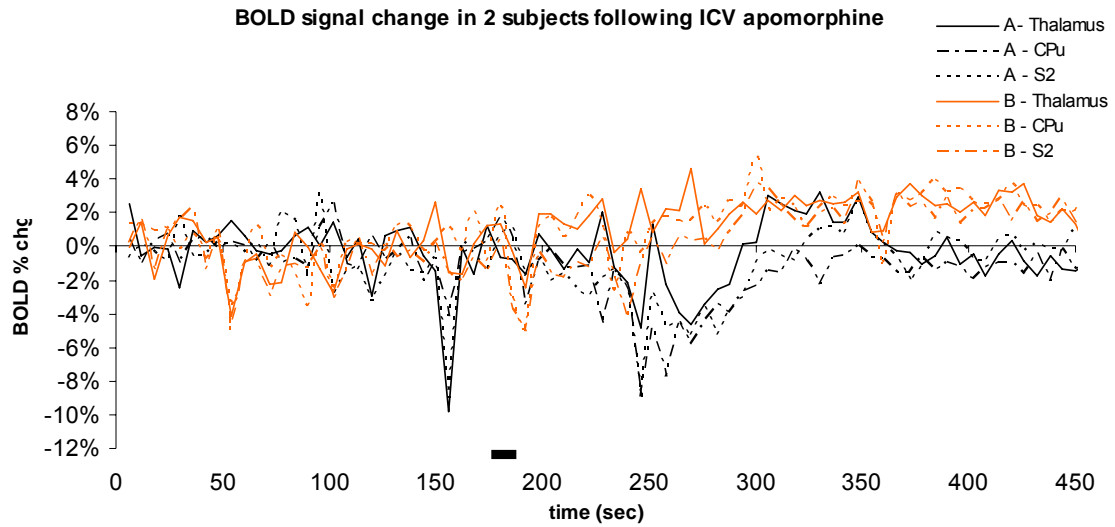


Figure 6 – 2: BOLD signal changes induced by apomorphine exhibit complex temporal dynamics and intersubject variability.

Changes in BOLD contrast following the ICV administration of apomorphine to conscious rats pretreated with saline exhibit complex temporal dynamics and intersubject variability. Time courses of measurements from three ROIs and two animals (A & B) are shown.

Figure 6-3

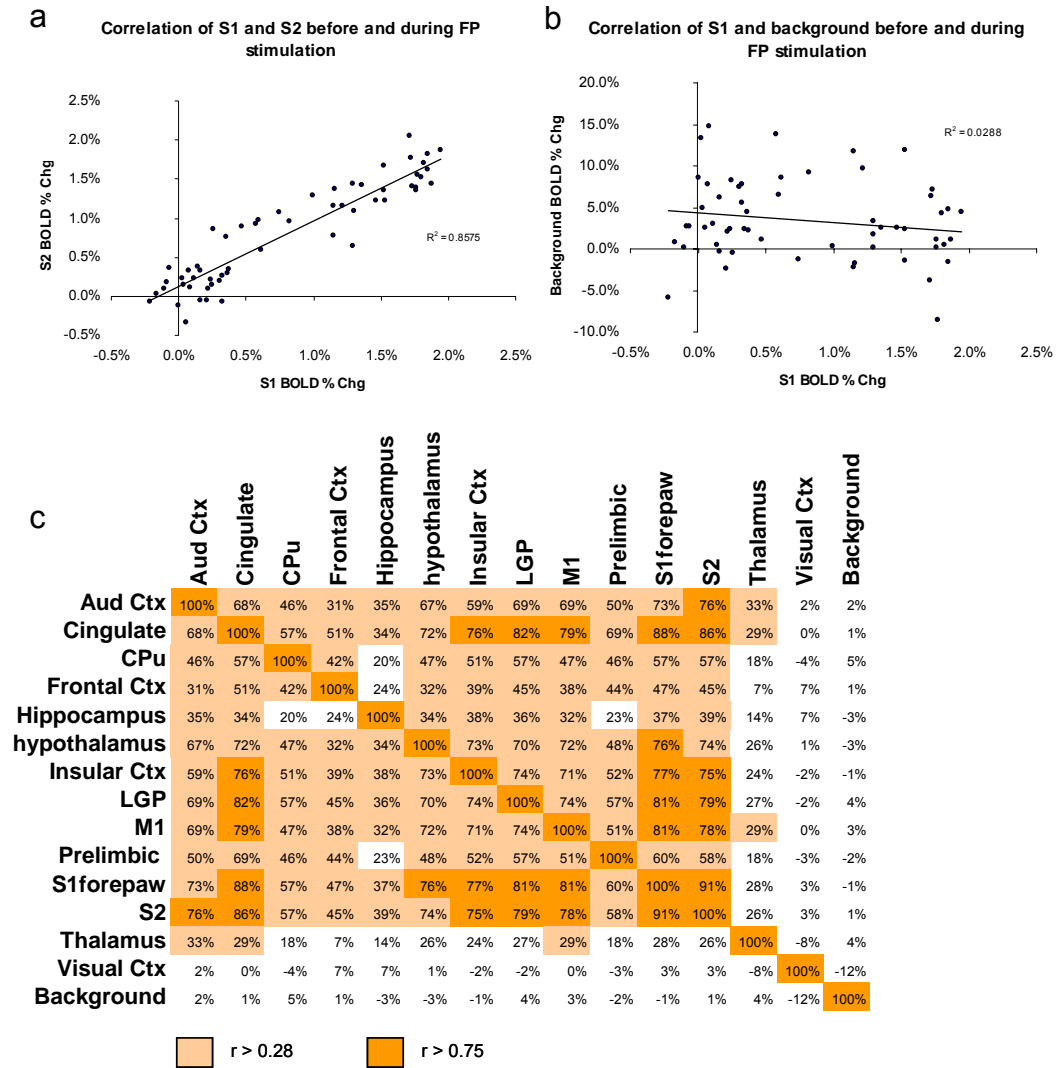


Figure 6 – 3: Correlation analysis of BOLD signal changes under electrical forepaw stimulation in anesthetized rats.

(a) Correlation of BOLD contrast changes in primary and secondary somatosensory regions following electrical stimulation of the forepaw in a representative anesthetized rat. (b) Correlation of BOLD contrast changes in the primary somatosensory region from the same rat compared with BOLD contrast changes measured from a background region of interest. (c) Correlation matrix showing group average correlation coefficients for multiple regions of interest ($N = 6$).


Figure 6-4

SALINE

	Amygdala	Aud Ctx	Cingulate	CPu	Entorhinal Ctx	Frontal Ctx	Hippocampus	hypothalamus	Insular Ctx	LGP	M1	PAG	Prelimbic	S1	S2	SN	Thalamus	Visual Ctx	VTA
Amygdala	100%	41%	25%	31%	40%	27%	15%	68%	56%	41%	18%	27%	17%	15%	47%	37%	38%	9%	2%
Aud Ctx	41%	100%	39%	30%	23%	36%	20%	39%	37%	32%	25%	44%	26%	21%	59%	37%	26%	40%	17%
Cingulate	25%	39%	100%	38%	11%	52%	26%	28%	35%	19%	46%	34%	63%	26%	44%	22%	27%	19%	8%
CPu	31%	30%	38%	100%	15%	32%	18%	27%	28%	32%	12%	26%	36%	7%	31%	21%	35%	2%	4%
Entorhinal Ctx	40%	23%	11%	15%	100%	14%	5%	24%	34%	28%	6%	20%	11%	10%	8%	48%	17%	-8%	4%
Frontal Ctx	27%	36%	52%	32%	14%	100%	12%	22%	23%	21%	34%	32%	38%	22%	41%	19%	27%	20%	6%
Hippocampus	15%	20%	26%	18%	5%	12%	100%	17%	23%	-3%	11%	20%	24%	14%	27%	17%	20%	19%	8%
hypothalamus	68%	39%	28%	27%	24%	22%	17%	100%	52%	28%	16%	28%	18%	11%	47%	32%	40%	11%	7%
Insular Ctx	56%	37%	35%	28%	34%	23%	23%	52%	100%	26%	24%	25%	27%	20%	53%	29%	27%	20%	1%
LGP	41%	32%	19%	32%	28%	21%	-3%	28%	26%	100%	22%	18%	18%	16%	32%	17%	26%	-2%	-4%
M1	18%	25%	46%	12%	6%	34%	11%	16%	24%	22%	100%	20%	36%	25%	30%	12%	7%	17%	-7%
PAG	27%	44%	34%	26%	20%	32%	20%	28%	25%	18%	20%	100%	25%	14%	36%	42%	19%	20%	19%
Prelimbic	17%	26%	63%	36%	11%	38%	24%	18%	27%	18%	36%	25%	100%	19%	32%	18%	17%	15%	8%
S1	15%	21%	26%	7%	10%	22%	14%	11%	20%	16%	25%	14%	19%	100%	35%	9%	10%	21%	1%
S2	47%	59%	44%	31%	8%	41%	27%	47%	53%	32%	30%	36%	32%	35%	100%	22%	37%	33%	12%
SN	37%	37%	22%	21%	48%	19%	17%	32%	29%	17%	12%	42%	18%	9%	22%	100%	25%	15%	22%
Thalamus	38%	26%	27%	35%	17%	27%	20%	40%	27%	26%	7%	19%	17%	10%	37%	25%	100%	5%	9%
Visual Ctx	9%	40%	19%	2%	-8%	20%	19%	11%	20%	-2%	17%	20%	15%	21%	33%	15%	5%	100%	9%
VTA	2%	17%	8%	4%	4%	6%	8%	7%	1%	-4%	-7%	19%	8%	1%	12%	22%	9%	9%	100%

DMSO

	Amygdala	Aud Ctx	Cingulate	CPu	Entorhinal Ctx	Frontal Ctx	Hippocampus	hypothalamus	Insular Ctx	LGP	M1	PAG	Prelimbic	S1	S2	SN	Thalamus	Visual Ctx	VTA
Amygdala	100%	32%	41%	40%	45%	21%	20%	66%	52%	17%	17%	20%	27%	-3%	57%	34%	29%	17%	20%
Aud Ctx	32%	100%	37%	34%	22%	21%	8%	39%	32%	31%	12%	42%	28%	11%	45%	30%	29%	26%	17%
Cingulate	41%	37%	100%	41%	35%	33%	10%	36%	47%	16%	40%	28%	63%	17%	56%	21%	21%	17%	17%
CPu	40%	34%	41%	100%	22%	25%	11%	41%	47%	20%	21%	20%	31%	4%	43%	18%	29%	21%	27%
Entorhinal Ctx	45%	22%	35%	22%	100%	17%	12%	27%	32%	2%	21%	8%	17%	6%	26%	47%	18%	16%	19%
Frontal Ctx	21%	21%	33%	25%	17%	100%	16%	26%	22%	19%	22%	25%	26%	3%	31%	17%	16%	18%	12%
Hippocampus	20%	8%	10%	11%	12%	16%	100%	30%	11%	18%	12%	17%	-2%	-6%	26%	15%	7%	10%	17%
hypothalamus	66%	39%	36%	41%	27%	26%	30%	100%	43%	32%	18%	39%	31%	0%	54%	30%	30%	23%	26%
Insular Ctx	52%	32%	47%	47%	32%	22%	11%	43%	100%	16%	25%	20%	32%	8%	54%	12%	37%	13%	7%
LGP	17%	31%	16%	20%	2%	19%	18%	32%	16%	100%	22%	45%	22%	8%	24%	25%	7%	3%	20%
M1	17%	12%	40%	21%	21%	22%	12%	18%	25%	22%	100%	26%	20%	10%	34%	20%	2%	-3%	7%
PAG	20%	42%	28%	20%	8%	25%	17%	39%	20%	45%	26%	100%	29%	9%	37%	27%	9%	21%	24%
Prelimbic	27%	28%	63%	31%	17%	26%	-2%	31%	32%	22%	20%	29%	100%	16%	41%	15%	7%	11%	10%
S1	-3%	11%	17%	4%	6%	3%	-6%	0%	8%	8%	10%	9%	16%	100%	15%	7%	8%	6%	-6%
S2	57%	45%	56%	43%	26%	31%	26%	54%	54%	24%	34%	37%	41%	15%	100%	30%	29%	18%	22%
SN	34%	30%	21%	18%	47%	17%	15%	30%	12%	25%	20%	27%	15%	7%	30%	100%	11%	9%	20%
Thalamus	29%	29%	21%	29%	18%	16%	7%	30%	37%	7%	2%	9%	7%	8%	29%	11%	100%	16%	-4%
Visual Ctx	17%	26%	17%	21%	16%	18%	10%	23%	13%	3%	-3%	21%	11%	6%	18%	9%	16%	100%	12%
VTA	20%	17%	17%	27%	19%	12%	17%	26%	7%	20%	7%	24%	10%	-6%	22%	20%	-4%	12%	100%

 r > 0.28


 r > 0.75

Figure 6 – 4: Correlation analysis of BOLD signal changes following apomorphine challenge in conscious rats pre-treated with saline or DMSO.

Average correlation coefficients are shown. N = 6 in each group.

Figure 6-5

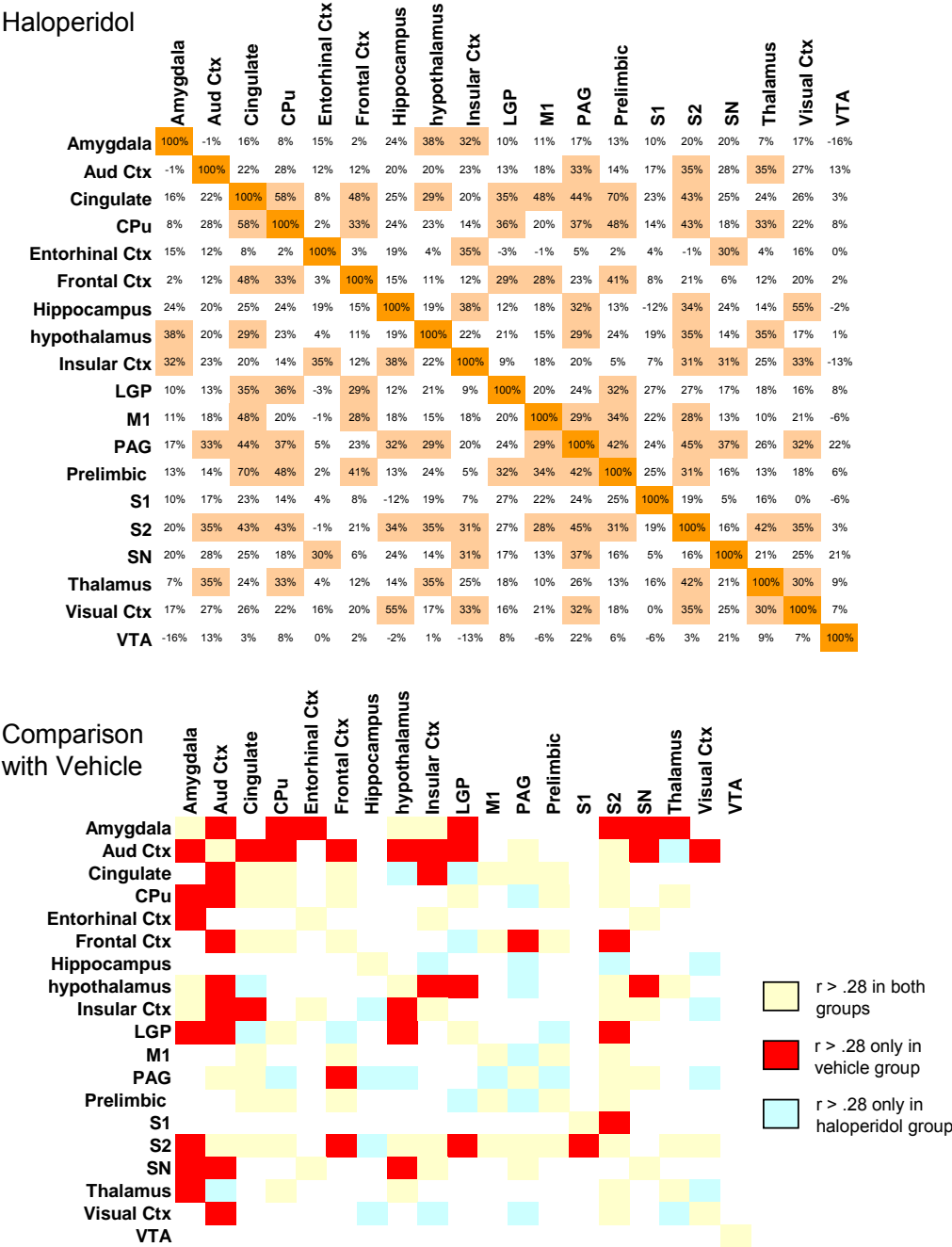


Figure 6 – 5: Correlation analysis of BOLD signal changes following apomorphine challenge in conscious rats pretreated with haloperidol.

Average correlation coefficients are shown. N = 6 in each group. Shading defined as in Figure 6 – 4.

Figure 6-6

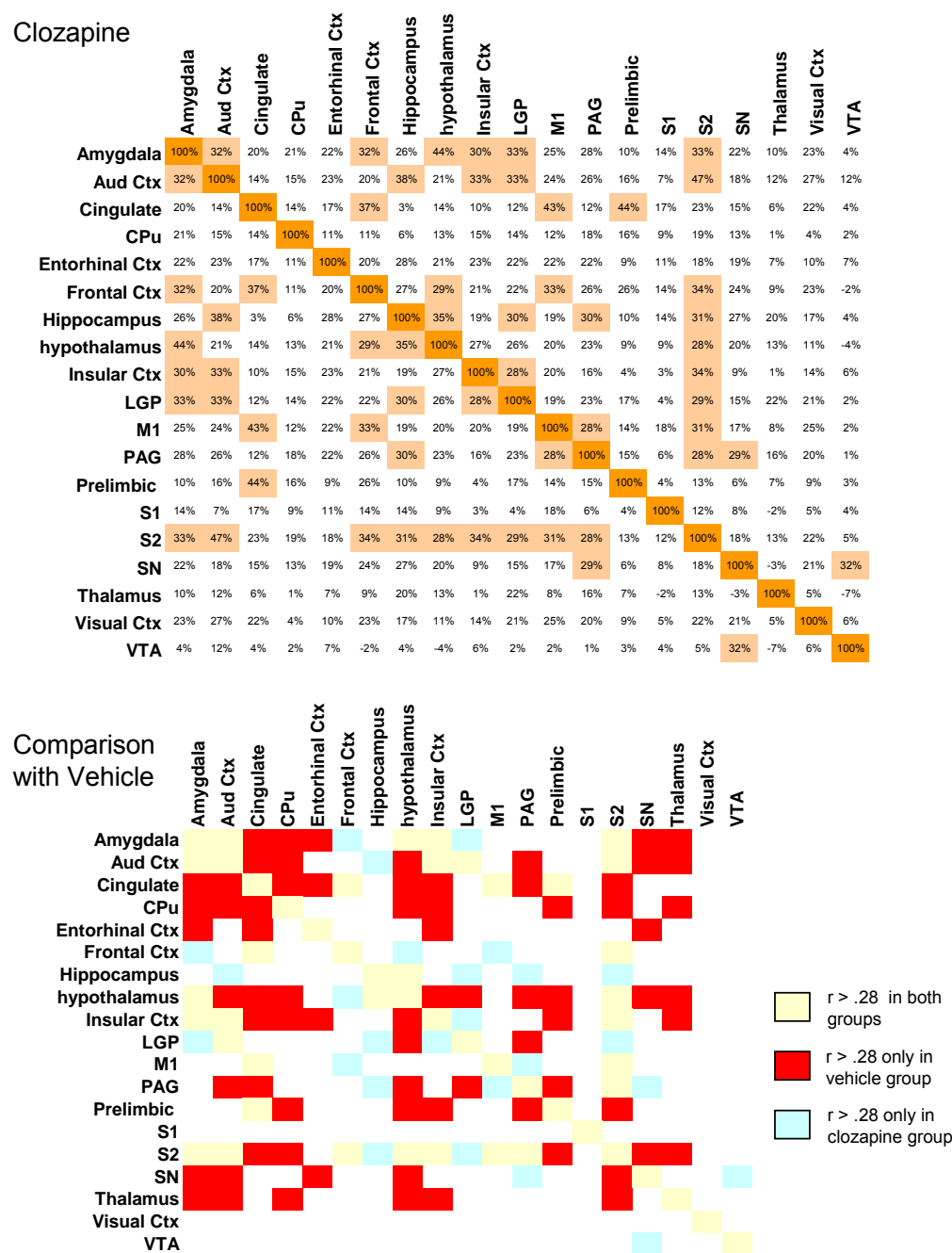


Figure 6 – 6: Correlation analysis of BOLD signal changes following apomorphine challenge in conscious rats pretreated with clozapine.

Average correlation coefficients are shown. N = 6 in each group. Shading defined as in Figure 6 – 4.

Figure 6-7

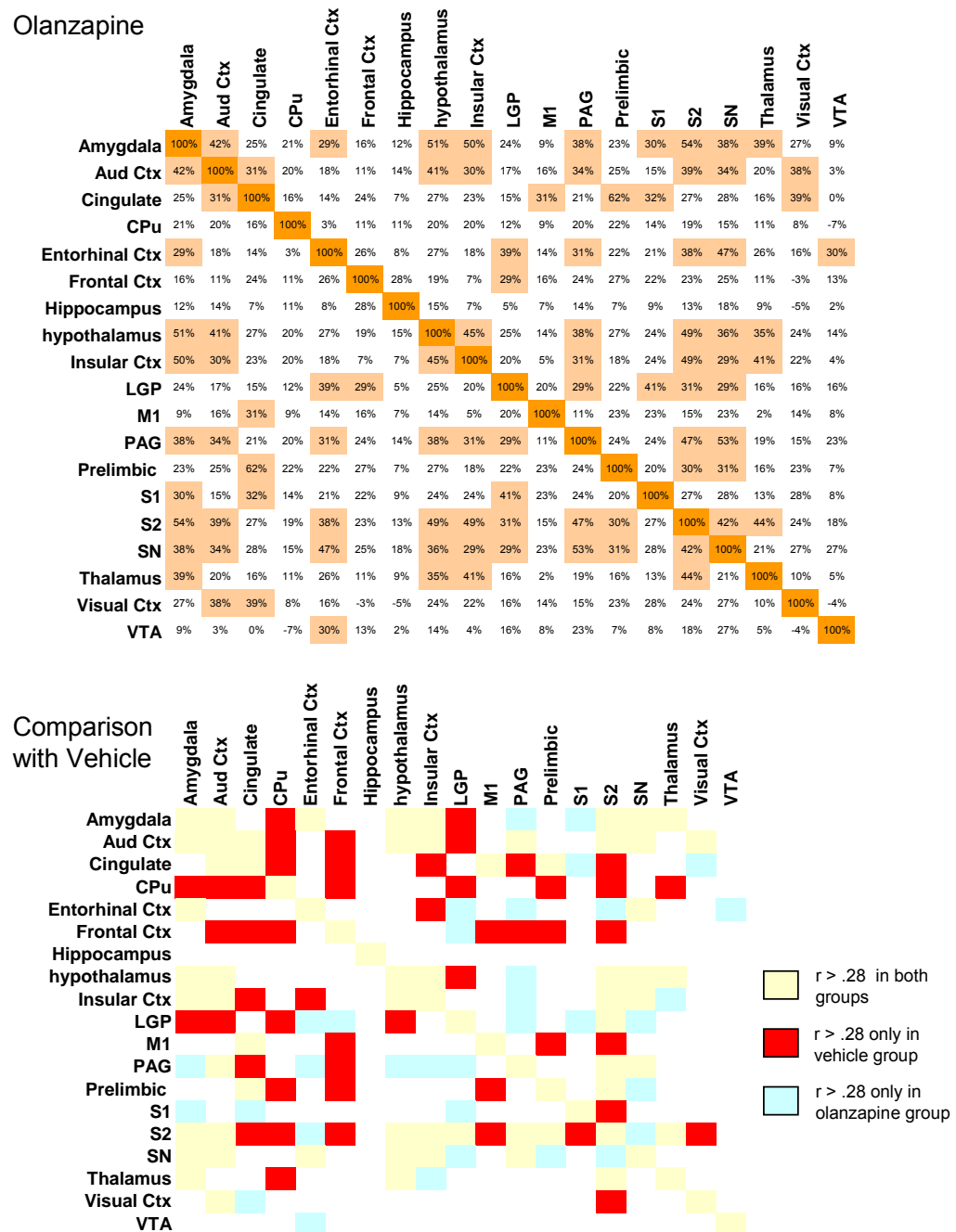


Figure 6 – 7: Correlation analysis of BOLD signal changes following apomorphine challenge in conscious rats pretreated with olanzapine.

Average correlation coefficients are shown. N = 6 in each group. Shading defined as in Figure 6 – 4.

Figure 6-8

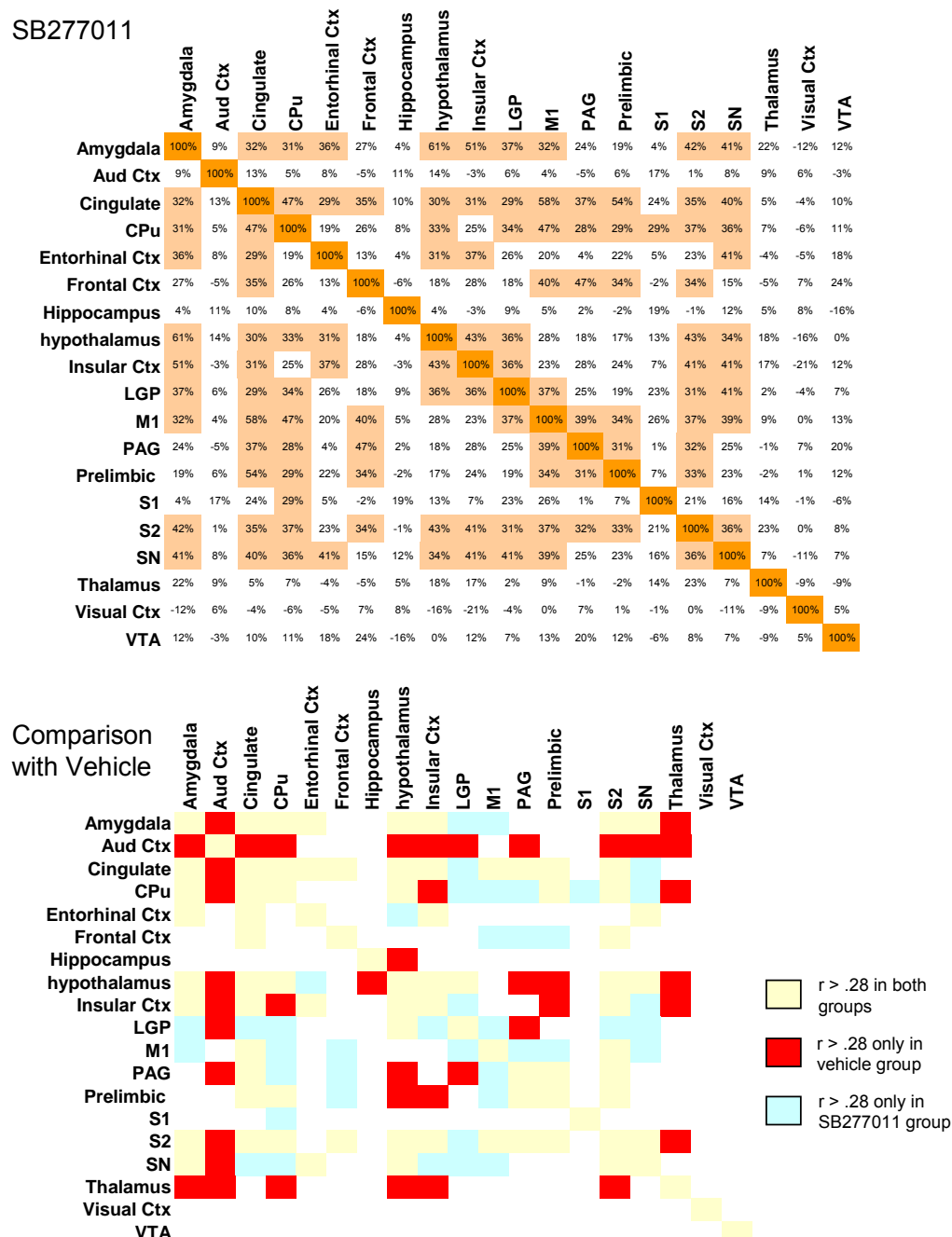


Figure 6 – 8: Correlation analysis of BOLD signal changes following apomorphine challenge in conscious rats pretreated with SB277011.

Average correlation coefficients are shown. N = 6 in each group. Shading defined as in Figure 6 – 4.

Similar patterns of disruption of correlations that were observed in control (vehicle pretreated) groups were seen among animals pretreated with typical, atypical, and investigational antipsychotic drugs. (a) Common features between haloperidol, clozapine, and olanzapine. (b) Common features between clozapine and olanzapine. (c) Common features between clozapine and SB277011. (d) Common features between olanzapine and SB277011.

CHAPTER VII

COMPREHENSIVE DISCUSSION

Marston Bates was an American zoologist in the 20th century who is quoted as having described research as “the process of going up alleys to see if they are blind.” This metaphor is not as cynical as it may first seem, and it astutely describes the presented work and ongoing efforts to validate and improve upon phMRI techniques for the investigation of psychotropic drugs. Although the avenues explored in the presented research failed to yield a universally superior technique for the investigation of the actions of drugs on neural activity within the brain, the limitations of these approaches are of value in the design and execution of future research, and the knowledge that these techniques provide relevant information under carefully controlled circumstances should motivate future phMRI investigations.

Pharmacological MRI is an emerging field with tremendous potential for the investigation of psychotropic compounds that is gaining widespread recognition in applications such as drug discovery (Wise and Tracey, 2006) and the study of addiction (Volkow et al., 2004). The growing literature of pharmacological MRI studies reflects the accelerating use of this technology in psychopharmacological research applications, in spite of unanswered questions that may significantly impact the interpretation of findings. Three questions, in particular, are of central importance for the interpretation of published work and for the design and execution of future psychopharmacological research using pmMRI; these questions are: Are the functional MRI measurements reliable surrogates of

changing neural activity in the presence of pharmacological agents? Is it relevant to investigate psychiatric phenomena such as reward or anxiolysis in anesthetized, rather than conscious animals? What are the methods that yield reproducible and meaningful results from phMRI experiments, and are they consistent in the investigations of different drugs, or between conscious and anesthetized animals? The methodological aspects of the research presented herein address these questions, and provide incremental advances in our understanding of their answers.

Impact of findings

In Chapters II and IV, novel techniques and technology were developed for the investigation of psychotropic compounds using MRI. These techniques permit dynamic observation of hemodynamic and putative metabolic changes using a non-invasive imaging modality that enables the identification of complex temporal changes that are obscured using traditional autoradiographic techniques (e.g. 2-deoxyglucose) or alternate imaging modalities (e.g. PET). The non-invasive nature of these protocols, and the similarity between MRI experiments performed in research settings and the MRI scans that are routinely performed in the clinic, holds promise that phMRI research in lower species will be easily translated to clinically observable phenomena. If this translation is realized, it would present an opportunity to validate animal models of psychiatric disease and exploit surrogate markers of drug action that are observed in the clinic for the development of novel drugs with improved efficacy.

In Chapter III, we illustrated that a multi-modal imaging approach can be used to obtain redundant measurements for use in the identification of artifacts unrelated to changing neural activity in response to a pharmacological challenge. While these redundant measures arguably contain little new information for traditional fMRI experiments using a sensory or cognitive stimulus (where BOLD signal changes are within published and normal physiological ranges), they were shown to be valuable in the investigation of a psychostimulant that induced unexpected changes in BOLD signal contrast. In the presented study, the collection of BOLD measurements alone may have led to erroneous inferences of changing neural activity, while the collection of multiple measurements, simultaneously, provided a sound basis for inference, and presented a novel approach for use in other pharmacological investigations. Many drugs of abuse are stimulants (e.g., methamphetamine), and it is logical to assume that investigations of these drugs will face many of the same challenges as were encountered in our investigation of cocaine.

In Chapter IV, a novel system was developed for multi-modal imaging in the conscious rat, representing a significant new capability for the MR research community. As we discovered in our investigation of morphine administered in the conscious animal (Chapter V), this technology faces many challenges related to animal motion that will need to be resolved before multi-modal imaging in the conscious animal supplants research performed with anesthetized preparations. Nonetheless, this technological advance is a necessary first step towards that end, and logical directions for the

improvement of the technology should guide the development of prototypes with greater resistance to problems associated with multi-modal imaging in the conscious animal.

In Chapter V, we addressed the debated issue of differences observed in the fMRI response to pharmacological challenge in conscious versus anesthetized animals. With the possible exception of general anesthetics, the primary interest in the investigation of psychoactive drugs is the effect that these drugs have on the conscious experience after acute or chronic administration. Given the number of published studies using anesthetized preparations, it is surprising that little effort has been made to demonstrate that the fMRI effects observed in anesthetized animals are, indeed, similar to those observed in conscious animals following the administration of a given psychoactive drug. Pertinacious resistance to imaging conscious animals may be related to the technical difficulty associated with these experiments, which is considerable, but our results from the administration of morphine to conscious and anesthetized animals provides evidence that this may be a necessary hardship in order to collect relevant data. Only in awake rats was an effect consistent with the pharmacodynamics of morphine observed, and we expect this result to motivate future research in the conscious animal.

In Chapter VI, we used a SE BOLD weighted imaging sequence with minimal anatomical distortion to investigate the effects that antipsychotic medications have on dopaminergic signaling induced by an apomorphine challenge delivered directly to the brain in the conscious rat. Our goals were to elucidate the changes induced in networks of signaling within the brain that are both within and beyond the primary dopaminergic pathways, and to develop a potential fingerprint of the actions of antipsychotic drugs for

use in the classification of novel antipsychotic compounds. The circumstances of this study were challenging, and several changes in the experimental approach are recommended for the reproduction of these and similar results in the future. Nonetheless, differences in the brains' response to a dopaminergic challenge were observed when animals were pretreated with various typical, atypical, and experimental antipsychotic drugs, and it is expected that this work will motivate future studies to examine the changes in the brains' response to dopaminergic challenge that occur following chronic treatment with these drugs, under therapeutically relevant conditions (Nestler et al., 2001; Katzung, 2004).

Considerations for phMRI data analysis

In addition to the methods and results reported herein, a number of unsuccessful data analysis strategies were explored that warrant consideration in the general context of phMRI experimentation. Unlike traditional fMRI experiments, which elicit a roughly binary response to cognitive or sensory stimuli, phMRI experiments elicit complex changes in the BOLD signal in response to a pharmacological challenge (see Chapters IV, V & VI). Consequently, traditional analysis techniques that rely on the statistical power of repetitive stimulus presentation or *a priori* hemodynamic response functions (Worsley and Friston, 1995; Buxton, 2002) are generally inapplicable to phMRI data. Additionally, techniques that rely on non-linear regression strategies (Xu et al., 2000; Xi et al., 2002; Luo et al., 2004) may detect changes that differ significantly from the pharmacodynamics of the drug under investigation, obscuring the meaning of statistical significance. Also unlike traditional fMRI experiments, each stimulus (drug) may have a

completely different set of effects on MRI measurements. From complex, direct actions on neural substrates to indirect actions on the peripheral physiology, no one protocol will be suitable for phMRI investigations of all drugs.

Emerging analysis strategies that are based on the correlated response of multiple brain areas to pharmacological challenge, such as principal components analysis (Thirion and Faugeras, 2003; Viviani et al., 2005; Liu et al., 2006; Wang et al., 2006), or the direct correlation analysis illustrated herein, represent a sensitive new tool for examining the coordinated responses of various brain regions, and may yield results which are more relevant to our understanding of the neural basis of action of psychotropic drugs than traditional fMRI data analysis methods. The raw correlation analysis approach presented in Chapter VI suffers from limited specificity, and further work on the receiver operating characteristics of this analysis is warranted.

Future directions

Investigation of the function of antipsychotic drugs

Clinical efficacy is observed in many, but not all schizophrenic patients, only after weeks of treatment with antipsychotic medications, implicating gradual neuroplastic changes as the potential therapeutic mechanism, rather than the acute effects of antipsychotic drugs on neurotransmission (Hyman and Nestler, 1996; Nestler et al., 2001; Squire et al., 2003). Several studies have revealed anatomical changes following chronic treatment with antipsychotic drugs, generally reflecting an increase in striatal structures in both animals (Benes et al., 1985; Chakos et al., 1998) and human patients (Chakos et

al., 1994; Keshavan et al., 1994; Gur et al., 1998) following treatment with typical antipsychotic drugs (e.g. haloperidol), but treatment with atypical antipsychotic drugs does not seem to cause a change in striatal volume, and can reverse presumed increases in striatal volume when patients are switched from typical to atypical antipsychotic drugs during the course of treatment (Scherk and Falkai, 2006). Further, evidence for neurogenesis as a result of treatment with antipsychotic drugs is lacking, suggesting that relevant neuroplastic changes following extended treatment with antipsychotic drugs are likely due primarily to synaptic remodeling (Konradi and Heckers, 2001).

Schizophrenia has been considered to be a disorder of functional connectivity between the prefrontal cortex and temporal cortices (Bogerts, 1997; Friston, 1998), and research has illustrated several changes in the architecture, function, and gene expression of striatal and extrastriatal (i.e. prefrontal cortex, hippocampus, and thalamus) neurons following treatment with haloperidol, for review, see (Konradi and Heckers, 2001). Functional MRI studies of task-related activation have revealed differences between schizophrenic patients and normal adults (Braus et al., 2002; Paulus et al., 2002; Kubicki et al., 2003; Honey et al., 2005; Tan et al., 2005), as well as between different treatments among schizophrenic patients (Zipursky et al., 1998; Honey et al., 1999; Juckel et al., 2006). These changes in function may be the result of changes in neurotransmission that result from synaptic remodeling as a result of exposure to antipsychotic drugs. Understanding these changes in neurotransmission in greater detail will have two immediate benefits: (1) the relevant changes in neurotransmission may be used as a screening tool for the characterization and development of novel antipsychotic drugs, and

(2) the changes in neurotransmission may be directly related to the pathology of schizophrenia, providing additional insights into the causes of positive symptoms, and the changes sufficient for their remission.

A canonical model of psychosis using animals does not exist, and while we have proposed an apomorphine challenge (Chapter VI) as a means to stimulate a relevant and measurable response that can be modulated by antipsychotic medications, other pharmacological models of psychosis may also be valuable for investigation. Antagonists of the NMDA receptor such as phencyclidine (Nestler et al., 2001) and MK801 (Wong et al., 1986), and antagonists of the 5-HT_{2A} receptor such as lysergic acid diethylamide (LSD) elicit psychotic symptoms such as dissociation and hallucinations (Katzung, 2004). The effects of these drugs can be modulated with antipsychotic medications (Miller et al., 1992; Schroeder et al., 2000; Linn et al., 2003; Hashimoto et al., 2005), and these modulations may be detectable by phMRI using techniques similar to those presented in Chapter VI. The insights gained from such experiments may reveal aspects of modulated neural signaling that relate directly to positive symptoms of psychosis (e.g., hallucinations) in a more specific manner than observations following a dopaminergic challenge such as apomorphine.

Further improvements in phMRI methodology are required

The research presented in Chapter V demonstrates significant differences in the phMRI response to morphine challenge in conscious vs. anesthetized rats. It is the opinion of the author that future phMRI studies will need to demonstrate consistency

between results obtained from anesthetized and conscious animals before inferences can be made regarding a drug's action in the conscious animal. The technical difficulty associated with performing phMRI experiments in conscious animals is considerable, primarily due to animal motion during image acquisition, and may explain the low frequency of published results using conscious preparations. However, novel restraint systems with integrated coil designs (Insight Neuroimaging Systems, LLC., Worcester, MA) greatly facilitate the process of imaging conscious animals, and the improvement of these systems and the methods for their use to further reduce animal motion is ongoing.

Multimodal imaging, specifically the measurement of CBF in the same experimental setting for measuring changes in BOLD or CBV, was shown to be an important capability in the interpretation of changes in neural activity following the administration of cocaine in Chapter III. The challenges of multimodal imaging in the conscious animal, specifically the use of arterial spin labeling techniques with multislice acquisition, are discussed in Chapter IV. These challenges will require significant experimental effort to address, and will likely require innovative changes in neck coil design, and may require the use of alternate labeling strategies such as spatially selective adiabatic inversion pulses (Zhan et al., 2002; Moffat et al., 2005). Currently, the technology is insufficient for the reliable detection of significant changes at the voxel level under several stimulus paradigms. While ROI based analysis is an effective means of increasing statistical power, it suffers from subjective influence and errors in the definition of ROIs, and can result in reduced statistical power when all voxels within the region are not activated equivalently. Future advances in this particular aspect of the

hardware and pulse sequences used in conscious animal phMRI experiments will enable redundant measurement of changing hemodynamics resulting from pharmacological challenge, permitting the identification of signal artifacts and the estimation of changes in metabolism related to neural activation.

Final comments

Like any contemporary research, the work presented in this dissertation is work still in progress. Pharmacological MRI methods will undergo many future improvements before the ability to monitor changes in neural activity elicited by psychoactive drugs is reliably measured and reproducible between laboratories. Similarly, the reported modulation of neural activity resulting from a dopaminergic challenge by pretreatment with antipsychotic drugs is a preliminary glimpse of a phenomenon that requires additional investigation; both to answer new questions raised earlier in this chapter, as well as to address limitations of the technique discussed in Chapter VI. Hopefully, the incremental progress reported in the present studies will motivate this research, and provide a basis for future investigations that will help to elucidate the pathological mechanisms of psychiatric diseases, and guide the development of novel therapies to treat them.

BIBLIOGRAPHY

- Abramoff MD, Magelhaes PJ, Ram SJ (2004) Image processing with ImageJ. *Biophotonics International* 11: 36-42
- Albert MS, Tseng CH, Williamson D, Oteiza ER, Walsworth RL, Kraft B, Kacher D, Holman BL, Jolesz FA (1996) Hyperpolarized ^{129}Xe MR imaging of the oral cavity. *J Magn Reson B* 111: 204-7
- Alberts B, Johnson A, Lewis J, Raff M, Roberts K, Walter P (2002) *Molecular Biology of the Cell*, 4th edn. Garland Science, Taylor & Francis Group, New York. 1463 pp
- Alvir JM, Lieberman JA, Safferman AZ, Schwimmer JL, Schaaf JA (1993) Clozapine-induced agranulocytosis. Incidence and risk factors in the United States. *N Engl J Med* 329: 162-7
- American Psychiatric Association (1994) *Diagnostic and Statistical Manual of Mental Disorders : DSM-IV*, 4th edn. American Psychiatric Association, Washington, DC. 932 pp
- Attwell D, Laughlin SB (2001) An energy budget for signaling in the grey matter of the brain. *J Cereb Blood Flow Metab* 21: 1133-45
- Barbier EL, Lamalle L, Decorps M (2001) Methodology of brain perfusion imaging. *J Magn Reson Imaging* 13: 496-520
- Bardo MT (1998) Neuropharmacological mechanisms of drug reward: Beyond dopamine in the nucleus accumbens. *Crit Rev Neurobiol* 12: 37-67
- Bartlett EJ, Brodie JD, Simkowitz P, Dewey SL, Rusinek H, Volkow ND, Wolf AP, Smith G, Wolkin A, Cancro R (1996) Time-dependent effects of a haloperidol challenge on energy metabolism in the normal human brain. *Psychiatry Res* 60: 91-9
- Bartlett EJ, Brodie JD, Simkowitz P, Schlosser R, Dewey SL, Lindenmayer JP, Rusinek H, Wolkin A, Cancro R, Schiffer W (1998) Effect of a haloperidol challenge on regional brain metabolism in neuroleptic-responsive and nonresponsive schizophrenic patients. *Am J Psychiatry* 155: 337-43
- Bauer WR, Nadler W, Bock M, Schad LR, Wacker C, Hartlep A, Ertl G (1999) The relationship between the BOLD-induced $T(2)$ and $T(2)^{*}$: A theoretical approach for the vasculature of myocardium. *Magn Reson Med* 42: 1004-10

- Becerra L, Breiter HC, Wise R, Gonzalez RG, Borsook D (2001) Reward circuitry activation by noxious thermal stimuli. *Neuron* 32: 927-46
- Becerra L, Iadarola M, Borsook D (2004) CNS activation by noxious heat to the hand or foot: Site-dependent delay in sensory but not emotion circuitry. *J Neurophysiol* 91: 533-41
- Belliveau JW, Kwong KK, Kennedy DN, Baker JR, Stern CE, Benson R, Chesler DA, Weisskoff RM, Cohen MS, Tootell RB, et al. (1992) Magnetic resonance imaging mapping of brain function. Human visual cortex. *Invest Radiol* 27 Suppl 2: S59-65
- Benes FM, Paskevich PA, Davidson J, Domesick VB (1985) The effects of haloperidol on synaptic patterns in the rat striatum. *Brain Res* 329: 265-73
- Benjamini Y, Hochberg Y (1995) Controlling the false discovery rate: A practical and powerful approach to multiple testing. *J. Roy. Stat. Soc. B.* 57: 289-300
- Blamire AM, Ogawa S, Ugurbil K, Rothman D, McCarthy G, Ellermann JM, Hyder F, Rattner Z, Shulman RG (1992) Dynamic mapping of the human visual cortex by high-speed magnetic resonance imaging. *Proc Natl Acad Sci U S A* 89: 11069-73
- Bloch F, Hansen WW, Packard M (1946) Nuclear induction. *Physical Review* 69: 127
- Bogerts B (1997) The temporolimbic system theory of positive schizophrenic symptoms. *Schizophr Bull* 23: 423-35
- Bomdorf H, Helzel T, Kunz D, Röschmann P, Tschendel O, Wieland J. (1988) Spectroscopy and imaging with a 4 Tesla whole-body MR system. *NMR in Biomedicine* 1: 151-158
- Boxerman JL, Bandettini PA, Kwong KK, Baker JR, Davis TL, Rosen BR, Weisskoff RM (1995a) The intravascular contribution to fMRI signal change: Monte Carlo modeling and diffusion-weighted studies in vivo. *Magn Reson Med* 34: 4-10
- Boxerman JL, Hamberg LM, Rosen BR, Weisskoff RM (1995b) MR contrast due to intravascular magnetic susceptibility perturbations. *Magn Reson Med* 34: 555-66
- Braus DF, Weber-Fahr W, Tost H, Ruf M, Henn FA (2002) Sensory information processing in neuroleptic-naïve first-episode schizophrenic patients: A functional magnetic resonance imaging study. *Arch Gen Psychiatry* 59: 696-701
- Breier A, Berg PH (1999) The psychosis of schizophrenia: Prevalence, response to atypical antipsychotics, and prediction of outcome. *Biol Psychiatry* 46: 361-4

- Breiter HC, Gollub RL, Weisskoff RM, Kennedy DN, Makris N, Berke JD, Goodman JM, Kantor HL, Gastfriend DR, Riorden JP, Mathew RT, Rosen BR, Hyman SE (1997) Acute effects of cocaine on human brain activity and emotion. *Neuron* 19: 591-611
- Brown M, Semelka R (1999) *MRI: Basic Principles and Applications*, 2nd ed. edn. Wiley-Liss, Inc., New York. 202 pp
- Buxton RB, Frank LR, Wong EC, Siewert B, Warach S, Edelman RR (1998) A general kinetic model for quantitative perfusion imaging with arterial spin labeling. *Magn Reson Med* 40: 383-96
- Buxton RB (2002) *Introduction to Functional Magnetic Resonance Imaging: Principles and Techniques*. Cambridge University Press, New York. 523 pp
- Buxton RB, Uludag K, Dubowitz DJ, Liu TT (2004) Modeling the hemodynamic response to brain activation. *Neuroimage* 23 Suppl 1: S220-33
- Bymaster FP, Rasmussen K, Calligaro DO, Nelson DL, DeLapp NW, Wong DT, Moore NA (1997) In vitro and in vivo biochemistry of olanzapine: A novel, atypical antipsychotic drug. *J Clin Psychiatry* 58 Suppl 10: 28-36
- Casey DE (1997) The relationship of pharmacology to side effects. *J Clin Psychiatry* 58 Suppl 10: 55-62
- Chakos MH, Lieberman JA, Bilder RM, Borenstein M, Lerner G, Bogerts B, Wu H, Kinon B, Ashtari M (1994) Increase in caudate nuclei volumes of first-episode schizophrenic patients taking antipsychotic drugs. *Am J Psychiatry* 151: 1430-6
- Chakos MH, Shirakawa O, Lieberman J, Lee H, Bilder R, Tamminga CA (1998) Striatal enlargement in rats chronically treated with neuroleptic. *Biol Psychiatry* 44: 675-84
- Chang C, Shyu BC (2001) A fmri study of brain activations during non-noxious and noxious electrical stimulation of the sciatic nerve of rats. *Brain Res* 897: 71-81
- Chen YC, Mandeville JB, Nguyen TV, Talele A, Cavagna F, Jenkins BG (2001) Improved mapping of pharmacologically induced neuronal activation using the iron technique with superparamagnetic blood pool agents. *J Magn Reson Imaging* 14: 517-24
- Cohen Z, Bouchelet I, Olivier A, Villemure JG, Ball R, Stanimirovic DB, Hamel E (1999) Multiple microvascular and astroglial 5-hydroxytryptamine receptor subtypes in human brain: Molecular and pharmacologic characterization. *J Cereb Blood Flow Metab* 19: 908-17

Colebatch JG, Deiber MP, Passingham RE, Friston KJ, Frackowiak RS (1991) Regional cerebral blood flow during voluntary arm and hand movements in human subjects. *J Neurophysiol* 65: 1392-401

Cooley J, Tukey O (1965) An algorithm for the machine calculation of complex fourier series. *Math Computation* 19: 297-301

Corbett AD, Henderson G, McKnight AT, Paterson SJ (2006) 75 years of opioid research: The exciting but vain quest for the holy grail. *Br J Pharmacol* 147 Suppl 1: S153-62

Corrigan MH, Gallen CC, Bonura ML, Merchant KM (2004) Effectiveness of the selective d4 antagonist sonepiprazole in schizophrenia: A placebo-controlled trial. *Biol Psychiatry* 55: 445-51

Cox RW (1996) AFNI: Software for analysis and visualization of functional magnetic resonance neuroimages. *Comput Biomed Res* 29: 162-73

Creese I, Burt DR, Snyder SH (1976) Dopamine receptor binding predicts clinical and pharmacological potencies of antischizophrenic drugs. *Science* 192: 481-3

Cunningham AS, Salvador R, Coles JP, Chatfield DA, Bradley PG, Johnston AJ, Steiner LA, Fryer TD, Aigbirhio FI, Smielewski P, Williams GB, Carpenter TA, Gillard JH, Pickard JD, Menon DK (2005) Physiological thresholds for irreversible tissue damage in contusional regions following traumatic brain injury. *Brain* 128: 1931-42

Curran MP, Perry CM (2001) Amisulpride: A review of its use in the management of schizophrenia. *Drugs* 61: 2123-50

Curry T, Dowdey J, Murry R (1990) Christensen's physics of diagnostic radiology, 4th Edition edn. Lea & Febiger, Philadelphia. 504 pp

Damadian R (1971) Tumor detection by nuclear magnetic resonance. *Science* 171: 1151-3

Davis TL, Kwong KK, Weisskoff RM, Rosen BR (1998) Calibrated functional MRI: Mapping the dynamics of oxidative metabolism. *Proc Natl Acad Sci U S A* 95: 1834-9

Delay J, Deniker P, Harl, Grasset A (1952a) [N-dimethylamino-propylchlorophenothiazine (4560 RP) therapy of confusional states.]. *Ann Med Psychol (Paris)* 110: 398-403

Delay J, Deniker P, Harl JM (1952b) [Therapeutic use in psychiatry of phenothiazine of central elective action (4560 RP).]. *Ann Med Psychol (Paris)* 110: 112-7

Detre JA, Leigh JS, Williams DS, Koretsky AP (1992) Perfusion imaging. *Magn Reson Med* 23: 37-45

Detre JA, Williams DS, Zhang W, Roberts DA, Leigh JS, Koretsky A (1995) Noninvasive perfusion MR imaging using spin labeling of arterial water. In: Le Bihan D (ed) *Diffusion and perfusion magnetic resonance imaging*. Raven, New York, pp 296-304

Dixon WT, Du LN, Faul DD, Gado M, Rossnick S (1986) Projection angiograms of blood labeled by adiabatic fast passage. *Magn Reson Med* 3: 454-62

Duong TQ, Silva AC, Lee SP, Kim SG (2000) Functional MRI of calcium-dependent synaptic activity: Cross correlation with CBF and BOLD measurements. *Magn Reson Med* 43: 383-92

Duong TQ, Iadecola C, Kim SG (2001) Effect of hyperoxia, hypercapnia, and hypoxia on cerebral interstitial oxygen tension and cerebral blood flow. *Magn Reson Med* 45: 61-70

Duong TQ, Yacoub E, Adriany G, Hu X, Ugurbil K, Kim SG (2003) Microvascular bold contribution at 4 and 7 T in the human brain: Gradient-echo and spin-echo fmri with suppression of blood effects. *Magn Reson Med* 49: 1019-27

Duyn JH, van Gelderen P, Talagala L, Koretsky A, de Zwart JA (2005) Technological advances in MRI measurement of brain perfusion. *J Magn Reson Imaging* 22: 751-3

Edelstein WA, Hutchison JM, Johnson G, Redpath T (1980) Spin warp NMR imaging and applications to human whole-body imaging. *Phys Med Biol* 25: 751-6

Farde L, Wiesel FA, Halldin C, Sedvall G (1988) Central D₂-dopamine receptor occupancy in schizophrenic patients treated with antipsychotic drugs. *Arch Gen Psychiatry* 45: 71-6

Farde L, Nordstrom AL, Wiesel FA, Pauli S, Halldin C, Sedvall G (1992) Positron emission tomographic analysis of central D₁ and D₂ dopamine receptor occupancy in patients treated with classical neuroleptics and clozapine. Relation to extrapyramidal side effects. *Arch Gen Psychiatry* 49: 538-44

Febo M, Segarra AC, Tenney JR, Brevard ME, Duong TQ, Ferris CF (2004) Imaging cocaine-induced changes in the mesocorticolimbic dopaminergic system of conscious rats. *J Neurosci Methods* 139: 167-76

Febo M, Segarra AC, Nair G, Schmidt K, Duong TQ, Ferris CF (2005) The neural consequences of repeated cocaine exposure revealed by functional MRI in awake rats. *Neuropsychopharmacology* 30: 936-43

Ferris CF, Snowdon CT, King JA, Duong TQ, Ziegler TE, Ugurbil K, Ludwig R, Schultz-Darken NJ, Wu Z, Olson DP, Sullivan Jr JM, Tannenbaum PL, Vaughan JT (2001) Functional imaging of brain activity in conscious monkeys responding to sexually arousing cues. *Neuroreport* 12: 2231-6

Ferris CF, Kulkarni P, Sullivan JM, Jr., Harder JA, Messenger TL, Febo M (2005) Pup suckling is more rewarding than cocaine: Evidence from functional magnetic resonance imaging and three-dimensional computational analysis. *J Neurosci* 25: 149-56

Ferris CF, Febo M, Luo F, Schmidt K, Brevard M, Harder JA, Kulkarni P, Messenger T, King JA (2006) Functional magnetic resonance imaging in conscious animals: A new tool in behavioural neuroscience research. *J Neuroendocrinol* 18: 307-18

Fiat D, Kang S (1992) Determination of the rate of cerebral oxygen consumption and regional cerebral blood flow by non-invasive ^{17}O in vivo nmr spectroscopy and magnetic resonance imaging: Part 1. Theory and data analysis methods. *Neurol Res* 14: 303-11

Fiat D, Dolinsek J, Hankiewicz J, Dujovny M, Ausman J (1993) Determination of regional cerebral oxygen consumption in the human: ^{17}O natural abundance cerebral magnetic resonance imaging and spectroscopy in a whole body system. *Neurol Res* 15: 237-48

Fiat D, Kang S (1993) Determination of the rate of cerebral oxygen consumption and regional cerebral blood flow by non-invasive ^{17}O in vivo NMR spectroscopy and magnetic resonance imaging. Part 2. Determination of CMRO_2 for the rat by ^{17}O NMR, and CMRO_2 , rCBF and the partition coefficient for the cat by ^{17}O mri. *Neurol Res* 15: 7-22

Fox PT, Raichle ME, Mintun MA, Dence C (1988) Nonoxidative glucose consumption during focal physiologic neural activity. *Science* 241: 462-4

Friston KJ (1998) The disconnection hypothesis. *Schizophr Res* 30: 115-25

Fullerton G, Cameron I (1988) Relaxation of biological tissues. In: Wehrli F, Shaw D, Kneeland J (eds) *Biomedical Magnetic Resonance Imaging*. VCH Publishers, Inc., New York, pp 115-155

Gilman S, Newman S (2003) *Manter and Gatz's Essentials of Clinical Neuroanatomy and Neurophysiology*, 10th edn. F.A. Davis Company, Philadelphia. 281 pp

GlaxoSmithKline (2003) *Imitrex (sumatriptan succinate) injection prescribing information*, Research Triangle Park, NC 27709

Gollub RL, Breiter HC, Kantor H, Kennedy D, Gastfriend D, Mathew RT, Makris N, Guimaraes A, Riorden J, Campbell T, Foley M, Hyman SE, Rosen B, Weisskoff R (1998) Cocaine decreases cortical cerebral blood flow but does not obscure regional activation in functional magnetic resonance imaging in human subjects. *J Cereb Blood Flow Metab* 18: 724-34

Gorelick DA (1998) The rate hypothesis and agonist substitution approaches to cocaine abuse treatment. *Adv Pharmacol* 42: 995-7

Grubb RL, Jr., Raichle ME, Eichling JO, Ter-Pogossian MM (1974) The effects of changes in PaCO₂ on cerebral blood volume, blood flow, and vascular mean transit time. *Stroke* 5: 630-9

Gur RE, Maany V, Mozley PD, Swanson C, Bilker W, Gur RC (1998) Subcortical MRI volumes in neuroleptic-naïve and treated patients with schizophrenia. *Am J Psychiatry* 155: 1711-7

Gurevich EV, Joyce JN (1999) Distribution of dopamine D₃ receptor expressing neurons in the human forebrain: Comparison with D₂ receptor expressing neurons. *Neuropsychopharmacology* 20: 60-80

Hafkenshiel J, Friedland C (1952) Physiology of the cerebral circulation in essential hypertension: The effects of 5% carbon dioxide mixtures on cerebral hemodynamics and oxygen metabolism. *Journal of Pharmacology and Experimental Therapeutics* 34: 391-392

Hallenga K (1991) Fourier transform NMR: Theoretical and practical aspects. In: *Modern NMR Techniques and Their Application in Chemistry*. Marcel Dekker, Inc., New York, pp 53-124

Hamon J, Paraire J, Velluz J (1952) [effect of r. P. 4560 on maniacal agitation.]. *Ann Med Psychol (Paris)* 110: 331-5

Han DD, Gu HH (2006) Comparison of the monoamine transporters from human and mouse in their sensitivities to psychostimulant drugs. *BMC Pharmacol* 6: 6

Hashimoto K, Fujita Y, Shimizu E, Iyo M (2005) Phencyclidine-induced cognitive deficits in mice are improved by subsequent subchronic administration of clozapine, but not haloperidol. *Eur J Pharmacol* 519: 114-7

Henderson LA, Richard CA, Macey PM, Runquist ML, Yu PL, Galons JP, Harper RM (2004) Functional magnetic resonance signal changes in neural structures to baroreceptor reflex activation. *J Appl Physiol* 96: 693-703

- Hess A, Sergejeva M, Budinsky L, Zeilhofer HU, Brune K (2006) Imaging of hyperalgesia in rats by functional MRI. *Eur J Pain*. In Press
- Hoge RD, Atkinson J, Gill B, Crelier GR, Marrett S, Pike GB (1999a) Investigation of BOLD signal dependence on cerebral blood flow and oxygen consumption: The deoxyhemoglobin dilution model. *Magn Reson Med* 42: 849-63
- Hoge RD, Atkinson J, Gill B, Crelier GR, Marrett S, Pike GB (1999b) Linear coupling between cerebral blood flow and oxygen consumption in activated human cortex. *Proc Natl Acad Sci U S A* 96: 9403-8
- Holcomb HH, Cascella NG, Thaker GK, Medoff DR, Dannals RF, Tamminga CA (1996) Functional sites of neuroleptic drug action in the human brain: PET/FDG studies with and without haloperidol. *Am J Psychiatry* 153: 41-9
- Holcomb HH, Lahti AC, Medoff DR, Weiler M, Dannals RF, Tamminga CA (2000) Brain activation patterns in schizophrenic and comparison volunteers during a matched-performance auditory recognition task. *Am J Psychiatry* 157: 1634-45
- Holden A, Wilman A, Wieler M, Martin WR (2006) Basal ganglia activation in Parkinson's disease. *Parkinsonism Relat Disord* 12: 73-7
- Honey G, Bullmore E (2004) Human pharmacological MRI. *Trends Pharmacol Sci* 25: 366-74
- Honey GD, Bullmore ET, Soni W, Varatheesan M, Williams SC, Sharma T (1999) Differences in frontal cortical activation by a working memory task after substitution of risperidone for typical antipsychotic drugs in patients with schizophrenia. *Proc Natl Acad Sci U S A* 96: 13432-7
- Honey GD, Pomarol-Clotet E, Corlett PR, Honey RA, McKenna PJ, Bullmore ET, Fletcher PC (2005) Functional dysconnectivity in schizophrenia associated with attentional modulation of motor function. *Brain* 128: 2597-611
- Horacek J, Bubenikova-Valesova V, Kopecek M, Palenicek T, Dockery C, Mohr P, Hoschl C (2006) Mechanism of action of atypical antipsychotic drugs and the neurobiology of schizophrenia. *CNS Drugs* 20: 389-409
- Hornak J (2002) The basics of MRI. Interactive Learning Software. <http://www.cis.rit.edu/htbooks/mri>
- Horvath I, Sandor NT, Ruttner Z, McLaughlin AC (1994) Role of nitric oxide in regulating cerebrocortical oxygen consumption and blood flow during hypercapnia. *J Cereb Blood Flow Metab* 14: 503-9

Hulvershorn J, Bloy L, Gualtieri EE, Leigh JS, Elliott MA (2005) Spatial sensitivity and temporal response of spin echo and gradient echo bold contrast at 3 T using peak hemodynamic activation time. *Neuroimage* 24: 216-23

Hyder F, Chase JR, Behar KL, Mason GF, Siddeek M, Rothman DL, Shulman RG (1996) Increased tricarboxylic acid cycle flux in rat brain during forepaw stimulation detected with $^1\text{H}[^{13}\text{C}]\text{NMR}$. *Proc Natl Acad Sci U S A* 93: 7612-7

Hyder F (2004) Neuroimaging with calibrated fMRI. *Stroke* 35: 2635-41

Hyman SE, Nestler EJ (1996) Initiation and adaptation: A paradigm for understanding psychotropic drug action. *Am J Psychiatry* 153: 151-62

Inturrisi CE, Schultz M, Shin S, Umans JG, Angel L, Simon EJ (1983) Evidence from opiate binding studies that heroin acts through its metabolites. *Life Sci* 33 Suppl 1: 773-6

Jacob SW, Herschler R (1986) Pharmacology of dmsO. *Cryobiology* 23: 14-27

Jochimsen TH, Norris DG, Mildner T, Moller HE (2004) Quantifying the intra- and extravascular contributions to spin-echo fmri at 3 t. *Magn Reson Med* 52: 724-32

Jones M, Hewson-Stoate N, Martindale J, Redgrave P, Mayhew J (2004) Nonlinear coupling of neural activity and cbf in rodent barrel cortex. *Neuroimage* 22: 956-65

Juckel G, Schlagenhauf F, Koslowski M, Wustenberg T, Villringer A, Knutson B, Wrase J, Heinz A (2006) Dysfunction of ventral striatal reward prediction in schizophrenia. *Neuroimage* 29: 409-16

Jung C, Weissleder R, Josephson L, Bengel H, Brady T (1996) Physical properties of MION-46 and AMI-227. *International Society of Magnetic Resonance in Medicine, 4th Annual Meeting*, p 1681

Kalisch R, Delfino M, Murer MG, Auer DP (2005) The phenylephrine blood pressure clamp in pharmacologic magnetic resonance imaging: Reduction of systemic confounds and improved detectability of drug-induced BOLD signal changes. *Psychopharmacology (Berl)* 180: 774-80

Kane J, Honigfeld G, Singer J, Meltzer H (1988) Clozapine for the treatment-resistant schizophrenic. A double-blind comparison with chlorpromazine. *Arch Gen Psychiatry* 45: 789-96

Kapur S, Mamo D (2003) Half a century of antipsychotics and still a central role for dopamine D_2 receptors. *Prog Neuropsychopharmacol Biol Psychiatry* 27: 1081-90

Kasischke KA, Vishwasrao HD, Fisher PJ, Zipfel WR, Webb WW (2004) Neural activity triggers neuronal oxidative metabolism followed by astrocytic glycolysis. *Science* 305: 99-103

Katzung B (2004) *Basic & Clinical Pharmacology*, 9th edn. The McGraw-Hill Companies, Inc., New York. 1202 pp

Kaufman MJ, Levin JM, Maas LC, Kukes TJ, Villafuerte RA, Dostal K, Lukas SE, Mendelson JH, Cohen BM, Renshaw PF (2001) Cocaine-induced cerebral vasoconstriction differs as a function of sex and menstrual cycle phase. *Biol Psychiatry* 49: 774-81

Keilholz SD, Silva AC, Raman M, Merkle H, Koretsky AP (2004) Functional MRI of the rodent somatosensory pathway using multislice echo planar imaging. *Magn Reson Med* 52: 89-99

Keilholz SD, Silva AC, Raman M, Merkle H, Koretsky AP (2006) Bold and cbv-weighted functional magnetic resonance imaging of the rat somatosensory system. *Magn Reson Med* 55: 316-24

Kelley AE (2004) Memory and addiction: Shared neural circuitry and molecular mechanisms. *Neuron* 44: 161-79

Kennedy C, Des Rosiers MH, Sakurada O, Shinohara M, Reivich M, Jehle JW, Sokoloff L (1976) Metabolic mapping of the primary visual system of the monkey by means of the autoradiographic [^{14}C]deoxyglucose technique. *Proc Natl Acad Sci U S A* 73: 4230-4

Keshavan MS, Bagwell WW, Haas GL, Sweeney JA, Schooler NR, Pettegrew JW (1994) Changes in caudate volume with neuroleptic treatment. *Lancet* 344: 1434

Kessler RM, Ansari MS, Riccardi P, Li R, Jayathilake K, Dawant B, Meltzer HY (2006) Occupancy of striatal and extrastriatal dopamine D(2) receptors by clozapine and quetiapine. *Neuropsychopharmacology*. In Press

Kety S, Schmidt C (1948) The effects of altered arterial tensions of carbon dioxide and oxygen on cerebral blood flow and cerebral oxygen consumption of normal young men. *Journal of Clinical Investigation* 27: 484-491

Khubchandani M, Mallick HN, Jagannathan NR, Mohan Kumar V (2003) Stereotaxic assembly and procedures for simultaneous electrophysiological and mri study of conscious rat. *Magn Reson Med* 49: 962-7

Kim SG, Rostrup E, Larsson HB, Ogawa S, Paulson OB (1999) Determination of relative CMRO₂ from CBF and BOLD changes: Significant increase of oxygen consumption rate during visual stimulation. *Magn Reson Med* 41: 1152-61

- King JA, Garelick TS, Brevard ME, Chen W, Messenger TL, Duong TQ, Ferris CF (2005) Procedure for minimizing stress for fMRI studies in conscious rats. *J Neurosci Methods* 148: 154-60
- Kinon BJ, Ahl J, Stauffer VL, Hill AL, Buckley PF (2004) Dose response and atypical antipsychotics in schizophrenia. *CNS Drugs* 18: 597-616
- Konradi C, Heckers S (2001) Antipsychotic drugs and neuroplasticity: Insights into the treatment and neurobiology of schizophrenia. *Biol Psychiatry* 50: 729-42
- Koob GF, Bloom FE (1988) Cellular and molecular mechanisms of drug dependence. *Science* 242: 715-23
- Koyama M, Hasegawa I, Osada T, Adachi Y, Nakahara K, Miyashita Y (2004) Functional magnetic resonance imaging of macaque monkeys performing visually guided saccade tasks: Comparison of cortical eye fields with humans. *Neuron* 41: 795-807
- Krings T, Erberich SG, Roessler F, Reul J, Thron A (1999) MR blood oxygenation level-dependent signal differences in parenchymal and large draining vessels: Implications for functional MR imaging. *AJNR Am J Neuroradiol* 20: 1907-14
- Kubicki M, McCarley RW, Nestor PG, Huh T, Kikinis R, Shenton ME, Wible CG (2003) An fMRI study of semantic processing in men with schizophrenia. *Neuroimage* 20: 1923-33
- Kumar A, Welti D, Ernst RR (1975) Imaging of macroscopic objects by NMR Fourier zeugmatography. *Naturwissenschaften* 62: 34-34
- Kwong KK, Belliveau JW, Chesler DA, Goldberg IE, Weisskoff RM, Poncelet BP, Kennedy DN, Hoppel BE, Cohen MS, Turner R, et al. (1992) Dynamic magnetic resonance imaging of human brain activity during primary sensory stimulation. *Proc Natl Acad Sci U S A* 89: 5675-9
- Laborit H, Huguenard P (1951) [Artificial hibernation by pharmacodynamic and physical means, in surgery.] *J Chir (Paris)* 67: 631-41
- Lahti AC, Holcomb HH, Medoff DR, Weiler MA, Tamminga CA, Carpenter WT, Jr. (2001) Abnormal patterns of regional cerebral blood flow in schizophrenia with primary negative symptoms during an effortful auditory recognition task. *Am J Psychiatry* 158: 1797-808
- Lahti KM, Ferris CF, Li F, Sotak CH, King JA (1998) Imaging brain activity in conscious animals using functional MRI. *J Neurosci Methods* 82: 75-83

- Lane HY, Hsu SK, Liu YC, Chang YC, Huang CH, Chang WH (2005) Dopamine D₃ receptor Ser9Gly polymorphism and risperidone response. *J Clin Psychopharmacol* 25: 6-11
- Lauterbur PC (1973) Image formation by induced local interactions: Examples employing nuclear magnetic resonance. *Nature* 242: 190-191
- Lee SW, Hilal SK, Cho ZH (1986) A multinuclear magnetic resonance imaging technique--simultaneous proton and sodium imaging. *Magn Reson Imaging* 4: 343-50
- Li KL, Suojanen JN (1995) Cocaine-induced changes in time course of regional cerebral blood volume and transit time as determined by dynamic MR imaging. *J Magn Reson Imaging* 5: 715-8
- Lindsley CW, Shipe WD, Wolkenberg SE, Theberge CR, Williams DL, Jr., Sur C, Kinney GG (2006) Progress towards validating the NMDA receptor hypofunction hypothesis of schizophrenia. *Curr Top Med Chem* 6: 771-85
- Linn GS, Negi SS, Gerum SV, Javitt DC (2003) Reversal of phencyclidine-induced prepulse inhibition deficits by clozapine in monkeys. *Psychopharmacology (Berl)* 169: 234-9
- Liu CS, Miki A, Hulvershorn J, Bloy L, Gualtieri EE, Liu GT, Leigh JS, Haselgrove JC, Elliott MA (2006) Spatial and temporal characteristics of physiological noise in fMRI at 3T. *Acad Radiol* 13: 313-23
- Liu ZM, Schmidt KF, Sicard KM, Duong TQ (2004) Imaging oxygen consumption in forepaw somatosensory stimulation in rats under isoflurane anesthesia. *Magn Reson Med* 52: 277-285
- Logothetis NK (2002) The neural basis of the blood-oxygen-level-dependent functional magnetic resonance imaging signal. *Philos Trans R Soc Lond B Biol Sci* 357: 1003-37
- Lu H, Golay X, Pekar JJ, Van Zijl PC (2003) Functional magnetic resonance imaging based on changes in vascular space occupancy. *Magn Reson Med* 50: 263-74
- Ludwig R, Bodgdanov G, King J, Allard A, Ferris CF (2004) A dual RF resonator system for high-field functional magnetic resonance imaging of small animals. *J Neurosci Methods* 132: 125-35
- Luo F, Wu G, Li Z, Li SJ (2003) Characterization of effects of mean arterial blood pressure induced by cocaine and cocaine methiodide on BOLD signals in rat brain. *Magn Reson Med* 49: 264-70

- Luo F, Xi ZX, Wu G, Liu C, Gardner EL, Li SJ (2004) Attenuation of brain response to heroin correlates with the reinstatement of heroin-seeking in rats by fMRI. *Neuroimage* 22: 1328-35
- Madsen PL, Holm S, Vorstrup S, Friberg L, Lassen NA, Wildschiodtz G (1991) Human regional cerebral blood flow during rapid-eye-movement sleep. *J Cereb Blood Flow Metab* 11: 502-7
- Madsen PL, Linde R, Hasselbalch SG, Paulson OB, Lassen NA (1998) Activation-induced resetting of cerebral oxygen and glucose uptake in the rat. *J Cereb Blood Flow Metab* 18: 742-8
- Magistretti PJ, Pellerin L, Rothman DL, Shulman RG (1999) Energy on demand. *Science* 283: 496-7
- Makiranta MJ, Ruohonen J, Suominen K, Sonkajarvi E, Salomaki T, Kiviniemi V, Seppanen T, Alahuhta S, Jantti V, Tervonen O (2004) BOLD-contrast functional MRI signal changes related to intermittent rhythmic delta activity in EEG during voluntary hyperventilation-simultaneous EEG and fMRI study. *Neuroimage* 22: 222-31
- Malisza KL, Docherty JC (2001) Capsaicin as a source for painful stimulation in functional MRI. *J Magn Reson Imaging* 14: 341-7
- Mandeville JB, Marota JJ, Ayata C, Moskowitz MA, Weisskoff RM, Rosen BR (1999) MRI measurement of the temporal evolution of relative CMRO(2) during rat forepaw stimulation. *Magn Reson Med* 42: 944-51
- Mandeville JB, Jenkins BG, Kosofsky BE, Moskowitz MA, Rosen BR, Marota JJ (2001) Regional sensitivity and coupling of BOLD and CBV changes during stimulation of rat brain. *Magn Reson Med* 45: 443-7
- Mandeville JB, Ekstrom L, Marota JJ, Jenkins BG, Vanduffel W (2005) Contrast-enhanced fMRI of cocaine action in awake non-human primate. *International Society of Magnetic Resonance in Medicine, 13th meeting. International Society for Magnetic Resonance in Medicine, Miami Beach, FL. Abstract 1506*
- Marota JJ, Mandeville JB, Weisskoff RM, Moskowitz MA, Rosen BR, Kosofsky BE (2000) Cocaine activation discriminates dopaminergic projections by temporal response: An fMRI study in rat. *Neuroimage* 11: 13-23
- Marsden CA (2006) Dopamine: The rewarding years. *Br J Pharmacol* 147 Suppl 1: S136-44

- Mata M, Fink DJ, Gainer H, Smith CB, Davidsen L, Savaki H, Schwartz WJ, Sokoloff L (1980) Activity-dependent energy metabolism in rat posterior pituitary primarily reflects sodium pump activity. *J Neurochem* 34: 213-5
- Medoff DR, Holcomb HH, Lahti AC, Tamminga CA (2001) Probing the human hippocampus using rCBF: Contrasts in schizophrenia. *Hippocampus* 11: 543-50
- Meltzer HY (1999) The role of serotonin in antipsychotic drug action. *Neuropsychopharmacology* 21: 106S-115S
- Meltzer HY, Arvanitis L, Bauer D, Rein W (2004) Placebo-controlled evaluation of four novel compounds for the treatment of schizophrenia and schizoaffective disorder. *Am J Psychiatry* 161: 975-84
- Middleton H, Black RD, Saam B, Cates GD, Cofer GP, Guenther R, Happer W, Hedlund LW, Johnson GA, Juvan K, et al. (1995) MR imaging with hyperpolarized ^3He gas. *Magn Reson Med* 33: 271-5
- Miller PL, Gay GR, Ferris KC, Anderson S (1992) Treatment of acute, adverse psychedelic reactions: "I've tripped and I can't get down". *J Psychoactive Drugs* 24: 277-9
- Moffat BA, Chenevert TL, Hall DE, Rehemtulla A, Ross BD (2005) Continuous arterial spin labeling using a train of adiabatic inversion pulses. *J Magn Reson Imaging* 21: 290-6
- Murray CJ, Lopez AD, The World Health Organization, Harvard School of Public Health, The World Bank (1996) *The Global Burden of Disease: A Comprehensive Assessment of Mortality and Disability from Diseases, Injuries, and Risk Factors in 1990 and Projected to 2020*. Harvard University Press, Cambridge, MA, USA. 976 pp
- Nair DG (2005) About being BOLD. *Brain Res Brain Res Rev* 50(2):229-43
- National Institutes of Health (1997) Effective medical treatment of opiate addiction. NIH Consensus Statement 15: 1-38
- National Library of Medicine (US) (2005) A.D.A.M. Medical encyclopedia. National Library of Medicine (US), Atlanta (GA) <http://www.nlm.nih.gov/medlineplus>
- Nelson RA, Boyd SJ, Ziegelstein RC, Herning R, Cadet JL, Henningfield JE, Schuster CR, Contoreggi C, Gorelick DA (2006) Effect of rate of administration on subjective and physiological effects of intravenous cocaine in humans. *Drug Alcohol Depend* 82: 19-24
- Nelson TR, Newman FD, Schiffer LM, Reith JD, Cameron SL (1985) Fluorine nuclear magnetic resonance: Calibration and system optimization. *Magn Reson Imaging* 3: 267-73

Nestler EJ, Hyman SE, Malenka RC (2001) *Molecular Neuropharmacology : A Foundation for Clinical Neuroscience*. McGraw-Hill, New York. 539 pp

Nestler EJ (2002) From neurobiology to treatment: Progress against addiction. *Nat Neurosci* 5 Suppl: 1076-9

Nguyen TV, Brownell AL, Iris Chen YC, Livni E, Coyle JT, Rosen BR, Cavagna F, Jenkins BG (2000) Detection of the effects of dopamine receptor supersensitivity using pharmacological mri and correlations with pet. *Synapse* 36: 57-65

Novartis Pharmaceutical Corporation (2005) Clozaril (clozapine) tablets, prescribing information, East Hanover (NJ)

O'Brien CP (2003) Research advances in the understanding and treatment of addiction. *Am J Addict* 12 Suppl 2: S36-47

Ogawa S, Lee TM, Nayak AS, Glynn P (1990) Oxygenation-sensitive contrast in magnetic resonance image of rodent brain at high magnetic fields. *Magn Reson Med* 14: 68-78

Ogawa S, Tank DW, Menon R, Ellermann JM, Kim SG, Merkle H, Ugurbil K (1992) Intrinsic signal changes accompanying sensory stimulation: Functional brain mapping with magnetic resonance imaging. *Proc Natl Acad Sci U S A* 89: 5951-5

Ogawa S, Menon RS, Tank DW, Kim SG, Merkle H, Ellermann JM, Ugurbil K (1993) Functional brain mapping by blood oxygenation level-dependent contrast magnetic resonance imaging. A comparison of signal characteristics with a biophysical model. *Biophys J* 64: 803-12

Paschal CB, Morris HD (2004) K-space in the clinic. *J Magn Reson Imaging* 19: 145-59

Paulus MP, Hozack NE, Zauscher BE, Frank L, Brown GG, McDowell J, Braff DL (2002) Parietal dysfunction is associated with increased outcome-related decision-making in schizophrenia patients. *Biol Psychiatry* 51: 995-1004

Paxinos G, Watson C (1998) *The Rat Brain in Stereotaxic Coordinates*, Fourth edn. Academic Press, Inc, San Diego, CA. 474 pp

Pekar J, Ligeti L, Ruttner Z, Lyon RC, Sinnwell TM, van Gelderen P, Fiat D, Moonen CT, McLaughlin AC (1991) In vivo measurement of cerebral oxygen consumption and blood flow using ¹⁷O magnetic resonance imaging. *Magn Reson Med* 21: 313-9

Pellerin L, Magistretti PJ (1994) Glutamate uptake into astrocytes stimulates aerobic glycolysis: A mechanism coupling neuronal activity to glucose utilization. *Proc Natl Acad Sci U S A* 91: 10625-9

Pitts DK, Udom CE, Marwah J (1987) Cardiovascular effects of cocaine in anesthetized and conscious rats. *Life Sci* 40: 1099-111

Porrino LJ, Domer FR, Crane AM, Sokoloff L (1988) Selective alterations in cerebral metabolism within the mesocorticolimbic dopaminergic system produced by acute cocaine administration in rats. *Neuropsychopharmacology* 1: 109-18

Purcell EM, Torrey HC, Pound RV (1946) Resonance absorption by nuclear magnetic moments in a solid. *Physical Review* 69: 37

Reavill C, Taylor SG, Wood MD, Ashmeade T, Austin NE, Avenell KY, Boyfield I, Branch CL, Cilia J, Coldwell MC, Hadley MS, Hunter AJ, Jeffrey P, Jewitt F, Johnson CN, Jones DN, Medhurst AD, Middlemiss DN, Nash DJ, Riley GJ, Routledge C, Stemp G, Thewlis KM, Trail B, Vong AK, Hagan JJ (2000) Pharmacological actions of a novel, high-affinity, and selective human dopamine D(3) receptor antagonist, SB-277011-A. *J Pharmacol Exp Ther* 294: 1154-65

Riad M, Tong XK, el Mestikawy S, Hamon M, Hamel E, Descarries L (1998) Endothelial expression of the 5-hydroxytryptamine_{1b} antimigraine drug receptor in rat and human brain microvessels. *Neuroscience* 86: 1031-5

Rohlf J (1994) *Modern Physics from [alpha] to z⁰*, First edn. John Wiley & Sons, Inc., New York. 646 pp

Roland PE, Eriksson L, Stone-Elander S, Widen L (1987) Does mental activity change the oxidative metabolism of the brain? *J Neurosci* 7: 2373-89

Rothman DL, Sibson NR, Hyder F, Shen J, Behar KL, Shulman RG (1999) In vivo nuclear magnetic resonance spectroscopy studies of the relationship between the glutamate-glutamine neurotransmitter cycle and functional neuroenergetics. *Phil Trans R Soc Lond B Biol Sci* 354: 1165-77

Rothman RB, Baumann MH (2003) Monoamine transporters and psychostimulant drugs. *Eur J Pharmacol* 479: 23-40

Roy C, Sherrington C (1890) On the regulation of the blood supply of the brain. *Journal of Physiology (London)* 11: 85-108

Scherk H, Falkai P (2006) Effects of antipsychotics on brain structure. *Curr Opin Psychiatry* 19: 145-50

Schmidt KF, Ziu M, Schmidt NO, Vaghasia P, Cargioli TG, Doshi S, Albert MS, Black PM, Carroll RS, Sun Y (2004) Volume reconstruction techniques improve the correlation between histological and in vivo tumor volume measurements in mouse models of human gliomas. *Journal of Neuro-Oncology* 68: 207-215

- Schmidt KF, Febo M, Shen Q, Luo F, Sicard KM, Ferris CF, Stein EA, Duong TQ (2006) Hemodynamic and metabolic changes induced by cocaine in anesthetized rat observed with multimodal functional MRI. *Psychopharmacology (Berl)* 185: 479-86
- Schmutz J, Eichenberger E (1982) *Chronicles of Drug Discovery*. Wiley, New York. pp 39-59
- Schroeder U, Schroeder H, Schwegler H, Sabel BA (2000) Neuroleptics ameliorate phencyclidine-induced impairments of short-term memory. *Br J Pharmacol* 130: 33-40
- Schwartz JC, Diaz J, Pilon C, Sokoloff P (2000) Possible implications of the dopamine d(3) receptor in schizophrenia and in antipsychotic drug actions. *Brain Res Brain Res Rev* 31: 277-87
- Schwarz AJ, Reese T, Gozzi A, Bifone A (2003) Functional MRI using intravascular contrast agents: Detrending of the relative cerebrovascular (rCBV) time course. *Magn Reson Imaging* 21: 1191-200
- Seeman P, Lee T (1975) Antipsychotic drugs: Direct correlation between clinical potency and presynaptic action on dopamine neurons. *Science* 188: 1217-9
- Seeman P, Lee T, Chau-Wong M, Wong K (1976) Antipsychotic drug doses and neuroleptic/dopamine receptors. *Nature* 261: 717-9
- Seeman P, Corbett R, Van Tol HH (1997) Atypical neuroleptics have low affinity for dopamine D₂ receptors or are selective for D₄ receptors. *Neuropsychopharmacology* 16: 93-110; discussion 111-35
- Shafer RA, Levant B (1998) The D₃ dopamine receptor in cellular and organismal function. *Psychopharmacology (Berl)* 135: 1-16
- Sharma T (2001) Quetiapine--efficacy in different domains. *Eur Neuropsychopharmacol* 11 Suppl 4: S385-90
- Shipley J (1998) M100907 phase IIb trial. Hoechst Marion Roussel Conference on M100907, West Palm Beach (FL)
- Shulman RG, Rothman DL, Behar KL, Hyder F (2004) Energetic basis of brain activity: Implications for neuroimaging. *Trends Neurosci* 27: 489-95
- Sibson NR, Dhankhar A, Mason GF, Rothman DL, Behar KL, Shulman RG (1998) Stoichiometric coupling of brain glucose metabolism and glutamatergic neuronal activity. *Proc Natl Acad Sci U S A* 95: 316-21

- Sicard K, Shen Q, Brevard ME, Sullivan R, Ferris CF, King JA, Duong TQ (2003) Regional cerebral blood flow and BOLD responses in conscious and anesthetized rats under basal and hypercapnic conditions: Implications for functional MRI studies. *J Cereb Blood Flow Metab* 23: 472-81
- Silva AC, Zhang W, Williams DS, Koretsky AP (1995) Multi-slice MRI of rat brain perfusion during amphetamine stimulation using arterial spin labeling. *Magn Reson Med* 33: 209-14
- Silva AC, Lee SP, Yang G, Iadecola C, Kim SG (1999) Simultaneous blood oxygenation level-dependent and cerebral blood flow functional magnetic resonance imaging during forepaw stimulation in the rat. *J Cereb Blood Flow Metab* 19: 871-9
- Silvennoinen MJ, Clingman CS, Golay X, Kauppinen RA, van Zijl PC (2003) Comparison of the dependence of blood R2 and R2* on oxygen saturation at 1.5 and 4.7 Tesla. *Magn Reson Med* 49: 47-60
- Skoubis PD, Hradil V, Chin CL, Luo Y, Fox GB, McGaraughty S (2006) Mapping brain activity following administration of a nicotinic acetylcholine receptor agonist, ABT-594, using functional magnetic resonance imaging in awake rats. *Neuroscience* 137: 583-91
- Sokoloff L, Reivich M, Kennedy C, Des Rosiers MH, Patlak CS, Pettigrew KD, Sakurada O, Shinohara M (1977) The [¹⁴C]deoxyglucose method for the measurement of local cerebral glucose utilization: Theory, procedure, and normal values in the conscious and anesthetized albino rat. *J Neurochem* 28: 897-916
- Squire LR, Bloom FE, McConnell SK, Roberts JL, Spitzer NC, Zigmond MJ (2003) *Fundamental Neuroscience*, 2nd edn. Academic Press, San Diego. 1426 pp
- Stanwood GD, Artymyshyn RP, Kung MP, Kung HF, Lucki I, McGonigle P (2000) Quantitative autoradiographic mapping of rat brain dopamine D₃ binding with [(125)I]7-OH-PIPAT: Evidence for the presence of D₃ receptors on dopaminergic and nondopaminergic cell bodies and terminals. *J Pharmacol Exp Ther* 295: 1223-31
- Stein EA, Fuller SA (1992) Selective effects of cocaine on regional cerebral blood flow in the rat. *J Pharmacol Exp Ther* 262: 327-34
- Stein EA (2001) Fmri: A new tool for the in vivo localization of drug actions in the brain. *J Anal Toxicol* 25: 419-24
- Strupp JP (1996) Stimulate: A GUI based fMRI analysis software package. *NeuroImage* 3: S607-S607

- Tan HY, Choo WC, Fones CS, Chee MW (2005) FMRI study of maintenance and manipulation processes within working memory in first-episode schizophrenia. *Am J Psychiatry* 162: 1849-58
- Taniwaki T, Okayama A, Yoshiura T, Togao O, Nakamura Y, Yamasaki T, Ogata K, Shigeto H, Ohyagi Y, Kira JI, Tobimatsu S (2006) Functional network of the basal ganglia and cerebellar motor loops in vivo: Different activation patterns between self-initiated and externally triggered movements. *Neuroimage* 31: 745-753
- Thirion B, Fugeras O (2003) Dynamical components analysis of fMRI data through kernel PCA. *Neuroimage* 20: 34-49
- Thulborn KR, Waterton JC, Matthews PM, Radda GK (1982) Oxygenation dependence of the transverse relaxation time of water protons in whole blood at high field. *Biochim Biophys Acta* 714: 265-70
- Trevor A, Katzung B, Masters S (2002) *Katzung & Trevor's Pharmacology: Examination & Board Review* 6th edn. The McGraw-Hill Companies, Inc., New York. 662 pp
- Turner R, Howseman A, Rees GE, Josephs O, Friston K (1998) Functional magnetic resonance imaging of the human brain: Data acquisition and analysis. *Exp Brain Res* 123: 5-12
- Ueki M, Linn F, Hossmann KA (1988) Functional activation of cerebral blood flow and metabolism before and after global ischemia of rat brain. *J Cereb Blood Flow Metab* 8: 486-94
- Uludag K, Dubowitz DJ, Yoder EJ, Restom K, Liu TT, Buxton RB (2004) Coupling of cerebral blood flow and oxygen consumption during physiological activation and deactivation measured with fMRI. *Neuroimage* 23: 148-55
- Van Camp N, Verhoye M, De Zeeuw CI, Van der Linden A (2006) Light stimulus frequency dependence of activity in the rat visual system as studied with high-resolution bold fMRI. *J Neurophysiol* 95: 3164-70
- Viviani R, Gron G, Spitzer M (2005) Functional principal component analysis of fMRI data. *Hum Brain Mapp* 24: 109-29
- Volkow ND, Fowler JS, Wang GJ (2004) The addicted human brain viewed in the light of imaging studies: Brain circuits and treatment strategies. *Neuropharmacology* 47 Suppl 1: 3-13
- Wang Z, Wang J, Calhoun V, Rao H, Detre JA, Childress AR (2006) Strategies for reducing large fMRI data sets for independent component analysis. *Magn Reson Imaging* 24: 591-6

Warach S, Dashe JF, Edelman RR (1996) Clinical outcome in ischemic stroke predicted by early diffusion-weighted and perfusion magnetic resonance imaging: A preliminary analysis. *J Cereb Blood Flow Metab* 16: 53-9

Weckesser M, Posse S, Olthoff U, Kemna L, Dager S, Muller-Gartner HW (1999) Functional imaging of the visual cortex with bold-contrast MRI: Hyperventilation decreases signal response. *Magn Reson Med* 41: 213-6

Williams DS, Detre JA, Leigh JS, Koretsky AP (1992) Magnetic resonance imaging of perfusion using spin inversion of arterial water. *Proc Natl Acad Sci U S A* 89: 212-6

Williams JT, Christie MJ, Manzoni O (2001) Cellular and synaptic adaptations mediating opioid dependence. *Physiol Rev* 81: 299-343

Wise RG, Tracey I (2006) The role of fMRI in drug discovery. *J Magn Reson Imaging* 23: 862-76

Wolf RL, Wang J, Wang S, Melhem ER, O'Rourke DM, Judy KD, Detre JA (2005) Grading of CNS neoplasms using continuous arterial spin labeled perfusion MR imaging at 3 tesla. *J Magn Reson Imaging* 22: 475-82

Wong EH, Kemp JA, Priestley T, Knight AR, Woodruff GN, Iversen LL (1986) The anticonvulsant MK-801 is a potent N-methyl-D-aspartate antagonist. *Proc Natl Acad Sci U S A* 83: 7104-8

Woolverton WL, Wang Z (2004) Relationship between injection duration, transporter occupancy and reinforcing strength of cocaine. *Eur J Pharmacol* 486: 251-7

Worsley KJ, Friston KJ (1995) Analysis of fMRI time-series revisited--again. *Neuroimage* 2: 173-81

Xi ZX, Wu G, Stein EA, Li SJ (2002) GABAergic mechanisms of heroin-induced brain activation assessed with functional MRI. *Magn Reson Med* 48: 838-43

Xi ZX, Wu G, Stein EA, Li SJ (2004) Opiate tolerance by heroin self-administration: An fMRI study in rat. *Magn Reson Med* 52: 108-14

Xiberas X, Martinot JL, Mallet L, Artiges E, Loc HC, Maziere B, Paillere-Martinot ML (2001) Extrastriatal and striatal D(2) dopamine receptor blockade with haloperidol or new antipsychotic drugs in patients with schizophrenia. *Br J Psychiatry* 179: 503-8

Xu H, Li SJ, Bodurka J, Zhao X, Xi ZX, Stein EA (2000) Heroin-induced neuronal activation in rat brain assessed by functional MRI. *Neuroreport* 11: 1085-92

Yablonskiy DA, Haacke EM (1994) Theory of NMR signal behavior in magnetically inhomogeneous tissues: The static dephasing regime. *Magn Reson Med* 32: 749-63

Yang SP, Krasney JA (1995) Cerebral blood flow and metabolic responses to sustained hypercapnia in awake sheep. *J Cereb Blood Flow Metab* 15: 115-23

Zacny JP, Lichtor JL, Flemming D, Coalson DW, Thompson WK (1994) A dose-response analysis of the subjective, psychomotor and physiological effects of intravenous morphine in healthy volunteers. *J Pharmacol Exp Ther* 268: 1-9

Zhan W, Gu H, Silbersweig DA, Stern E, Yang Y (2002) Inversion profiles of adiabatic inversion pulses for flowing spins: The effects on labeling efficiency and labeling accuracy in perfusion imaging with pulsed arterial spin-labeling. *Magn Reson Imaging* 20: 487-94

Zhang W, Silva AC, Williams DS, Koretsky AP (1995) NMR measurement of perfusion using arterial spin labeling without saturation of macromolecular spins. *Magn Reson Med* 33: 370-6

Zipursky RB, Zhang-Wong J, Lambe EK, Bean G, Beiser M (1998) MRI correlates of treatment response in first episode psychosis. *Schizophr Res* 30: 81-90

APPENDIX A

SUPPLEMENTAL GROUPWISE CORRELATION ANALYSES

Saline STDERR																			
	Amygdala	Aud Ctx	Cingulate	CPu	Entorhinal Ctx	Frontal Ctx	Hippocampus	hypothalamus	Insular Ctx	LGP	M1	PAG	Prelimbic	S1	S2	SN	Thalamus	Visual Ctx	VTA
Amygdala	0%	11%	12%	13%	8%	8%	6%	5%	8%	10%	13%	13%	6%	13%	5%	7%	13%	4%	3%
Aud Ctx	11%	0%	13%	17%	14%	13%	14%	5%	10%	12%	14%	12%	11%	17%	6%	9%	13%	12%	8%
Cingulate	12%	13%	0%	14%	13%	6%	12%	5%	5%	11%	13%	9%	3%	16%	13%	9%	9%	8%	5%
CPu	13%	17%	14%	0%	11%	15%	11%	14%	11%	13%	4%	15%	12%	11%	16%	10%	14%	8%	5%
Entorhinal Ctx	8%	14%	13%	11%	0%	12%	5%	8%	11%	18%	15%	9%	11%	17%	13%	5%	5%	10%	5%
Frontal Ctx	8%	13%	6%	15%	12%	0%	8%	6%	9%	10%	11%	10%	9%	14%	8%	13%	6%	5%	5%
Hippocampus	6%	14%	12%	11%	5%	8%	0%	10%	9%	3%	7%	9%	9%	11%	11%	9%	14%	12%	5%
hypothalamus	5%	5%	5%	14%	8%	6%	10%	0%	5%	9%	9%	7%	5%	11%	2%	4%	10%	5%	7%
Insular Ctx	8%	10%	5%	11%	11%	9%	9%	5%	0%	11%	12%	9%	3%	13%	3%	7%	10%	7%	8%
LGP	10%	12%	11%	13%	18%	10%	3%	9%	11%	0%	13%	13%	3%	12%	8%	10%	10%	13%	4%
M1	13%	14%	13%	4%	15%	11%	7%	9%	12%	13%	0%	10%	6%	17%	15%	10%	6%	9%	6%
PAG	13%	12%	9%	15%	9%	10%	9%	7%	9%	13%	10%	0%	10%	9%	5%	7%	6%	12%	4%
Prelimbic	6%	11%	3%	12%	11%	9%	9%	5%	3%	3%	6%	10%	0%	11%	7%	8%	11%	4%	6%
S1	13%	17%	16%	11%	17%	14%	11%	11%	13%	12%	17%	9%	11%	0%	18%	9%	11%	9%	2%
S2	5%	6%	13%	16%	13%	8%	11%	2%	3%	8%	15%	5%	7%	18%	0%	6%	14%	9%	4%
SN	7%	9%	9%	10%	5%	13%	9%	4%	7%	10%	10%	7%	8%	9%	6%	0%	6%	9%	6%
Thalamus	13%	13%	9%	14%	5%	6%	14%	10%	10%	6%	6%	11%	11%	14%	6%	0%	10%	3%	
Visual Ctx	4%	12%	8%	8%	10%	5%	12%	5%	7%	13%	9%	12%	4%	9%	9%	9%	10%	0%	8%
VTA	3%	8%	5%	5%	5%	5%	5%	7%	8%	4%	6%	4%	6%	2%	4%	6%	3%	8%	0%

DMSO STDERR																			
	Amygdala	Aud Ctx	Cingulate	CPu	Entorhinal Ctx	Frontal Ctx	Hippocampus	hypothalamus	Insular Ctx	LGP	M1	PAG	Prelimbic	S1	S2	SN	Thalamus	Visual Ctx	VTA
Amygdala	0%	10%	11%	11%	9%	7%	11%	5%	7%	15%	10%	14%	9%	4%	7%	7%	14%	7%	5%
Aud Ctx	10%	0%	9%	13%	13%	11%	13%	13%	7%	9%	13%	11%	9%	9%	11%	11%	11%	7%	7%
Cingulate	11%	9%	0%	14%	9%	10%	10%	8%	11%	9%	16%	13%	7%	9%	12%	8%	14%	7%	7%
CPu	11%	13%	14%	0%	9%	9%	8%	13%	16%	14%	13%	13%	11%	5%	15%	13%	16%	7%	7%
Entorhinal Ctx	9%	13%	9%	9%	0%	13%	9%	10%	11%	14%	10%	17%	7%	11%	10%	10%	5%	12%	13%
Frontal Ctx	7%	11%	10%	9%	13%	0%	10%	8%	7%	7%	10%	7%	10%	4%	10%	5%	12%	9%	4%
Hippocampus	11%	13%	10%	8%	9%	10%	0%	13%	8%	9%	10%	16%	8%	4%	15%	11%	12%	8%	6%
hypothalamus	5%	13%	8%	13%	10%	8%	13%	0%	10%	7%	9%	10%	9%	8%	6%	9%	14%	7%	5%
Insular Ctx	7%	7%	11%	16%	11%	7%	8%	10%	0%	10%	11%	9%	9%	7%	8%	10%	14%	7%	13%
LGP	15%	9%	9%	14%	14%	7%	9%	7%	10%	0%	10%	11%	4%	11%	12%	10%	15%	6%	6%
M1	10%	13%	16%	13%	10%	10%	10%	9%	11%	10%	0%	15%	15%	4%	16%	11%	7%	3%	8%
PAG	14%	11%	13%	13%	17%	7%	16%	10%	9%	11%	15%	0%	10%	8%	15%	11%	10%	8%	3%
Prelimbic	9%	9%	7%	11%	7%	10%	8%	9%	9%	4%	15%	10%	0%	6%	12%	8%	15%	5%	5%
S1	4%	9%	9%	5%	11%	4%	4%	8%	7%	11%	4%	8%	6%	0%	12%	4%	10%	9%	6%
S2	7%	11%	12%	15%	10%	10%	15%	6%	8%	12%	16%	15%	12%	12%	0%	8%	17%	8%	5%
SN	7%	11%	8%	13%	10%	5%	11%	9%	10%	10%	11%	11%	8%	4%	8%	0%	10%	5%	10%
Thalamus	14%	11%	14%	16%	5%	12%	12%	14%	14%	15%	7%	10%	15%	10%	17%	10%	0%	7%	16%
Visual Ctx	7%	7%	7%	7%	12%	9%	8%	7%	7%	6%	3%	8%	5%	9%	8%	5%	7%	0%	5%
VTA	5%	7%	7%	7%	13%	4%	6%	5%	13%	6%	8%	3%	5%	6%	5%	10%	16%	5%	0%

Figure A – 1: Standard errors of group mean correlation matrices in saline and DMSO pretreatment groups (N = 6)

Haloperidol STDERR																				
	Amygdala	Aud Ctx	Cingulate	CPu	Entorhinal Ctx	Frontal Ctx	Hippocampus	hypothalamus	Insular Ctx	LGP	M1	PAG	Prelimbic	S1	S2	SN	Thalamus	Visual Ctx	VTA	
Amygdala	0%	13%	8%	9%	10%	14%	8%	13%	10%	5%	8%	8%	10%	11%	11%	8%	10%	5%	4%	
Aud Ctx	13%	0%	12%	13%	14%	10%	22%	20%	18%	15%	7%	14%	16%	8%	16%	13%	11%	15%	9%	
Cingulate	8%	12%	0%	15%	13%	11%	16%	6%	18%	7%	14%	8%	7%	14%	13%	11%	9%	14%	6%	
CPu	9%	13%	15%	0%	16%	13%	17%	7%	21%	11%	8%	13%	16%	4%	17%	14%	9%	14%	3%	
Entorhinal Ctx	10%	14%	13%	16%	0%	6%	8%	13%	12%	5%	10%	19%	15%	9%	18%	8%	13%	11%	12%	
Frontal Ctx	14%	10%	11%	13%	6%	0%	10%	5%	13%	6%	11%	9%	9%	20%	12%	7%	7%	7%	7%	
Hippocampus	8%	22%	16%	17%	8%	10%	0%	17%	14%	11%	12%	12%	12%	21%	19%	10%	22%	16%	3%	
hypothalamus	13%	20%	6%	7%	13%	5%	17%	0%	23%	4%	10%	6%	6%	8%	14%	7%	15%	12%	14%	
Insular Ctx	10%	18%	18%	21%	12%	13%	14%	23%	0%	8%	13%	17%	14%	13%	26%	6%	21%	10%	9%	
LGP	5%	15%	7%	11%	5%	6%	11%	4%	8%	0%	6%	7%	9%	9%	9%	8%	9%	8%	6%	
M1	8%	7%	14%	8%	10%	11%	12%	10%	13%	6%	0%	11%	7%	16%	7%	6%	10%	13%	4%	
PAG	8%	14%	8%	13%	19%	9%	12%	6%	17%	7%	11%	0%	9%	11%	6%	10%	7%	12%	9%	
Prelimbic	10%	16%	7%	16%	15%	9%	12%	6%	14%	9%	7%	9%	0%	8%	13%	12%	9%	10%	7%	
S1	11%	8%	14%	4%	9%	20%	21%	8%	13%	9%	16%	11%	8%	0%	6%	5%	11%	7%	5%	
S2	11%	16%	13%	17%	18%	12%	19%	14%	26%	9%	7%	6%	13%	6%	0%	14%	12%	14%	9%	
SN	8%	13%	11%	14%	8%	7%	10%	7%	6%	8%	6%	10%	12%	5%	14%	0%	9%	7%	4%	
Thalamus	10%	11%	9%	9%	13%	7%	22%	15%	21%	9%	10%	7%	9%	11%	12%	9%	0%	12%	9%	
Visual Ctx	5%	15%	14%	14%	11%	7%	16%	12%	10%	8%	13%	12%	10%	7%	14%	7%	12%	0%	3%	
VTA	4%	9%	6%	3%	12%	7%	3%	14%	9%	6%	4%	9%	7%	5%	9%	4%	9%	3%	0%	

Clozapine STDERR																				
	Amygdala	Aud Ctx	Cingulate	CPu	Entorhinal Ctx	Frontal Ctx	Hippocampus	hypothalamus	Insular Ctx	LGP	M1	PAG	Prelimbic	S1	S2	SN	Thalamus	Visual Ctx	VTA	
Amygdala	0%	11%	12%	14%	10%	9%	13%	11%	13%	9%	11%	9%	10%	7%	10%	11%	7%	11%	4%	
Aud Ctx	11%	0%	10%	14%	7%	7%	9%	12%	11%	7%	7%	9%	4%	8%	8%	8%	8%	13%	8%	
Cingulate	12%	10%	0%	4%	8%	8%	13%	9%	9%	11%	15%	11%	5%	5%	8%	7%	3%	13%	7%	
CPu	14%	14%	4%	0%	10%	6%	13%	12%	13%	15%	7%	9%	11%	9%	16%	3%	4%	6%	3%	
Entorhinal Ctx	10%	7%	8%	10%	0%	7%	14%	11%	14%	10%	9%	9%	8%	7%	9%	7%	7%	9%	2%	
Frontal Ctx	9%	7%	8%	6%	7%	0%	12%	7%	11%	11%	15%	11%	7%	7%	7%	10%	8%	15%	5%	
Hippocampus	13%	9%	13%	13%	14%	12%	0%	11%	15%	13%	16%	13%	7%	11%	11%	12%	14%	16%	6%	
hypothalamus	11%	12%	9%	12%	11%	7%	11%	0%	13%	9%	10%	7%	10%	6%	9%	12%	12%	11%	10%	
Insular Ctx	13%	11%	9%	13%	14%	11%	15%	13%	0%	12%	10%	10%	10%	9%	11%	14%	2%	14%	5%	
LGP	9%	7%	11%	15%	10%	11%	13%	9%	12%	0%	14%	9%	6%	10%	9%	11%	8%	10%	4%	
M1	11%	7%	15%	7%	9%	15%	16%	10%	10%	14%	0%	9%	13%	11%	10%	11%	4%	15%	6%	
PAG	9%	9%	11%	9%	9%	11%	13%	7%	10%	9%	9%	0%	8%	6%	7%	10%	8%	11%	3%	
Prelimbic	10%	4%	5%	11%	8%	7%	7%	10%	10%	6%	13%	8%	0%	7%	6%	7%	2%	8%	6%	
S1	7%	8%	5%	9%	7%	7%	11%	6%	9%	10%	11%	6%	7%	0%	13%	2%	1%	5%	5%	
S2	10%	8%	8%	16%	9%	7%	11%	9%	11%	9%	10%	7%	6%	13%	0%	11%	8%	13%	5%	
SN	11%	8%	7%	3%	7%	10%	12%	12%	14%	11%	11%	10%	7%	2%	11%	0%	7%	10%	5%	
Thalamus	7%	8%	3%	4%	7%	8%	14%	12%	2%	8%	4%	8%	2%	1%	8%	7%	0%	6%	8%	
Visual Ctx	11%	13%	13%	6%	9%	15%	16%	11%	14%	10%	15%	11%	8%	5%	13%	10%	6%	0%	6%	
VTA	4%	8%	7%	3%	2%	5%	6%	10%	5%	4%	6%	3%	6%	5%	5%	5%	8%	6%	0%	

Figure A – 2: Standard errors of group mean correlation matrices in haloperidol and clozapine pretreatment groups (N = 6)

Olanzapine STDERR

	Amygdala	Aud Ctx	Cingulate	CPu	Entorhinal Ctx	Frontal Ctx	Hippocampus	hypothalamus	Insular Ctx	LGP	M1	PAG	Prelimbic	S1	S2	SN	Thalamus	Visual Ctx	VTA
Amygdala	0%	13%	14%	9%	13%	7%	9%	8%	12%	10%	12%	4%	7%	14%	10%	9%	15%	17%	8%
Aud Ctx	13%	0%	16%	13%	15%	11%	8%	14%	14%	12%	13%	10%	11%	15%	15%	13%	12%	17%	11%
Cingulate	14%	16%	0%	13%	16%	11%	9%	15%	9%	12%	19%	13%	10%	13%	14%	14%	7%	11%	9%
CPu	9%	13%	13%	0%	8%	9%	7%	11%	9%	15%	12%	10%	8%	12%	10%	9%	9%	10%	3%
Entorhinal Ctx	13%	15%	16%	8%	0%	11%	9%	11%	15%	9%	14%	12%	11%	13%	11%	10%	8%	22%	8%
Frontal Ctx	7%	11%	11%	9%	11%	0%	14%	6%	11%	11%	10%	7%	9%	13%	8%	7%	5%	12%	5%
Hippocampus	9%	8%	9%	7%	9%	14%	0%	6%	6%	5%	6%	6%	6%	8%	5%	10%	6%	7%	3%
hypothalamus	8%	14%	15%	11%	11%	6%	6%	0%	8%	12%	13%	8%	9%	16%	10%	10%	12%	17%	6%
Insular Ctx	12%	14%	9%	9%	15%	11%	6%	8%	0%	11%	8%	7%	6%	12%	12%	10%	13%	14%	10%
LGP	10%	12%	12%	15%	9%	11%	5%	12%	11%	0%	11%	10%	8%	15%	13%	11%	7%	16%	11%
M1	12%	13%	19%	12%	14%	10%	6%	13%	8%	11%	0%	11%	18%	15%	12%	14%	4%	13%	6%
PAG	4%	10%	13%	10%	12%	7%	6%	8%	7%	10%	11%	0%	6%	12%	7%	7%	9%	14%	8%
Prelimbic	7%	11%	10%	8%	11%	9%	6%	9%	6%	8%	18%	6%	0%	10%	9%	10%	7%	10%	5%
S1	14%	15%	13%	12%	13%	13%	8%	16%	12%	15%	15%	12%	10%	0%	17%	15%	11%	14%	11%
S2	10%	15%	14%	10%	11%	8%	5%	10%	12%	13%	12%	7%	9%	17%	0%	11%	15%	16%	9%
SN	9%	13%	14%	9%	10%	7%	10%	10%	10%	11%	14%	7%	10%	15%	11%	0%	10%	17%	9%
Thalamus	15%	12%	7%	9%	8%	5%	6%	12%	13%	7%	4%	9%	7%	11%	15%	10%	0%	8%	6%
Visual Ctx	17%	17%	11%	10%	22%	12%	7%	17%	14%	16%	13%	14%	10%	14%	16%	17%	8%	0%	15%
VTA	8%	11%	9%	3%	8%	5%	3%	6%	10%	11%	6%	8%	5%	11%	9%	9%	6%	15%	0%

SB277011 STDERR

	Amygdala	Aud Ctx	Cingulate	CPu	Entorhinal Ctx	Frontal Ctx	Hippocampus	hypothalamus	Insular Ctx	LGP	M1	PAG	Prelimbic	S1	S2	SN	Thalamus	Visual Ctx	VTA
Amygdala	0%	6%	14%	16%	16%	23%	6%	11%	17%	12%	17%	20%	16%	8%	11%	14%	18%	19%	15%
Aud Ctx	6%	0%	8%	6%	10%	10%	6%	9%	5%	5%	9%	4%	10%	10%	9%	8%	6%	5%	
Cingulate	14%	8%	0%	14%	19%	19%	10%	13%	19%	12%	19%	18%	9%	13%	17%	12%	11%	11%	19%
CPu	16%	6%	14%	0%	23%	19%	6%	13%	21%	17%	19%	17%	16%	17%	20%	20%	10%	11%	17%
Entorhinal Ctx	16%	10%	19%	23%	0%	27%	13%	14%	18%	15%	22%	25%	16%	14%	23%	14%	5%	12%	13%
Frontal Ctx	23%	10%	19%	19%	27%	0%	4%	22%	23%	20%	19%	8%	13%	8%	18%	27%	13%	12%	10%
Hippocampus	6%	10%	10%	6%	13%	4%	0%	7%	6%	9%	7%	9%	5%	14%	7%	8%	2%	7%	4%
hypothalamus	11%	6%	13%	13%	14%	22%	7%	0%	18%	13%	15%	16%	12%	9%	11%	14%	20%	17%	16%
Insular Ctx	17%	9%	19%	21%	18%	23%	6%	18%	0%	12%	21%	19%	15%	5%	17%	17%	16%	16%	17%
LGP	12%	5%	12%	17%	15%	20%	9%	13%	12%	0%	15%	14%	14%	8%	14%	10%	11%	12%	13%
M1	17%	5%	19%	19%	22%	19%	7%	15%	21%	15%	0%	18%	18%	14%	16%	16%	11%	8%	16%
PAG	20%	9%	18%	17%	25%	8%	9%	16%	19%	14%	18%	0%	13%	15%	13%	18%	6%	7%	8%
Prelimbic	16%	4%	9%	16%	16%	13%	5%	12%	15%	14%	18%	13%	0%	4%	11%	14%	4%	7%	12%
S1	8%	10%	13%	17%	14%	8%	14%	9%	5%	8%	14%	15%	4%	0%	18%	5%	16%	8%	7%
S2	11%	10%	17%	20%	23%	18%	7%	11%	17%	14%	16%	13%	11%	18%	0%	17%	17%	11%	18%
SN	14%	9%	12%	20%	14%	27%	8%	14%	17%	10%	16%	18%	14%	5%	17%	0%	11%	17%	21%
Thalamus	18%	8%	11%	10%	5%	13%	2%	20%	16%	11%	11%	6%	4%	16%	17%	11%	0%	10%	9%
Visual Ctx	19%	6%	11%	11%	12%	12%	7%	17%	16%	12%	8%	7%	7%	8%	11%	17%	10%	0%	9%
VTA	15%	5%	19%	17%	13%	10%	4%	16%	17%	13%	16%	8%	12%	7%	18%	21%	9%	9%	0%

Figure A – 3: Standard errors of group mean correlation matrices in olanzapine and SB277011 pretreatment groups (N = 6)

Figure A-4

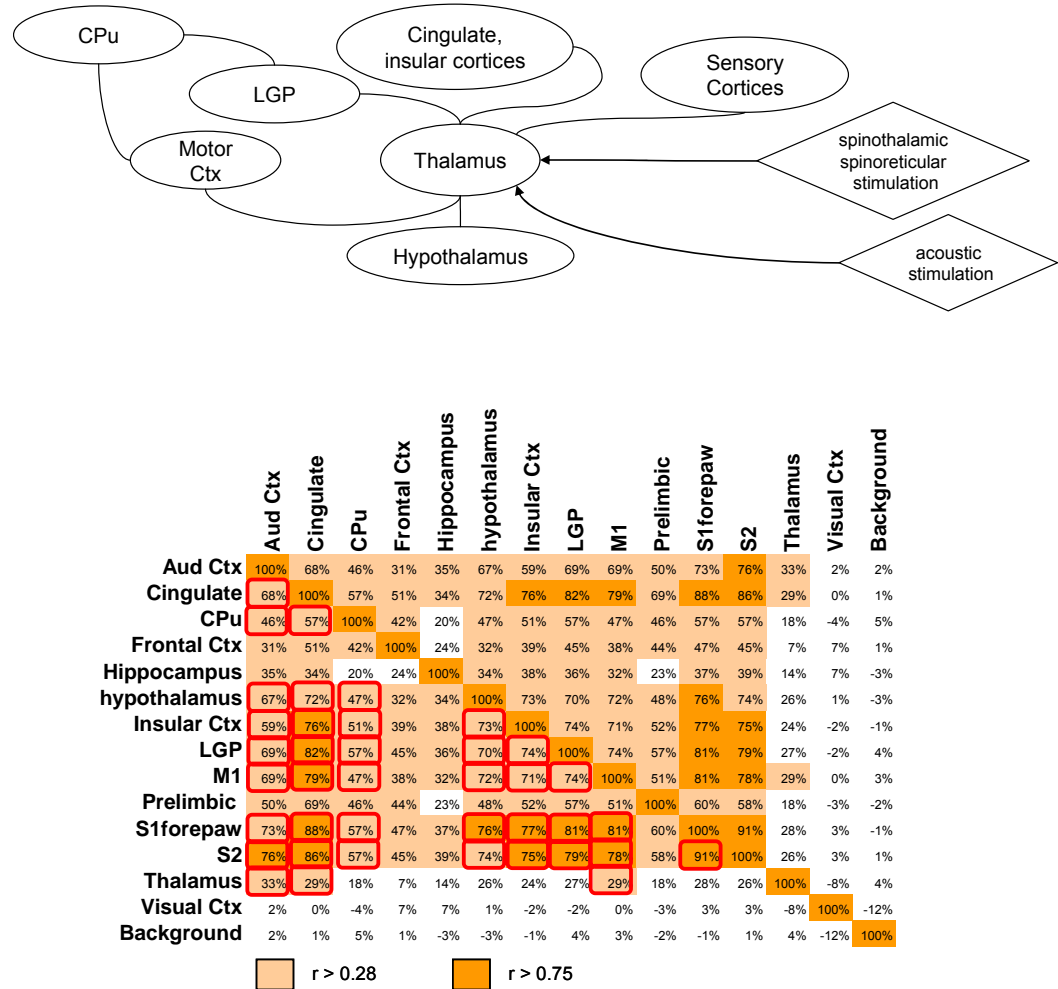


Figure A – 4: Correlations observed among sensory and motor pathways in electrical forepaw stimulation analysis.

All of the highly significant correlations ($r > 0.75$) and several other significant correlations ($r > 0.28$) are shown circled in red boxes (bottom panel). These regions recapitulate the sensory and motor circuitry expected to be stimulated following electrical forepaw stimulation (top panel).

Figure A-5

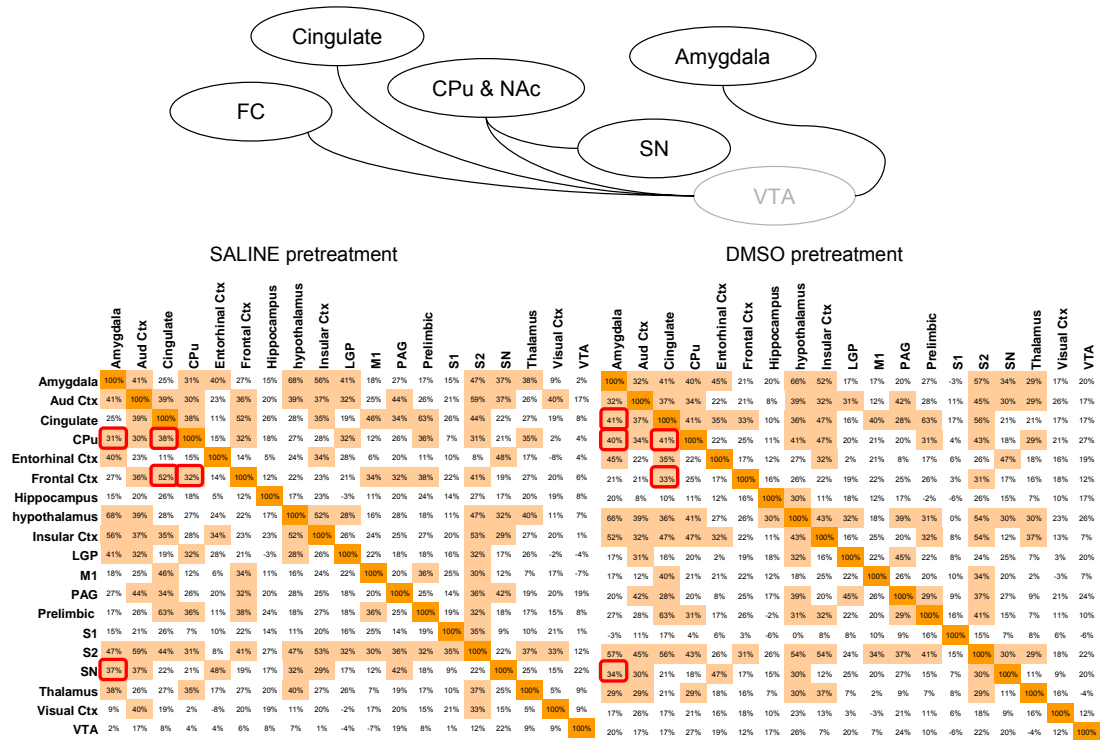


Figure A – 5: Correlation between regions of the mesolimbic dopamine network following ICV apomorphine administration.

Red boxes indicate correlations exceeding 0.28 (bottom panel) that were observed between components of the mesolimbic dopamine network (top panel) in animals that were pretreated with vehicle only. Shading defined as in Figure A – 4.

Figure A-6

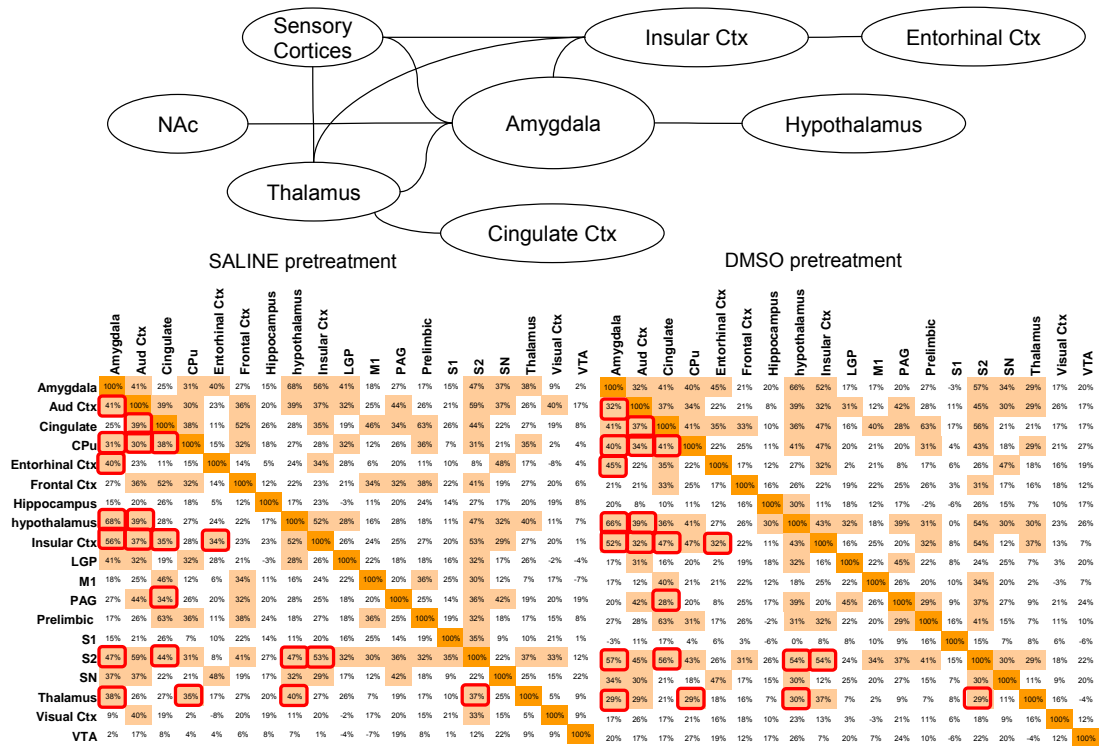


Figure A – 6: Correlation between regions associated with nociception and sensory information processing following ICV apomorphine administration.

Red boxes indicate correlations exceeding 0.28 (bottom panel) that were observed between components of known sensory and nociceptive information processing networks (top panel) in animals that were pretreated with vehicles only. Shading defined as in Figure A – 4.

Figure A-7

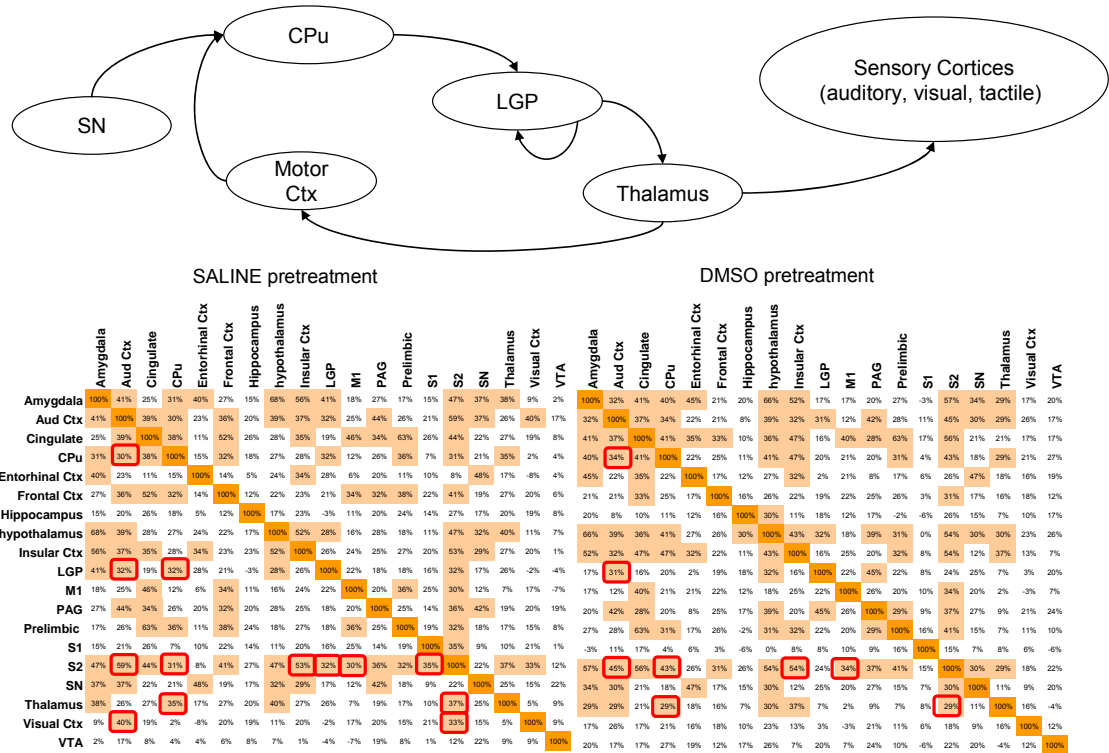


Figure A – 7: Correlation between regions associated with motor control and sensory information processing following ICV apomorphine administration.

Red boxes indicate correlations exceeding 0.28 (bottom panel) that were observed between components of known motor control and sensory information processing networks (top panel) in animals that were pretreated with vehicles only. Shading defined as in Figure A – 4.

APPENDIX B

CONSIDERATIONS IN CHOOSING AN IMAGING METHOD FOR phMRI EXPERIMENTS

The neuroscience investigator planning to use phMRI to probe the effects of drugs on neural activity within the brain is faced with several questions that dramatically affect the study design. The answers to these questions are not easily obtained, and guidance for making assumptions in phMRI study design is scant. Beyond the question of whether to perform experiments using conscious or anesthetized animals, the variety of technical approaches and data presented in this dissertation raises some specific questions regarding technical strategy: *Should I try to acquire multiple measures simultaneously? Which is better, BOLD, CBF, or CBV? Can I administer my drugs peripherally, or will ICV administration be necessary? What spatial and temporal resolution should I use, and with which acquisition protocol?* All of these questions are motivated by the more important general concern: *How can I be sure that this approach will work?*

Experiments using conscious animals

In Chapter 5, data are presented which support the argument that, in the context of understanding the relevant changes in neural activity that are induced by a psychotropic drug of interest, equivalence must be demonstrated between anesthetized and conscious preparations before conclusions can be drawn from experiments performed in anesthetized animals alone. Currently, few drugs have been investigated by phMRI in

conscious animals, and the burden of proof is on the investigator to perform any validating experiments before working with anesthetized preparations. In addition to the technical difficulty of performing experiments using conscious animals, factors may confound the comparison of data acquired from conscious animals to data acquired from anesthetized animals. These factors include the stress and sensory stimulation of conscious rats that are restrained inside the magnet and exposed to auditory stimulation during an MRI scan. These factors can be minimized by acclimation to the restraint apparatus and auditory experience of an MRI scan, and acclimation has been shown to reduce corticosterone release with repeated exposure to a simulated scanning environment (King et al., 2005).

Considerations for selecting the functional imaging modality, image acquisition protocol, and route of drug administration

Regrettably, there is no single approach that is ideal for all pharmacological MRI investigations, and there is no guarantee that a particular approach will be successful under novel circumstances. Dependency on the drug under investigation, the brain regions being investigated, the nature of data analysis, available resources (such as proprietary blood pool contrast agents), and study design (single session or longitudinal) are all important factors in determining the best approach. In any case, a single completed study is insufficient grounds for determining the best approach for investigating an unrelated drug. For example, consider the data presented in Chapter 3.

Based on the data presented in Chapter 3, one might draw the conclusion that BOLD measurements should be avoided for their propensity to produce erroneous or misleading results. This conclusion is premature in the absence of a comparative analysis of BOLD and alternative functional MR imaging modalities under the specific study conditions being considered. It is true that BOLD imaging is prone to contamination by a wider spectrum of physiological and experimental phenomena than contrast agent enhanced CBV or arterial spin labeling CBF measurements, but neither of these alternate modalities is failsafe. In Chapter 3, simultaneous acquisition of CBF and BOLD changes provided evidence to support the claim that negative BOLD changes observed along the cortical surface were artifacts, rather than changes indicative of reduced neural activity in these regions. However, the decision to collect this multi-modal information is dependent on several factors that may be best informed by understanding the specific limitations encountered in the presented research.

Figure B – 1 illustrates some of the limitations of various phMRI imaging modalities, acquisition protocols, and routes of administration, as determined from the research presented in the studies herein. As shown in Figure B – 1, phMRI Study Feature 1, phMRI investigations that anticipate neural activation, especially potent and widespread activation as seen with psychostimulants, suffer few, if any, limitations using specific functional imaging modalities. The significant hemodynamic response that results from neural stimulation is easily detected using BOLD, CBF, or CBV methods and specific anomalies such as those presented in Chapter 3 are readily detected and resolved with multimodal or sequential, unimodal imaging experiments. Imaging

conscious animals during the administration of psychostimulants can be challenging due to the increase in motor activity following drug administration, potentially causing severe motion artifacts.

Neural deactivation paradigms, such as the investigation of sedative drugs, present a different set of challenges (Figure B – 1, Study Feature 2). Reductions in CBF and CBV following neural deactivation have not been widely reported. CBF changes were shown to be undetectable in rats following morphine administration in Chapter 5, and decreases in BOLD signal contrast and CBF due to visual sensory deprivation have been shown to be smaller in amplitude than increases in these measures due to visual sensory stimulation in humans (Uludag et al., 2004). As a result, it is reasonable to assume that CBF measurements following neural deactivation using arterial spin labeling may be especially difficult to make in conscious rats, summarily complicating the measurement of changes in CMRO₂. Currently, the ease of measuring changes in CBV in conscious rats due to neural deactivation is difficult to anticipate, but CBV data reported among conscious rats under pHMRI neural stimulation paradigms is encouraging (Skoubis et al., 2006).

In analyses that require whole brain coverage (Figure B – 1, Study Feature 3), such as analyses examining functionally interconnected brain regions that are distal from one another (see Chapter 6), adequate coverage of ventral regions of the rat brain mandates a spin echo sequence that does not suffer from susceptibility or warping artifacts present in gradient echo or echo-planar-imaging (EPI) acquisition protocols. This problem is not an issue when regionally specific investigations are being performed of dorsal cortical areas

(see Chapter 2, and Figure B – 1, Study Feature 4), but remains an issue if the regions investigated are located in ventral or subcortical brain areas affected by the large sinuses of the ear canals in the rat skull (Figure B – 1, Study Feature 5). Multi-subject analyses that require data set coregistration are especially sensitive to non-linear deformations due to EPI image acquisition, and this workhorse of functional imaging is generally problematic in rat studies where this geometric distortion is especially prominent (Figure 6 – 1, Figure B – 1, Study Feature 6). In all acquisition protocols, a balance must be struck between spatial and temporal resolution and required sensitivity. In the studies presented herein, spatial resolution of $468 \times 468 \times 1500 \mu\text{m}^3$ and acquisition times of 2 sec (EPI) or 6 sec (RARE) represented the minimum volume and repetition times able to detect significant changes in BOLD contrast due to hemodynamic effects at 4.7T.

Peripheral administration of drugs often causes physiological changes that can have especially profound effects on the BOLD signal, preventing its reliable use, and complicating the estimation of changes in CMRO_2 (Figure B – 1, Study Feature 8). It is likely that changes in CBV, and, if measurable, changes in CBF will provide a robust alternate to BOLD imaging under these conditions. Evidence supporting this speculation can be found in the case of apomorphine administration, which was shown in rats not to affect CBV measurements using a blood pool contrast agent (Nguyen et al., 2000), but was shown to affect BOLD measurements in anesthetized (Kalisch et al., 2005) and conscious rats (pilot data not shown). Intracerebral ventricular (ICV) administration of the drug under investigation, as opposed to intravenous (IV), intraperitoneal (IP), or

subcutaneous (SC) administration, can be used to effectively prevent these physiological changes under many circumstances, as illustrated in Chapter 6 and in (Febo et al., 2005).

CBV measurements using blood pool contrast agents provide a unique combination of sensitivity that is greater than CBF measurements using arterial spin labeling, and resistance to physiological changes that affect the BOLD signal, suggesting that CBV may be an important tool for pHMRI research in the future. Unfortunately, the limited availability and high cost of contrast agents with a long half-life in the blood, such as MION (which has a half life in the blood of more than 4 hours; Jung et al., 1996), remains a formidable resource constraint that hinders CBV pHMRI studies (Figure B – 1, Study Feature 9). In addition to other applications, the future availability of effective blood pool contrast agents for CBV studies will enable validation of the findings made from the BOLD signal analysis performed in Chapter 6, presumably without the need for ICV administration of apomorphine. Furthermore, peripheral administration of the drug being assayed by pHMRI is a necessary feature of longitudinal studies using the same animal in multiple experiments (Figure B -1, Study Feature 7), such as those described in the discussion presented in Chapter 7. These advantages may make CBV measurements an indispensable aspect of future pHMRI research, in conjunction with non-invasive BOLD, CBF, and multimodal imaging techniques.

Figure B-1

phMRI Study Feature	Modality				Acquisition			Administration	
	BOLD	CBF	CBV	CMRO2	GE EPI	SE EPI	RARE	IP / IV / SC	ICV
1 Expecting neural activation (e.g. stimulant)	●	●	●	●	●	●	●	○	○
2 Expecting neural deactivation (e.g. sedative)	●	⊘	?	⊘	●	●	⊘	○	○
3 Analysis requires whole brain exploration	●	●	●	●	⊘	⊘	●	○	○
Analysis requires localized exploration									
4 of dorsal cortical regions	●	●	●	●	●	●	●	○	○
5 of subcortical or ventral regions	●	●	●	●	⊘	⊘	●	○	○
6 Analysis of effects across animals	●	●	●	●	⊘	⊘	●	○	○
7 Longitudinal study within same animal	○	○	○	○	○	○	○	●	⊘
8 Drug effects peripheral systems (e.g. HR, RR)	⊘	●	●	⊘	○	○	○	⊘	●
9 Limited access to MION or other contrast agent	○	○	⊘	○	○	○	○	○	○

● suggested for ⊘ suggested against ○ not pertinent

Figure B – 1: Considerations for phMRI study design based on experiences gleaned from the present studies.

Limitations of several aspects of phMRI techniques were encountered in the presented research and the recommended approaches under these conditions, gleaned from the experiences herein, are indicated in the figure. Discussion of these specific study features is included in the text of Appendix B.